ABSTRACT

DEVELOPMENT AND CHARACTERIZATION OF METHODOLOGY AND TECHNOLOGY FOR THE ALIGNMENT OF FMRI TIME SERIES

by
Carlo Ciulla

This dissertation has developed, implemented and tested a novel computer based system (AUTOALIGN) that incorporates an algorithm for the alignment of functional Magnetic Resonance Image (fMRI) time series. The algorithm assumes the human brain to be a rigid body and computes a head coordinate system on the basis of three reference points that lie on the directions correspondent to two of the eigenvectors of inertia of the volume, at the intersections with the head boundary. The eigenvectors are found weighting the inertia components with the voxel's intensity values assumed as mass. The three reference points are found in the same position, relative to the origin of the head coordinate system, in both test and reference brain images. Intensity correction is performed at sub-voxel accuracy by tri-linear interpolation. A test fMR brain volume in which controlled simulations of rigid-body transformations have been introduced has preliminarily assessed system performance. Further experimentation has been conducted with real fMRI time series. Rigid-body transformations have been retrieved automatically and the values of the motion parameters compared to those obtained by the Statistical Parametric Mapping (SPM99), and the Automatic Image Registration (AIR 3.08). Results indicated that AUTOALIGN offers sub-voxel accuracy in correcting both misalignment and intensity among time points in fMR images time series, and also that its performance is comparable to that of SPM99 and AIR3.08.

DEVELOPMENT AND CHARACTERIZATION OF METHODOLOGY AND TECHNOLOGY FOR THE ALIGNMENT OF FMRI TIME SERIES

by
Carlo Ciulla

A Dissertation
Submitted to the Faculty of
New Jersey Institute of Technology
in Partial Fulfillment of the Requirements for the Degree of
Doctor of Philosophy in Computer and Information Science

Department of Computer Science

May 2002

APPROVAL PAGE

DEVELOPMENT AND CHARACTERIZATION OF METHODOLOGY AND TECHNOLOGY FOR THE ALIGNMENT OF FMRI TIME SERIES

Carlo Ciulla

Dr. Fadi P. Deek, Dissertation Advisor — Date
Associate Dean of College of Computing Sciences
and Associate Professor of Information Systems, NJIT

Dr. Frank Shih, Committee Member — Date
Professor of Computer Science, NJIT

Dr. Andrew Kalnin, Committee Member — Date
Assistant Professor of Radiology, UMDNJ

Dr. James McHugh, Committee Member — Date
Professor of Computer Science, NJIT

Dr. Murray Turoff, Committee Member — Date
Hurlburt Professor of Management Information Systems, NJIT

BIOGRAPHICAL SKETCH

Author: Carlo Ciulla

Degree: Doctor of Philosophy in Computer and Information Science

Date: May 2002

Undergraduate and Graduate Education:

- Doctor of Philosophy in Computer and Information Science
  New Jersey Institute of Technology, Newark, NJ, USA, 2002

- Master of Science in Information Systems
  New Jersey Institute of Technology, Newark, NJ, USA, 2000

- Eng. Degree (Laurea) in Management Engineering
  University of Palermo, Faculty of Engineering, Palermo, Italy, 1994

Specialization: Computational Engineering in Biomedical Applications

Publications:

C. Ciulla and F.P. Deek,
"Performance Assessment of an Algorithm for the Alignment of fMRI Time Series". Brain Topography, 2002, 14(2): 1-20.

C. Ciulla and F.P. Deek,
"Development and Characterization of an Automatic Technique for the Alignment of fMRI Time Series". Brain Topography, 2001, 14(1): 41-56.

C. Ciulla, T. Takeda, H. Endo, T. Kumagai, M. Morabito and R. Xiao,
"MEG Measurements of 40Hz Auditory Evoked Response in Human Brain". C. Aine, Y. Okada, G. Stroink, S. Swithenby and C. Wood (Eds.) Biomag96: Proceedings of the Tenth International Conference on Biomagnetism Springer-Verlag (2000).

C. Ciulla,
"Development and Characterization of Techniques for Neuroimaging Alignment." Master's Thesis, New Jersey Institute of Technology, Newark, NJ, USA, May 2000.

C. Ciulla, T. Takeda and H. Endo,
"MEG Characterization of Spontaneous Alpha Rhythm in the Human Brain." Brain Topography, 1999, 11(3): 211-222.

C. Ciulla, T. Takeda and H. Endo,
"Temporal Analysis of Alpha Activity in Human Brain using a Whole-Head MEG System." The Journal of Japan Biomagnetism and Bioelectromagnetics Society, May 1996, 9(1): 168-171.

C. Ciulla, T. Takeda, M. Morabito, H. Endo, T. Kumagai and R. Xiao,
"MEG Measurements of 40Hz Auditory Evoked Response in Human Brain." Visualization of Information Processing in the Human Brain: Recent Advances in MEG and Functional MRI. Electroenceph. Clin. Neurophysiol., 1996, Suppl. 47: 121-127.

C. Ciulla, T. Takeda, R. Xiao, M. Morabito, T. Kumagai and H. Endo,
"Temporal Analysis of Alpha Activity in Human Brain using a Whole-Head MEG System." BPES 95 Proceedings of the 10th Symposium on Biological and Physiological Engineering. Sapporo, Japan, November 1995: 9-12.

Ciulla, C., Takeda, T., Xiao, R., Kumagai, T., Endo, H. and Morabito, M,
"Hemispheric and Regional Coherence of Gamma Band Activity in Human Brain Recorded by a whole-head MEG System." Visualization of Information Processing in the Human Brain: Recent Advances in MEG and Functional MRI. Tokyo Institute of Psychiatry. The 10th International Symposium. Tokyo, October 1995, 100-101.

Xiao, R., Takeda, T., Kumagai, T., Ciulla, C., Endo, H. and Morabito, M,
"MEG Measurement with Color Visual Stimuli." Visualization of Information Processing in the Human Brain: Recent Advances in MEG and Functional MRI. Tokyo Institute of Psychiatry. The 10th International Symposium. Tokyo, October 1995, 105.

Symposiums and Presentations:

The 10th Tokyo Institute of Psychiatry (TIP) International Symposium. Tokyo, Japan; October 1995.

BPES' 95. The 10th Symposium on Biological and Physiological Engineering. Sapporo, Japan; November 1995.

Biomag 96. Santa Fè, New Mexico, USA; February 1996.

The Japanese Biomag. Tokyo, Japan; May 1996.

ISBET'97 Brain fields in Psychiatry. Zurich, Switzerland; March 1997.

Academic Medical Centre. AMC, Amsterdam, The Netherlands; November 1997.

Rutgers - Department of Psychology. Newark, NJ, USA; October 1998.

University Hospital – UMDNJ. Newark, NJ, USA; November 2000.

New Jersey Institute of Technology - NJIT. Newark, NJ, USA; September 2001.

Medical Imaging Research Laboratory - MIRL. Salt Lake City, UT, USA; December 2001.

Department of Neurology, University of Pennsylvania Medical School, Philadelphia, PA, USA; April 2002.

Unit of Integrative Neuroimaging, Clinical Brain Disorders Branch - NIMH, NIH. Bethesda, MD, USA; May 2002.

This dissertation is dedicated to any student whom believes in mastery, command and combined use of Mathematics, Engineering and Computer Science

ACKNOWLEDGMENT

My greatest gratitude is for Dr. Fadi P. Deek, dissertation Advisor, for his special attention and invaluable contribution in addressing both the scientific and technological issues of this dissertation. I would like to extend my gratitude to Prof. F. Shih and Prof. McHugh for the great suggestions furnished during technological and scientific development of the software system and particularly to Dr. Andrew Kalnin for his constant attention to issues relevant to literature review and availability of fMRI data for experimentation. Discussions had with Prof. Turoff during the proposal defense have greatly enhanced both presentation of literature review and assessment of algorithm's performance. Also, I would like to thank Dr. Wen Liu of the Department of Radiology at the New Jersey Medical School, for his availability in discussing issues related to fMRI acquisition. This PhD dissertation was supported by New Jersey Information-Technology Opportunities for the Workforce, Education and Research (NJ I-TOWER), a New Jersey Institute of Technology (NJIT) project funded by the New Jersey Commission on Higher Education. Some fMRI data used in this research were provided by the functional Imaging Laboratory of the University of Medicine and Dentistry of New Jersey (UMDNJ Newark, NJ). Other fMRI time series used for experimentation were those made available by the fMRI Data Center of the Dartmouth College (Hanover, NH). Their recording parameters are described in Buckner et al. (2000).

TABLE OF CONTENTS

Chapter	Page
1 INTRODUCTION	1
1.1 Brain Image Registration	1
1.2 Brain Image Rigid Registration	5
1.3 Alignment of fMRI Time Series	10
1.4 Research Aims	11
1.5 Manuscript Organization	13
2 RELATED RESEARCH	14
2.1 Performance of Rigid Registration in Brain Imaging	14
2.1.1 Extrinsic Algorithms	14
2.1.2 Intrinsic Algorithms	17
2.1.3 Findings	28
2.2 A Framework for Brain Image Rigid Registration	29
2.2.1 Mono-modal Applications	29
2.2.2 Multi-modal Applications	32
2.2.3 Findings	35
3 SCIENTIFIC METHODOLOGY	37
3.1 Motivation	37
3.2 Research Methods	39
3.3 Scientific Approach	40
3.4 Technological Effort	47
3.5 Testing and Validation	48

TABLE OF CONTENTS
(Continued)

Chapter **Page**

3.6 Contributions..... 49

3.7 Head Motion Simulation..... 51

3.8 Head Coordinate System of The 3-fiducial Markers Technique..... 52

3.9 The AUTOALIGN Technique..... 57

3.10 AUTOALIGN Registration Algorithm..... 59

3.10.1 Extraction of the Tensors of Inertia..... 59

3.10.2 Localization of the Fiducial Markers..... 59

3.10.3 Construction of the Head Coordinate System..... 62

3.10.4 Determination of the Rigid-Body Transformation..... 64

3.10.5 Interpolation..... 69

3.10.6 Accuracy Estimation..... 70

4 TECHNOLOGY DEVELOPMENT..... 71

4.1 General Description of AUTOALIGN Computer Based System..... 71

4.2 Detailed Description..... 80

4.2.1 Generally Object Oriented..... 80

4.2.2 Structure Chart Based..... 93

5 METHODOLOGY VALIDATION..... 106

5.1 Preliminary Analysis with Simulated Data..... 106

5.2 Validation with Real fMRI Time Series..... 111

5.3 Robustness to Noise..... 122

5.4 Reliability of the Three Points Method..... 125

TABLE OF CONTENTS
(Continued)

Chapter **Page**

5.5 Performance Comparison with Existing Algorithms..... 128

6 DISCUSSION..... 131

6.1 Performance of Algorithms for Brain Image Registration..... 131

6.2 Creation of the AUTOALIGN Technique..... 135

6.3 AUTOALIGN Algorithm..... 138

6.3.1 Background..... 138

6.3.2 Testing and Validation..... 139

6.3.3 Robustness to Noise..... 140

6.3.4 The Axis of Minor Resolution..... 142

6.3.5 AUTOALIGN Point-Based Registration..... 142

6.3.6 Types of fMRI Motion Related Effects..... 143

7 CONCLUSIONS..... 145

7.1 Algorithmic Performance in Brain Image Rigid Registration..... 145

7.2 AUTOALIGN Technique Characteristics..... 146

7.3 Performance of AUTOALIGN Algorithm for fMRI..... 147

7.4 Summary..... 151

7.5 On the Future of fMRI Alignment Research..... 152

7.5.1 On the Tri-linear Interpolation Effectiveness..... 153

7.5.2 Implications for Future Research..... 158

APPENDIX A AUTOALIGN DATA DESCRIPTION..... 160

TABLE OF CONTENTS
(Continued)

Chapter **Page**

APPENDIX B PRELIMINARY TEST OF THE AUTOALIGN TECHNIQUE..... 170

REFERENCES..... 178

LIST OF TABLES

Table **Page**

2.1 Performance of Fiducial Markers Algorithms..... 16

2.2 Performance of Voxel Based Registration..... 21

2.3 Performance of Mutual Information Approaches..... 22

2.4 Performance of Feature Based Algorithms..... 24

2.5 Performance of Anatomical Landmarks Based Algorithms..... 25

2.6 Performance of Segmentation Based Algorithms..... 27

2.7 Performance of a Real Time Algorithm..... 28

2.8 Performance of Principal Axes Based Algorithms..... 28

5.1 "Amis" Values..... 115

5.2 AUTOALIGN Accuracy Average Values..... 116

5.3 Performance Coefficient (P) of VB and MMI Approaches..... 129

5.4 Performance Coefficient (P) of FB, ALB and SB Approaches..... 130

5.5 Performance Coefficient (P) of FIB and MB Approaches..... 130

7.1 Methodology Characteristics Used to Create AUTOALIGN..... 147

7.2 Erone's Triangle Area..... 148

B.1 Preliminary Test Results of the AUTOALIGN Technique..... 176

LIST OF FIGURES

Figure **Page**

2.1 A Framework for Brain Image Rigid Registration..... 36

4.1 The Architectural Framework of a Visual Information System..... 73

4.2 Architectural Framework of an Image Database System..... 74

4.3 Architectural Framework of a Computer Based System for Brain Image Registration..... 75

4.4 Architectural Diagram of AUTOALIGN Computer Based System for Brain Image Registration..... 78

4.5 AUTOALIGN Graphical User Interface (GUI)..... 79

4.6 AUTOALIGN Level 0 Diagram..... 81

4.7 AUTOALIGN Level 1 Diagram (Two fMRI Scans)..... 83

4.8 AUTOALIGN Level 2 Diagram (All fMRI Scans)..... 84

4.9 AUTOALIGN Level 2 Diagram (Display Scan)..... 86

4.10 AUTOALIGN Level 2 Diagram (Unit Vectors)..... 87

4.11 AUTOALIGN Level 2 Diagram (Align Scan)..... 89

4.12 AUTOALIGN Level 2 Diagram (ReDisplay)..... 89

4.13 AUTOALIGN Level 2 Diagram (Diff. Image)..... 91

4.14 AUTOALIGN Level 2 Diagram (Align All to Ref.)..... 92

4.15 AUTOALIGN Structure Chart Level 0..... 94

4.16 AUTOALIGN Structure Chart Level 1: Input..... 94

4.17 AUTOALIGN Structure Chart Level 1: Two fMRI Scans..... 95

4.18 AUTOALIGN Structure Chart Level 2: Display Scan..... 96

4.19 AUTOALIGN Structure Chart Level 2: Unit Vectors..... 98

LIST OF FIGURES
(Continued)

Figure **Page**

4.20 AUTOALIGN Structure Chart Level 2: Align Scan 99

4.21 AUTOALIGN Structure Chart Level 2: Re-Display..... 100

4.22 AUTOALIGN Structure Chart Level 1: All fMRI Scans 101

4.23 AUTOALIGN Structure Chart Level 2: Align All to Ref 103

4.24 AUTOALIGN Structure Chart Level 2: Diff. Image 104

4.25 AUTOALIGN Structure Chart Level 1: Output 105

5.1 Functional MRI Data Shown in three 2D Composite Views (Axial, Sagittal and Coronal) 108

5.2 Location of Fiducial Markers into the Artificial fMRI 109

5.3 Preliminary Analysis 110

5.4 fMR Difference Images 112

5.5 Angles Estimation Plot with Real fMRI Data 113

5.6 Translation Estimation Plot with Real fMRI Data 114

5.7 Plot of Registration Accuracy after AUTOALIGN Motion Correction 117

5.8 Brain Images Before and After AUTOALIGN Alignment 119

5.9 Location of the Three Fiducial Markers into the Real fMRI 120

5.10 Difference Images Obtained with Real fMR 121

5.11 Plot of Average Values of Estimated Motion Parameters Versus Noise Level (2^N where N=1, 2, 3, 4, 5) 124

5.12 Bar Plot of Average Difference Values between Unit Vectors of Z-eigenvector (white) and Z-axis (black) 127

6.1 Location of Intensity Changes Used for Noise Simulations (N=5) 141

LIST OF FIGURES
(Continued)

Figure **Page**

7.1 "Amis" Plot across Algorithms for 1st 2nd and 3rd Experimental Sessions 149

7.2 "Amis" Plot across Algorithms for exp1-01, exp1-02 and exp1-04 Experimental Sessions 150

7.3 Voxel Ψ (a), Trilinear Function (b) and Region of Efficacy (c) 159

B.1 AUTOALIGN and SPM99 Estimation of Pitch Angles 171

B.2 AUTOALIGN and SPM99 Estimation of Roll Angles 172

B.3 AUTOALIGN and SPM99 Estimation of Yaw Angles 173

B.4 AUTOALIGN and SPM99 Estimation of Pitch, Roll and Yaw Angles 175

B.5 Sample Alignment Result of AUTOALIGN 177

CHAPTER 1

INTRODUCTION

1.1 Brain Image Registration

Image registration is a basic requirement in neuro-imaging and all methods aimed to the construction and use of brain atlases (Toga and Thompson 2000). Data must either undergo some alignment procedure or be assumed to be in register to allow any analysis, within or across subjects or sessions. As it is for many image-processing applications, also in neuro-imaging it is necessary to form a voxel-by-voxel / pixel-by-pixel comparison of two images (3D / 2D) of the same object field obtained from different sensors, or two images of an object field taken from the same sensor at different times. To form this comparison, it is necessary to spatially register the images and thereby correct for relative translational shifts, magnification differences, and rotational shifts, as well as geometrical and intensity distortions of each image (Althof et al. 1997).

Presently, neuro-imaging techniques such as fMRI (functional Magnetic Resonance Imaging), MRI (Magnetic Resonance Imaging), PET (Positron Emission Tomography) and CT (Computerized Tomography), among others, require head motion correction. Correction of any head movements that may occur during scanning must be employed prior to any data analysis, in order to minimize head motion artifacts. Several automated methodologies have been applied in the past with some success. Most of these methodologies rely on the assumption that the human brain is a rigid body subject to rigid motion during the period of scanning (Pellizzari et al. 1989; Alpert et al. 1990; Woods et al. 1992, 1993, 1998a,

1998b; Maurer et al. 1997; West et al. 1997, 1999), others assume that motion-related artifacts are still present after alignment is performed (Friston et al. 1996), and some uses algorithms that can model elastic deformations (Thompson and Toga 2000).

Registration of 3D medical images to a standard was obtained by the principal axes method by Faber and Stokely (1988). The principal axes of an object were defined as those orthogonal axes about which the moments of inertia are minimized and thus it was shown that if two objects are identical, except for a rotation and/or a translation, they could be registered by matching their principal axes. Alpert et al. (1990) developed a computational technique called registration by the principal axes transformation. This methodology assumes the brain to be a rigid body and was developed for the registration of volumes, which are rotated and translated in the transverse section plane. The performance of the method was studied with image data from PET, CT and MRI. It was found that progressively, coarser sampling of data sets led to some degradation in the performance of the method.

There is agreement in literature about the need in neuro-imaging for sub-voxel registration accuracy. It has been estimated that registration accuracy of the order of 0.05 voxels (typically 50 μm) is required to avoid mis-registration artifacts in MRI (Lemieux et al. 1998). Maximization of mutual information (MMI) has recently been proposed as a new approach for multi-modal medical image registration. Mutual information (MI) was introduced as a robust similarity measure for medical data (Viola and Wells 1995; Collignon at al. 1995) and proved superior to optimize transformations of both mono and multi-modal registration. Since then,

several separate studies have found excellent results for mutual information based medical image registration (Wells and Viola 1996; Maes et al. 1997; Meyer et al. 1997; Studholme et al. 1997; Thevenaz et al. 1998, 2000; Holden et al. 2000). Studholme et al. (1996) presented a comparative study of several voxel-based registration methods (e.g. various correlation measures, corresponding variance, moments of the joint histogram, joint entropy, and mutual information). In term of robustness, they concluded that mutual information performed extremely well when compared to other measures.

West et al. (1997) aimed recently to perform a blinded evaluation of a group of brain image registration techniques using as a gold standard a prospective bone-implanted marker-based registration method described by Maurer et al. (1997). Their results indicated that brain registration techniques have the potential to produce satisfactory results much of the time but that visual inspection is necessary to guard against large errors and that the most accurate registration standard for clinical data was is obtainable with the bone-implanted markers and has an accuracy of around 500 μm. The brain registrations made by West et al. (1997) were performed in parallel at several sites with registration algorithms that were published earlier in literature. Several authors participated to the experiment. Some methods were used that were applicable only to CT-to-MR or PET-to-MR registration, and some were suitable for both cases.

In order to distinguish between registration solutions that are clinically satisfactory and those that are not, one approach is to rely on a human observer to inspect the registration results and reject images that have been registered with

insufficient accuracy. Therefore, a methodology was developed for evaluating the efficacy of the visual assessment of registration accuracy (Fitzpatrick et al. 1998). Such methodology was applied to the registration solution proposed earlier by Maurer et al. (1997) and was obtained using external fiduciary markers screwed into the patient's skull that were visible in both MRI and CT images. The latter, to be fully automatic needs a technique for finding and localizing externally attached markers. Thus, a method was developed and tested for CT (Computerized Tomography) and MRI (Magnetic Resonance Imaging) by Wang et al. (1996).

Also, functional fMRI data series present the problem of head motion-related artifacts. Despite restraints to inhibit head movement, even willing and co-operative subjects still show head displacements (Friston et al. 1996). With some subjects (i.e. very young), head restraints appear to be ineffective in preventing motion. In such circumstances head movement of several millimeters or more is not uncommon. As suggested by Friston et al. (1996) simply moving the images back into register is not sufficient to remove all motion-related effects. Movement-related effects will still persist even after perfect realignment. Grootoonk et al. (2000) emphasized the existence of residual intensity errors in fMRI time series even after realignment. In particular, it was demonstrated that if a non-ideal interpolation scheme is used to resample realigned images, this could account for a major component of the residual artifacts.

1.2 Brain Image Rigid Registration

Brain imaging is a vast component of a larger set of applications in the modern clinical setting and as such it assumes relevant importance since it consists of imaging modalities devoted to recording from the human brain. Brain imaging can be partitioned into two main categories: anatomical and functional. While the former is devoted to the visualization of the anatomy of the human brain, the latter aims to reveal information about tissue metabolism underlying anatomy. The following anatomical imaging techniques were considered in this dissertation: X-ray, CT (Computer Tomography) and MRI (Magnetic Resonance Imaging); together with functional imaging techniques like: SPECT (Single-Photon Emission Computed Tomography), PET (Positron Emission Tomography) and fMRI (functional Magnetic Resonance Imaging).

Because signal intensities recorded from the human brain are very weak, replications of recording need to be conducted in order to obtain successful imaging (e.g. fMRI). Thus, registration of brain images obtained with the same modality but at different times can be a necessity. Also, some brain imaging applications are in their nature complementary to each other. An example of this kind is the anatomical structure of the human brain recorded by MRI and the functional activation of the same recorded with techniques like PET and/or fMRI. Registration is then employed in order to determine a voxel-to-voxel mapping (alignment) between images of different modalities (co-registration).

According to the elegant outline proposed by Rouet et al. (2000), a registration algorithm is composed by several steps. Preliminarily, an optional pre-processing

procedure is applied in order to segment the image or extract features of interest. However, any processing procedures prior to registration can affect the results of the subsequent alignment. Next the registration algorithm requires to adopt either rigid or non-rigid body assumptions (Bookstein 1989; Miller et al. 1993; Collins et al. 1995; Davatzikos 1996; Shormann et al. 1996; Thompson and Toga 1996; Iosifescu et. al. 1997; Thompson et al. 1997; Toga 1994; Warfield et al. 1996; Coley et al. 2000; Rouet et al. 2000; Toga and Thompson 2000; Wang and Staib 2000) to model the transformation. Then, a cost function between target and transformed images and an optimization procedure that maximize it need to be defined, so that the registration parameters can be found. The choice of the cost function is the step of the registration algorithm that determines the approach used to elaborate the relationships between images to align. The last step is that of fusing and/or interpreting the registered images, which implies estimation of the voxel's intensity from the values of the original image. This is accomplished by interpolation. Similarly, Grootoonk et al. (2000) reports two processes governing brain image rigid registration. The first is that of estimating for each image the six rigid-body parameters, which define the spatial transformation. The second is that of re-sampling each image according to the spatial transformation.

Previous research surveyed the broad topic of image registration (Brown 1992) and compiled a general overview of the algorithms classifying them in: (i) correlation-based; (ii) fourier-based; (iii) point-based and (iv) elastic registration methods. Other research surveyed the more focused medical image registration and its applications (Maurer and Fitzpatrick 1993; van den Elsen et al. 1993; Maintz

and Viergever 1998; Fitzpatrick et al. 2000). Audette et al. (2000) reviewed surface registration approaches and presented them as a subset of the medical image registration techniques discussed by Maintz and Viergever (1998). Among the surface-based algorithms, the authors did not include those approaches based on manually identified landmarks. Consistent with Audette et al. (2000), this dissertation considers approaches based on landmarks extracted automatically from surfaces as feature-based algorithms and distinguish them from algorithms based on manually selected landmarks. Also, consistent with Maintz and Viergever (1998), principal axes based approaches, which reduce the image content to vectors and scalars, are considered here as distinct from algorithms of the voxel-based category, which for definition, uses the full image content. Therefore, on the basis of the knowledge provided in literature, the present dissertation classifies the bulk of registration algorithms that rely on the rigid-body assumption in either extrinsic (artificial objects attached to the patient) or intrinsic: (i) voxel-based (e.g. maximization of mutual information); (ii) feature-based; (iii) anatomical landmarks based; (iv) segmentation-based and (v) principal axes based.

Brain imaging techniques necessitate automatic procedures in order to determine voxel-to-voxel mapping between images. Mapping consists of registration, which enables reliable analysis of brain images of the same modality (e.g. fMRI), or co-registration, which enables projection of images of one modality onto another. One example is functional recordings onto anatomical datasets. In either case, a large body of literature has been reported and a rich web of

methodologies has been proposed in order to determine the voxel-to-voxel mapping using several different assumptions and/or properties of the brain images.

The most basic assumption that features a registration algorithm is that of rigid or non-rigid (Rouet et al. 2000; Wang and Staib 2000; Toga and Thompson 2000; Thompson and Toga 2000) motion. Several properties of the brain images have been used: voxel relationships such as intensity differences (Friston et al. 1995), statistical similarities such as variance of intensity ratios (Woods at al. 1992, 1993, 1998a, 1998b) or mutual information (Wells et al. 1995, 1996; Maes et al. 1997, 1999; Studholme et al. 1997; Thevenaz et al. 1998; Thevenaz and Unser 2000; Holden et al. 2000), features (Maintz et al. 1995, 1996a, 1996b, 1997), landmarks (Grachev et al. 1999; Kruggel et al. 1999; Pennec et al. 2000) and vectors and scalars (Faber and Stokely 1988; Alpert et al. 1990). Also, extrinsic properties of brain images determined by fiducial markers have been used (Maurer et al. 1993, 1994, 1995, 1996, 1997) and a mathematical formulation has been given to assess accuracy of point-based registration (Fitzpatrick et al. 1998; Fitzpatrick and West 2001; West et al. 2001).

Focusing on brain image rigid registration, it can be inferred that in general: (i) excellent results, independent from modality, can be obtained with fiducial markers (Maurer et al. 1997); (ii) moment based registration algorithms provide simple and fast methodologies (Alpert et al. 1990; Faber and Stokely 1988); (iii) mutual information approaches provide robust co-registration of functional and anatomical datasets (Hill et al. 1993, 1994; Collignon et al. 1995a, 1995b; Wells et al. 1995, 1996; Studholme et al. 1996); (iv) voxel-based approaches (Friston et al. 1995;

Woods et al. 1992, 1993, 1998a, 1998b) are more prone to perform successful within-modality registration. However, each of the above methodologies presents limitations. Fiducial markers, for example, need to have consistency such to be detected and imaged independently from any modalities. Also, either affixed or screwed, markers necessitate algorithms to localize them accurately into the brain images (Wang et al. 1996). Moment based registration algorithms are particularly sensitive to sampling axial resolution (Faber and Stokely 1988). Mutual information approaches are subject to long and time-wise expensive optimization processes and need to be initialized close to the optimal solution (Maes et al. 1997). Voxel-based methods provide excellent mean for within-modality registration but their similarity measures are based on assumptions made on the nature of the relationships between voxel's intensity.

Though literature on brain image rigid registration is rich and diverse, few studies made comparative evaluation of performances across algorithms. The most comprehensive one in term of variety of approaches compared and most consistent in term of equality of modalities and size of brain images used for evaluation, was reported by West et al. (1997, 1999). Other studies have focused on investigating which optimization strategies were the best for multi-resolution rigid registration based on maximization of mutual information (Maes et al. 1999), and which brain image similarity measure was the best between joint-entropy (e.g. mutual information) and correlation based cost-functions (Holden et al. 2000).

1.3 Alignment of fMRI Time Series

Considerable efforts have been devoted to the alignment of functional Magnetic Resonance Images. Cox (1996) released software for visualization and analysis of fMRI, which by means of markers allow co-registration of anatomical and functional datasets. As far as voxel-based methods are concerned, Friston et al. (1995) developed the Statistical Parametric Mapping, which can also be used for alignment of fMRI time series by a least-square non-iterative method that minimizes differences between two images intensity values. Also Thevenaz et al. (1998) proposed an algorithm based on least-square minimization of intensity differences but proposed as an optimizer, a variant of the Marquardt-Levenberg (ML) method.

Biswal and Hyde (1997) presented a contour-based technique and showed that local changes in signal intensity, such as those due to magnetic field variations, constitute a limitation for intensity-based fMRI registration. Along the same line, Kybic et al. (1999) studied the non-linear geometrical distortions of echo-planar images (EPI) that are caused by local magnetic field inhomogeneities and reported an algorithm to register EPI images to MRI.

Eddy et al. (1996) explored the issue of within-plane motion in fMRI and proposed a two-dimensional method that estimates, before image reconstruction, translations and rotations in the Fourier domain (k-space). Also, Maas et al. (1997) addressed the problem of in-plane motion and proposed the DART registration algorithm, which was based on the separation of rotational and translational motion

components and allowed reduction of complexity eliminating the need of iterative implementations.

Lee et al. (1996, 1998) reported a prospective real-time methodology to solve the problem of through-plane motion, which occurs when an anatomical section of the brain goes in and out of the imaging plane.

As far as the accuracy obtainable by intensity correction, it has been shown that motion related effects are still present after registration (Friston et al. 1996) and is attributable to interpolation (Grootoonk et al. 2000) or magnetic field inhomogeneities (Andersson et al. 2001). Various interpolation paradigms were evaluated (Ostuni et al. 1997) and it was found the tri-cubic spline to be the most accurate and the tri-linear to be the most practical in term of computational time. Also, Freire and Mangin (2001) presented evidence supporting the argument that, alignment algorithms, especially those based on least-square measures, might produce artifacts in motion free fMRI data, suggesting not to resample time series if motion estimates are small compared to the voxel's size.

1.4 Research Aims

This dissertation focus on fMRI and starting from the assumption that to screw fiduciary markers into the patient's skull is not feasible either for research or for diagnostic purposes proposes that fiducial markers can be automatically found by principal axes transformation methods. At this purpose, the principal axes / tensor-based transformation method reported by Alpert et al. (1990) and Faber and

Stokely (1988), has been merged to a method that uses three points to identify the position of the brain in the scanning volume. The latter was successfully employed to co-register MRI with MEG data during previous work investigating the origin of the 40 Hz Auditory Steady State Response (Ciulla et al. 1996) and the spontaneous Alpha Rhythm (Ciulla et al. 1999). A new and fully automatic technique to align fMRI time series has been developed, implemented and tested on a SGI Origin 2400 workstation and it consists of a software package written using Matlab, Open GL and ANSI C.

Thus, aiming to both exploit accuracy of point-based registration and speed of computation of moment-based registration, a fiducial markers methodology used earlier (Ciulla et al. 1999, 2000) was combined with a tensor-based approach to obtain the AUTOALIGN registration technique (Ciulla and Deek 2001a). This dissertation gives a full mathematical description of the AUTOALIGN algorithm, developed on the basis of the registration technique, and assesses its performance by comparing results obtained in fMRI to those of SPM99 and AIR3.08 with the same dataset. Issues explored by this research are discussed on the basis of the knowledge provided in literature.

Also, this dissertation aims to bring further contribution to the literature by focusing on brain image rigid registration and by placing emphasis on algorithmic performance, extending the work of previous evaluations (West et al. 1997, 1999; Maes et al. 1999; Holden et al. 2000) to a larger number of registration techniques. A framework is advanced that groups the most successful brain image rigid registration techniques on the basis of the imaging modality in which they were

employed, and analyze performance of each algorithm in term of accuracy, computational time and approach used for validation.

1.5 Manuscript Organization

This manuscript is organized as follow. In chapter 2 is given a detailed outline of the current published literature in brain rigid image registration. In chapter 3 is explained what this research consists of, what scientific approaches were used and technological efforts were spent in term of software implementation. A preliminary study is described to develop and test separately AUTOALIGN components and later pipeline them to form the novel approach. Also, advantages of the novel computer based system are outlined together with the registration algorithm that has been developed. Chapter 3 also includes a detailed description of all mathematics incorporated into the AUTOALIGN algorithm and implemented into software. In chapter 4, components of the software system are defined by architectural diagrams based on object oriented methodologies. Diagrams describe AUTOALIGN internal functions. A picture of the Graphical User Interface (GUI) is included such to provide the reader with all the functionality elements of the software system. A data description is given in Appendix A that refers to the terms used in both object oriented diagrams and structure charts. In chapter 5 results are given to show the potentiality of the new algorithm and how it compares in terms of performance to existing methods. Chapters 6 and 7 respectively discuss value of this dissertation with respect to the current knowledge and outline conclusions.

CHAPTER 2

RELATED RESEARCH

This chapter presents a review of the literature on algorithms that adopt the rigid-body assumption to solve the problem of brain image registration. It is also advanced a framework that considers two important issues in order to outline performance in brain image registration: methodology used to elaborate relationship between the volumes to register and imaging modality. Using the literature as a basis, identified methodologies were classified in either extrinsic, which rely on external objects affixed to the head, and intrinsic, which rely on information provided by the brain images alone. Performance of published algorithms was analyzed devoting particular attention to accuracy, computational time and validation approach. It was found that algorithms offering the best performance are, within the extrinsic classification, those based on fiducial markers and, within the intrinsic classification, those using relationships between voxel's intensity. For each imaging modality, the framework also identifies the algorithm that is most promising in term of accuracy.

2.1 Performance of Rigid Registration in Brain Imaging

2.1.1 Extrinsic Algorithms

Extrinsic algorithms rely on external objects (attached or screwed) to the subject's head in order to determine the matching transformation between brain images to be

registered. As such, these algorithms are easy to implement and require no need of optimization procedures. External objects can be fiducial markers (Erickson and Jack 1993; Maurer et al. 1993, 1994, 1995), stereotaxic frames (Zhang et al. 1990) or head-holding devices (Evans et al. 1988, 1989). They provide fixed reference points into the brain images.

While use of stereotaxic frames is invasive, head-holding devices present the disadvantage of difficult and not precise positioning during each scanning. A drawback with the use of external fiducial markers is that the technology must ensure that the markers are always imaged. Since the physics may vary from one imaging modality to another, type and consistency of markers may vary also. For the high resolution requirements of CT and MR images, specific fiducial marker systems that fit onto stereotaxic frame-base rings have been used, but these can cause pain and discomfort for the patient (Henri et al. 1991).

Also, as indicated by research, all of the above methods require prospective planning studies, making relatively difficult retrospective analysis of scans without extrinsic reference (Hogan et al. 1996). Registration results have been documented with either two (Dobbins et al. 1993) or four (Arendsen and Bentum 1991; Bellers and De Bruijn 1993) fiducial markers. The mismatch error obtained in co-registration of SPECT and MR studies by use of fiducial markers has been reported, with a phantom model, to be no greater than 3 mm (Erickson and Jack 1993).

Later, Maurer et al. (1997) developed a method based on invasive fiducial markers and reported a registration accuracy of 0.5 mm for CT, MR and X-ray

images. To date, this is claimed to be the most accurate fiducial markers registration method; also one of the most accurate among all co-registration techniques and had been used by West et al. (1997, 1999) as "gold standard" within an experiment aimed to compare the accuracy of several other alignment techniques.

Fitzpatrick et al. (1998b) developed a methodology for the evaluation of the efficacy of the visual assessment of registration accuracy and applied it to the registration solution proposed earlier by Maurer et al. (1997). Table 2.1 summarizes the most accurate results that can be obtained by the use of fiducial markers. Data are presented together with the modality and the approach chosen for validation.

Table 2.1 Performance of Fiducial Markers Algorithms

From left to right are reported author, modality, accuracy, time, validation approach, resolution and computer technology.

Author	*Modality*	*Accuracy*	*Time*	*Validation Approach*	*Resolution*	*Computer Tech.*
Maurer et al. (1997)	X-ray CT MR	0.5 mm (500 μm)	10,000 Steps Algorithm	Phantom	512 x 512 x (28-55) 256 x 256 x (26-55)	"convent. workstation"
Wang et al. (1996)	CT-MR	0.4-0.6 mm	(Time to find markers) 87 sec (CT) 18 sec (MR)	Registr. tested accuracy of localization algor.	512 x 512 x (27-34) 256 x 256 x (20-26)	SGI Indy R 4400SC 150 MHz

Contrary to voxel-based registration algorithms, which use the full image content to find the matching transformation between images to align, accuracy of fiducial-based algorithms is largely dependent on a number of factors determined

by the fiducials themselves. These factors have been clearly outlined and a mathematical expression (Target Registration Error – TRE) that characterizes their influence on registration accuracy has been provided (Fitzpatrick et al. 1998a; Fitzpatrick and West 2001; West et al. 2001). It was demonstrated that the target registration error, which provides a more objective measure of accuracy than the fiducial registration error (FRE), depends on number of fiducials, fiducial configuration and localization error (FLE). According to Fitzpatrick et al. (1998a), an increase of number of fiducials is accompanied by a reduction of TRE if the root-mean-square distance of the reference points (fiducials) from the principal axes of the fiducial configuration, remains constant. Earlier work (Schonemann 1966) showed that the problem of fitting two three-dimensional point sets has unique solution if and only if the point sets contain at least three non-collinear points. Combining such knowledge with the work of (Fitzpatrick et al. 1998a; Fitzpatrick and West 2001; West et al. 2001) and provided that fiducials are accurately localized (Wang et al. 1996), allows fiducial marker based registration to step on a solid scientific ground.

2.1.2 Intrinsic Algorithms

2.1.2.1 Voxel Based. Registration algorithms using patient related image information maximize a similarity measure between two images. The similarity measure may apply directly to the original gray value images (van den Elsen et al. 1994; Thevenaz et al. 1998) particularly when two images of the same modality are to be registered. In multi-modality image registration, however, the physical

realities of the two images can be quite different, thus statistical similarity based registration might be preferred (Woods et al. 1992, 1993; Hajnal et al. 1995; Chen et al. 1998, 1999; Ashburner et al. 1999).

Cross-correlation is the basic statistical approach to brain image registration (Maintz et al. 1994, 1995, 1996a; van den Elsen et al. 1994). Other cost-functions were also employed: (i) Fourier-based correlation (De Castro and Morandi 1987; Eddy et al. 1996); (ii) variance intensity ratios (Hill et al. 1993, 1994; Woods et al. 1992, 1993, 1998a, 1998b); (iii) intensity differences - least square methods (Hajnal et al. 1995; Jacq and Roux 1995; Friston et al. 1995; Thevenaz et al. 1998b; Nikou et al. 1998), which work best under Gaussian noise assumptions; (iv) motion flow (Vemuri et al. 1998); (v) Bayesian statistics (Ashburner et al. 1999) and (vi) entropy (Atkinson et al. 1997).

Various optimization strategies were used in the literature: (i) steepest descent (Ashburner et al. 1999); (ii) multivariate Newton methods (Woods et al. 1998a, 1998b); (iii) quasi-Newton methods (Vemuri et al. 1998); (iv) simplex minimization (Eddy et al. 1996); (v) simulated annealing (Nikou et al. 1998); (vi) Powell method (van den Elsen et al. 1994) and (vii) Levenburg-Marquardt methods (Hajnal et al. 1995; Unser et al. 1995; Woods et al. 1998a, 1998b; Thevenaz et al. 1998b).

Best results in terms of accuracy were reported in (Friston et al. 1995; Hajnal et al. 1995; Nikou et al. 1998). It is significant to report that all of these studies have used intensity differences as cost-function to minimize in the least square sense. In term of computational time the fastest optimization procedures were: Levenburg-

Marquardt based (Thevenaz et al. 1998b), Newton based (Woods et al. 1998a, 1998b) and non-iterative (Friston et al. 1995), all of which solved 3D registration and co-registration problems. Table 2.2 reports on what was learned in term of accuracy, computational time and validation procedures for the brain imaging registration algorithms that belongs to the voxel-based classification.

Among the voxel-based classification, maximization of mutual information algorithms (MMI) has been recently proposed as new approaches for multi-modal brain image registration. The Mutual Information (MI) metric has been rigorously derived from information theory. It describes the statistical dependence of two random variables, and is suitable to determine the amount of redundant information contained in both variables. Therefore, methodologies that have been proposed apply the concept of mutual information (MI) to measure the statistical dependence between the intensities of corresponding voxels in two images.

The joint probability distribution, which is closely related to MI, can be graphically displayed as a 2D compound histogram. The optimal transformation is found, if the dispersion of significant clusters in the histogram is minimized, which coincides with MI reaching its maximum (Viola and Wells 1995; Collignon at al. 1995a, 1995b). Because no assumptions are made regarding the nature of the dependence and no limiting constraints are imposed on the image content of the modalities involved, MI is a very general and powerful criterion, allowing robust, fully automated affine registration of multi-modal images with different contrast and resolution in a variety of applications without the need for segmentation or other preprocessing (Maes et al. 1997).

Various strategies have been proposed for maximization of mutual information: (i) Powell's method (Powell 1964) used in (Hill et al. 1993, 1994; Collignon et al. 1995a, 1995b; Studholme et al. 1995; Hastreiter et al. 2000); (ii) downhill simplex (Maes et al. 1999); (iii) conjugate-gradient (Clarckson et al. 1999); (iv) multi-resolution search (Studholme et al. 1997) and (v) stochastic optimization (Wells et al. 1995, 1996).

Comparative evaluation of the optimization strategies has been carried out by Maes et al. (1999). It was found that considerable speed up, without loss of robustness, is achieved with simplex, conjugate-gradient and Levenberg-Marquardt methods. Lately, Thevenaz and Unser (2000) proposed a Levenberg-Marquardt based new optimizer for solving the problem of inter-modal image registration. Best results in term of computational time have been reported in by Thevenaz et al. (1998a) and Thevenaz and Unser (2000) with 2D MR images using Levenberg-Marquardt optimization, and by Wells et al. (1995, 1996) for CT-MR and PET-MR three-dimensional co-registration using stochastic optimization.

Image noise limits overall accuracy of automated algorithms such as MMI, and also as research shows, cost functions related to standard similarity measures are generally nonlinear, yielding many local minima in the cost function. Consequently, MMI registration algorithms must be initialized close to the optimal solution in order to obtain satisfactory solutions (Wells et al. 1995, 1996; Nikou et al. 1998). Table 2.3 shows performance of this class of algorithms. As it can be seen, mutual information approaches offer most of the time accurate registrations but they are subject to long and expensive optimization processes.

Table 2.2 Performance of Voxel Based Registration

Some algorithms had their accuracy compared to a "gold standard" (Med. Val. Ref. to GS) based on bone-implanted markers (Maurer et al. 1997).

Author	*Modality*	*Accuracy*	*Time*	*Validation Approach*	*Resolution*	*Computer Tech.*
Van den Elsen et al. (1994)	CT-MR	(Med. Val. Ref. to GS) 1.6 mm	1-2 hours	Vanderbilt medical database	512 x 512 x (28;34) 256 x 256 x (20;26)	SGI Indigo 2
West et al. (1999)	CT-MR PET-MR	(V. based) 1.8 - 2.9 mm (surface) 5.7 - 6.1 mm (V. based) 2.7 - 4.0 mm (surface) 3.9 - 4.4 mm	3 min – 2 hs.	Vanderbilt medical database	512 x 512 x (28;34) 256 x 256 x (20;26)	various
Thevenaz et al. (1998b)	PET fMRI	0.08-0.10 pixels	3 - 4 min	Controlled Motion	128 x 128 x 21	Sparc 20
Maas et al. (1997)	fMRI	(2D) -0.09° rot -0.035 pix.	1.7-7.5 sec.	phantom	128 x 128 64 x 64	HP 735/125
Nikou et al. (1998)	MR-MR MR- SPECT	< 1° rot < 1 vox. trasl.	35 min – 1 h	2D, 3D Controlled Motion	128 x 128 x128	HP 715/80
Friston et al. (1995)	fMRI PET MRI	100 μm	Order of minutes	Motion simulation	64 x 64 x 5.0 mm 256 x 256 x 118 128 x 128 x 43	Sparc
Woods et al. (1992, 1993)	PET - MRI	1.745 mm	3 - 9 min	phantom	128 x 128 x 15	Sparc IPX
Ashburner et al. (1999)	MRI	(2D) Not reported	400 sec	Simulated data	200 x 256	Sparc Ultra 2
Althof et al. (1997)	CR	(2D) 0.2 pix.	18.8 – 27.6 sec.	Comp to center of mass algor.	1760 x 2140	Sparc 10 Sun M.V.
Vemuri et al. (1998)	MRI	True Motion Error (%) 20° 1.2 2 2 (0.56) 30° 1.2 2 2 (0.5) 40° 1.2 2 2 (2.47)	1.35-9.2 min	Synthetic and real data	256 x 256 x (105 - 124)	UltraSparc 1
Maintz et al. (1997)	CT-MR PET-MR	(Val. Ref. to Fiducials) 1.1-1.7 mm 2.3 –10.6 mm	Heavily dependent on image's information content	Vanderbilt medical database	256 x 256 x 200 256 x 256 x 100 256 x 256 x128	Not reported
Woods et al. (1993) Woods et al. (1998a, 1998b)	PET-MR PET MRI	(Med. Val. Ref. to GS) 2.3 mm < 2.00 mm < 0.5 mm	20 - 30 min 26 - 323 sec. 2.8 - 13 min	Vanderbilt medical database	512 x 512 x (28;34) 256 x 256 x (20;26) 128 x 128 x 15	Sun Sparc IPX
Woods et al. (1992)	PET	< 1.745 mm	3 – 6 min	3D brain phantom	128 x 128 x 15	Sparc 2
Eddy et al. (1996)	fMRI	(2D) 0.02 - 0.3 pix.	not reported	Simulated data	128 x 128 64 x 64	Not reported
Van den Elsen et al. (1994)	CT-MRI	0.5 pix. 0.5 deg.	not reported	Comp. to marker based	256 x 256 x 250 320 x 320 x 145	Not reported
Hajnal et al. (1995)	MRI	< 0.001 pix. (tr) < 0.003 deg (rot)	2 – 4 h (reg) 5 h (resl)	Simulated data	256 x 256 x 140	Sparc 10

Table 2.3 Performance of Mutual Information Approaches

Author	*Modality*	*Accuracy*	*Time*	*Validation Approach*	*Resolution*	*Computer Tech.*
Collignon et al. (1995a, 1995b)	CT-MR PET-MR	(Med. Val. Ref. to GS) 1.5 mm 3.6 mm	10-30 min	Vanderbilt medical database	512 x 512 x (28;34) 256 x 256 x (20;26) 128 x 128 x 15	IBM RS 6000/3AT
Hill et al. (1993, 1994) and Studholme et al. (1995)	CT-MR PET-MR	(Med. Val. Ref. to GS) 1.2 mm 3.2 mm	20 min	Vanderbilt medical database	512 x 512 x (28;34) 256 x 256 x (20;26) 128 x 128 x 15	Sparc 20/61
Thevenaz et al. (1998a)	CT-MR PET-MR MR	(3D Volumes) 1.40-1.53 mm 0.9-1.7 mm (2D Image) 0.034 – 1.75 pixels	Not Reported 2.7 – 7.6 sec	Vanderbilt medical database	512 x 512 x (28;34) 256 x 256 x (20;26) 128 x 128 x 15	Not reported
Holden et al. (2000)	MRI	(Med. Val.) 78-122 μm	Not Reported	Product of 2 transf. compos.	256 x 256 x 94	Not reported
Hastreiter et al. (2000)	MRI	Not reported	19.2 min	Not reported	256 x 256 x 128	SGI Onyx 2 195 MHz
Maes et al. (1999)	CT-MR	0.5-3.1 mm	91-2,597 sec	Vanderbilt medical database	256 x 256 x 128 512 x 512 x 48	current workstations
Wells et al. (1995, 1996)	CT-MR PET-MR	$\lvert \Delta\Theta \rvert < 3.18°$ and $\lvert \Delta\Theta \rvert > 2.70°$	20 - 111 Iter. 6 min. 5,000 - 10,000 Iter.	Controlled rigid-body transf.	256 x 256 x 24 512 x 512 x 29	DEC Alpha 3000/60
Thevenaz and Unser (2000)	MRI	(2D) 0.01 pix.	16.3-17.3 sec	Random transf.	256 x 256	Sun Ultra 30
Clarkson et al. (1999)	Surface model derived from MR/CT	1.05 – 1.61 mm	Not reported	Known transf.	256 x 256 x 150 512 x 512 x 142	Not reported
Hill et al. (1997)	MRI	0.35 – 0.54 mm (tr)	20 min.	Re-imaging with subject moved	Not reported	Sparc Ultra 1-140

2.1.2.2 Feature Based. The idea behind feature-based registration algorithms is that of extracting from the brain image features that can be used for matching. Features commonly used in brain image matching are edges (Borgefors 1988) and ridges (Levin et al. 1988; Zhang et al. 1990; Hill et al. 1991; Lemoine et al. 1991; van den Elsen et al. 1992, 1993b; Turkington et al. 1993; Erickson and Jack 1993;

Li et al. 1993; Liu et al. 1994; Thirion 1994; Collignon et al. 1995c; Hogan et al. 1995; Maintz et al. 1995, 1996a, 1996b, 1997).

Because of the physics behind imaging modalities, when a brain image is depicted as intensity landscape, the skull offers valuable information content that can be used for matching purposes. Precisely, the skull forms a positive ridge in the CT image and a negative ridge in the MR image. Furthermore, since the skull is assumed to be a virtually undeformable structure, "ridge images" are well suited for registration under the rigid-body assumption. "Ridgness" extracting operators are for example derivative of Gaussian, and if they are applied to brain images, resulting feature images show a remarkable similarity that can be caught even by visual comparison. "Edgeness" images are on the other hand a measure of the local steepness of the intensity landscape. CT and MR brain "edgeness" images offer often less visual similarity than "ridgeness" images (Maintz et al. 1995, 1996a, 1996b, 1997).

Cost-functions used within the feature-based classification were: (i) correlation-based (Maintz et al. 1995, 1996b, 1997; Biswal and Hyde 1997); (ii) squared distances between surface points (Hemler et al. 1995; Meyer et al. 1995; Pennec et al. 2000); (iii) chamfer distance (Jiang et al. 1992a, 1992b); (iv) root mean-square distance (Hogan et al. 1995, 1999).

The most used optimization strategy (Maintz et al. 1995, 1996b, 1997) was the hierarchical multi-resolution Powell based method reported by van den Elsen et al. (1995). Other strategies were also employed: (i) Levenberg-Marquardt (Hemler et al. 1995) and (ii) stochastic optimization (Hill et al. 1991). Excellent results were

obtained in term of accuracy by Pennec et al. (2000) and in term of computational time by Hill et al. (1991). Table 2.4 summarizes performance characteristics of algorithms belonging to the feature-based classification.

Table 2.4 Performance of Feature Based Algorithms

Author	*Modality*	*Accuracy*	*Time*	*Validation Approach*	*Resolution*	*Computer Tech.*
Hemler et al. (1995)	CT-MR	(Med. Val. Ref. to GS) 1.4 mm	Not reported	Vanderbilt medical database	512 x 512 x (28-34) 256 x 256 x (20-26)	Not reported
Maintz et al. (1995, 1996b, 1997)	CT-MR PET-MR	(Med. Val. Ref. to GS) 5.1 mm 3.5 mm	1-12 hours 40 minutes	Vanderbilt medical database	512 x 512 x (28;34) 256 x 256 x (20;26) 128 x 128 x 15	HP 700
Jiang et al. (1992a, 1992b)	CT-MR PET-MR	(Med. Val. Ref. to GS) 5.7 mm 4.0 mm	3-20 min	Vanderbilt medical database	512 x 512 x (28;34) 256 x 256 x (20;26) 128 x 128 x 15	SGI Challenge
Biswal and Hyde (1997)	fMRI	2D 0.21 ± 0.07 pixels	Not reported	Motion simulation & phantom	64 x 64	Not reported
Hogan et al. (1999)	MR-SPECT MR-CT	2.1 – 2.5 mm 1.0 - 4.5 mm	Not Reported	Markers	0.859 x 0.859 x 1.5 mm 0.488 x 0.488 x 3 mm	"convent. workstation"
Meyer et al. (1995)	MR-PET	3 – 4 mm	Not Reported	Error vector magn. betw. point pairs	Not reported	Vistra 800 ex SC
Hogan et al. (1995)	CT-MR	0.9-8.0 mm	40 min	Fiducial markers registr.	0.859 x 0.859 x 1.5 mm 128 x 128 x 96	"convent. workstation"
Hedley et al. (1991a, 1991b)	Phantom	2D translations not reported	44 sec -14 min	Phantom	64 x 64	Sun 4
Hill et al. (1991)	MRI CT	< 2 mm	1 min	Point registr.	256 x 256 x 52	Sun Sparc 10
Maintz et al. (1996a)	CT MRI	0.02 – 4.34 mm (tr) 0.05 – 2.94 deg (rot)	Not reported	Ref. transf. obtained with markers	1 x 1 x 1 mm 0.9 x 0.9 x 1.5 mm	Not reported
Pennec et al. (2000)	CT MR	0.04 mm 0.06 mm	Not reported	Synthetic data	1 x 1 x 1.5 mm 0.97 x 0.97 x 1.5 mm	Not reported

2.1.2.3 Anatomical Landmarks Based. Anatomical landmarks have been used by several researchers as matching features within multi-modal image registration (Evans et al. 1988, 1991; Boesecke et al. 1990; Hawkes et al. 1990; Strasters et al. 1997), for which the purpose is to register two volumes by measuring different properties of an object. However, the selection of landmarks is recognized to be a

difficult problem whether done automatically or manually. For many images, this is a serious drawback because registration accuracy cannot be better than what it is achieved by the initial selection of landmarks.

Variance of intensity ratios (Woods et al. 1998a, 1998b) was used as cost function by Grachev et al. (1999) to assess inter-subject registration accuracy based on anatomical landmarks localization. Optimization strategies were: (i) Newton-based (Grachev et al. 1999; Kruggel et al. 1999); (ii) conjugate-gradient (Kruggel et al. 1999) and (iii) Powell's method (Kruggel et al. 1999).

The Newton's method was found to produce the most accurate results (Kruggel et al. 1999) within a study that compared orientation and origin of automatically generated axes, with manually generated reference alignments. Table 2.5 summarizes performance of the most successful registration algorithms based on anatomical landmarks.

Table 2.5 Performance of Anatomical Landmarks Based Algorithms

Author	*Modality*	*Accuracy*	*Time*	*Validation Approach*	*Resolution*	*Computer Tech.*
Maguire et al. (1991)	CT-MR	(Med. Val. Ref. to GS) 3.3 mm 3.6 mm	15-30 min	Vanderbilt medical database	512 x 512 x (28;34) 256 x 256 x (20;26) 128 x 128 x 15	Sparc 10/51
Grachev et al. (1999)	MR	< 1 mm for the majority of subcortical landmarks (15) out of a total of 128 landmarks	Not reported	Talairach and Tournoux (1988); Woods et al., (1998a, 1998b)	256 x 256 x 160	Not reported
Kruggel et al. (1999)	CT-MR PET-MR	1.2 ± 0.4 mm 0.8° ± 0.5°	20 minutes	Reference alignment manually generated	128 x (0.86 - 1) mm x (1.4 – 1.5) mm	"convent. workstation"

2.1.2.4 Segmentation Based, Principal Axes Based and Real Time Algorithms

Other categories that are considered in this review are: segmentation, principal axes and real time approaches. The first category is mainly characterized by application of spatial pre-processing techniques aimed to segment the brain image prior registration. The work in this area has been initiated by Pellizzari et al. (1989). A considerable performance evaluation of segmentation-based techniques (Pellizzari et al. 1989; Lemoine et al. 1994; Malandain et al. 1994a, 1994b, 1995) has been conducted within the experiment performed by West et al. (1997).

Cost-functions used within the segmentation-based algorithms were: (i) distance between 3D surfaces (Pellizzari et al. 1989; Lemoine et al. 1994) and (ii) potential field (Malandain et al. 1994a, 1994b, 1995). Optimization strategies were: (i) Powell method (Pellizzari et al. 1989; Lemoine et al. 1994) and (ii) potential minimization (Malandain et al. 1994a, 1994b, 1995). The best results were obtained by Lemoine et al. (1994) in the order of 1.6 mm of accuracy, and by Malandain et al. (1994a, 1994b, 1995) in terms of computational time, respectively for CT-MR and PET-MR registrations.

Principal axes registration is characterized by simplicity of implementation and restricted computational demand. This is because no cost-functions are computed nor iterative strategies are employed for optimization. The theory of this class of registration approaches was presented by Faber and Stokely (1988) and used to align SPECT images. It assumes that brain volumes are registered by matching their principal axes and centers of gravity. Later, this method was used also by Alpert et al. (1990), and it was confirmed that progressively coarser sampling

resolution lead to degradation of performance. Other applications were reported in (Banerjee and Toga 1994; Pavia et al. 1994).

Real time approaches are prone to correct intra-image through-plane motion. Being different from motion occurring between individual image acquisitions, which can be corrected retrospectively, intra-image motion occurs during acquisition when the anatomical section of interest moves in and out of the excited plane (Lee et al. 1996, 1998). Within the real time approaches, it is interesting to note how the impressive time of the adaptive methodology reported by Lee et al. (1996, 1998), is accompanied by high accuracy (0.5 mm), though such on-line method is unique compared to the rest of the other registration algorithms that involve data post-processing. Tables 2.6, 2.7 and 2.8 show performance of these three categories of registration approaches.

Table 2.6 Performance of Segmentation Based Algorithms

Author	*Modality*	*Accuracy*	*Time*	*Validation Approach*	*Resolution*	*Computer Tech.*
Lemoine et al. (1994)	CT-MR PET-MR	(Med. Val. Ref. to GS) 1.6 mm 4.6 mm	15 min	Vanderbilt medical database	512 x 512 x (28;34) 256 x 256 x (20;26) 128 x 128 x 15	Sun Sparc 20
Malandain et al. (1994a, 1994b, 1995)	CT-MR PET-MR	(Med. Val. Ref. to GS) 4.3 mm 4.2 mm	3 min 40 sec	Vanderbilt medical database	512 x 512 x (28;34) 256 x 256 x (20;26) 128 x 128 x 15	DEC Alpha 3000
Pellizzari et al. (1989)	CT-MR PET-MR	(Med. Val. Ref. to GS) 2.7 mm 2.9 mm	20 min	Vanderbilt medical database	512 x 512 x (28;34) 256 x 256 x (20;26) 128 x 128 x 15	SGI Indigo 2

Table 2.7 Performance of a Real Time Algorithm

Author	*Modality*	*Accuracy*	*Time*	*Validation Approach*	*Resolution*	*Computer Tech.*
Lee et al. (1996, 1998)	fMRI	0.5 mm in the range ± 0.36 ± 12 deg	100 msec	Computer controlled Phantom	256 x 256 x (25;51)	Sparc 5

Table 2.8 Performance of Principal Axes Based Algorithms

Author	*Modality*	*Accuracy*	*Time*	*Validation Approach*	*Resolution*	*Computer Tech.*
Faber and Stokely (1988)	SPECT	0.39 voxels (x) 0.08 voxels (y) 0.22 voxels (z)	Order of seconds	Simulated data	64 x 64 x 64 32 x 32 x 32	"convent. workstation"
Alpert et al. (1990)	PET MR	1 mm	2 min.	Simulated data	256 x 256 x 63 128 x 128 x 12 mm	DEC VAX 11/780

2.1.3 Findings

As far as accuracy, computational time and validation approaches, for registration and co-registration algorithms, findings can be summarized as follow:

(i) Comparison between data reported in tables 2.2, 2.3 (algorithms that use relationships between voxel's intensity) and 2.4 (feature-based algorithms), 2.5 (anatomical landmarks algorithms), 2.6 (segmentation-based), suggests that voxel-based algorithms, including those based on the maximization of mutual information (MMI), allow higher level of accuracy in brain rigid registration than feature, anatomical landmark and segmentation based algorithms.

(ii) Though data reported in tables 2.6 and 2.5 suggests that anatomical landmarks based algorithms allow for higher level of accuracy than feature-based algorithms, for both classes of algorithms accuracy is strongly dependent on the localization precision of either features or landmarks.

(iii) Comparison of data reported in tables 2.1 and 2.8 suggests that fiducial markers algorithms allow for higher level of accuracy than principal axes methods. However, accuracy of the former category is strongly dependent on correct localization of markers into the brain images.

(iv) For the voxel-based classification (other than MMI), cost-functions accompanied by best accuracy of within-modality registration were those based on intensity differences to be minimized in the least square sense (Friston et al. 1995; Hajnal et al. 1995; Nikou et al. 1998).

(v) Optimization strategies accompanied by shortest computational time were: Levenburg-Marquardt (Thevenaz et al. 1998b; Thevenaz and Unser 2000), used for MMI in order to solve 2D registrations; stochastic optimization (Hill et al. 1991; Wells et al. 1995, 1996), used respectively for feature-based and MMI algorithms and Newton's method (Kruggel et al. 1999; Woods et al. 1998a, 1998b), used respectively for anatomical landmark and voxel-based algorithms.

(vi) Most commonly adopted validation approaches were brain images with controlled motion and brain images of the Vanderbilt medical database.

2.2 A Framework for Brain Image Rigid Registration

2.2.1 Mono-modal Applications

2.2.1.1 Computer Tomography (CT). Registrations of CT scans were reported in (Levin et al. 1988; Hill et al. 1991; Lemoine et al. 1991; Maintz et al. 1996a; Althof et al. 1997; Pennec et al. 2000). The best results in terms of accuracy were

obtained by Maurer et al. (1997) with fiducial markers. Validation techniques used for CT registrations were reference points (Hill et al. 1991; Maintz et al. 1996a), phantom (Maurer et al. 1997) and synthetic data (Pennec et al. 2000).

2.2.1.2 Magnetic Resonance (MR). Several studies performed MR mono-modal registrations (Levin et al. 1988; Hedley et al. 1991a, 1991b; Hill et al. 1991; Lemoine et al. 1991; Rosseau et al. 1991; Jiang et al. 1992a, 1992b; Mandava et al. 1992; Li et al. 1993; Morris et al. 1993; Turkington et al. 1993; Maurer et al. 1993, 1994, 1995, 1996, 1997; Collignon et al. 1995a, 1995b; Hajnal et al. 1995; Friston et al. 1995; Maintz et al. 1995; Atkinson et al. 1997; Rutherford et al. 1997; Lemieux et al. 1998; Nikou et al. 1998; Vemuri et. al. 1998; Chen et al. 1998, 1999; Ashburner et al. 1999; Grachev et al. 1999; Kruggel and von Cramen 1999; Holden et al. 2000; Hastreiter et. al. 2000; Pennec et al. 2000).

Also, two different approaches in MRI inter-subject registration were disseminated to the research community: (i) the piecewise linear Talaraich stereotaxic transformation method (Talairach. and Tournoux 1988) and (ii) the non-linear transformation method AIR of Woods et al. (1992, 1993, 1998a, 1998b). It was reported that accurate registration (0.5 mm) for MR data is obtainable with bone-implanted markers (Maurer et al. 1997). However, voxel-based methods reported by Friston et al. (1995) and Holden et al. (2000) seem to obtain even better accuracy.

Computational time to perform MR registration is significantly small (order of sec.) for 2D applications (Thevenaz et al. 1998a; Thevenaz and Unser 2000) but can also increase dramatically up to several hours (Hajnal et al. 1995) for 3D

applications. Various validation approaches were used for MR registration. Among those were: phantom (Maurer et al. 1997), brain images with known motion (Hajnal et al. 1995; Thevenaz and Unser 2000) and subject re-imaging (Hill et al. 1997).

2.2.1.3 Positron Emission Tomography (PET). The two most effective approaches to perform registration of PET images were introduced by Friston et al. (1991a, 1991b, 1995) and Woods et al. (1992, 1993). Recently, Unser et al. (1995) described a registration algorithm that uses the concept of multi-resolution analysis, which consists of representing a signal by a sequence of fine-to-coarse continuous functions providing approximations at various resolutions.

Other approaches can be found in (Levin et al. 1988; Alpert et al. 1990; Turkington et al. 1993; Thevenaz et al. 1998). Based on the data collected in this survey, processing time for PET registrations is usually in the order of minutes (Friston et al. 1995; Thevenaz et al. 1998b; Woods et al. 1998a, 1998b), and validation approaches have used both controlled motion simulations and brain images of the Vanderbilt medical database.

2.2.1.4 Single Photon Emission Computed Tomography (SPECT). This type of registration was performed by Faber and Stokely (1988) to validate principal axes transformation methods, and Maintz et al. (1997) to validate feature-based registration algorithms. Other SPECT registrations were reported in (Turkington et al. 1993; Pavia et al. 1994; Kybic et al. 2000; Kybic and Unser 2000). Both in terms of accuracy and processing time, the work of Faber and Stokely (1998)

remains the one offering the best performance. Simulated data were used to validate the algorithm.

2.2.1.5 Functional Magnetic Resonance (fMR). Various algorithms have been proposed to correct head-motion related artifacts in fMRI (Eddy et al. 1996; Cox 1996; Maas et al. 1997; Biswal and Hyde 1997; Lee et al. 1996, 1998). Recently, Thevenaz et al. (1998) described a voxel-based technique and Ciulla and Deek (2001a) reported an application of a principal-axes/fiducial-markers approach. Friston et al. (1995) developed the Statistical Parametric Mapping (SPM), a software package that can be used for both alignment and analysis of fMRI time series. To date, this application seems the most accurate (100μm) and also is relatively fast. Validation approaches for fMRI registration were phantom (Maas et al. 1997) and controlled motion simulation (Friston et al. 1995; Eddy et al. 1996; Biswal and Hyde 1997; Ciulla and Deek 2001).

2.2.2 Multi-modal Applications

2.2.2.1 Computer Tomography – Magnetic Resonance. Many studies have performed CT-MR registrations (Maguire et al. 1991; Jiang et al. 1992a, 1992b; Hill et al. 1993, 1994; Hill and Hawkes 1994; Lemoine et al. 1994; Malandain et al. 1994a, 1994b, 1995; van den Elsen et al. 1994; Hemler et al. 1995; Hogan et al. 1996; Collignon et al. 1995a; Viola and Wells 1995; Wang et al. 1996; Wells et al. 1995, 1996; Maintz et al. 1994, 1996a, 1996b, 1997, 1998; Studholme et al. 1996, 1997; Thevenaz and Unser 1998; Clarkson et al. 1999; Maes et al. 1999; Panigrahy et al. 2000). CT-MR highly accurate registration of head volumes were obtained by

van den Elsen (1994) with a voxel-based algorithm, by Wang et al. (1996) and Maurer et al. (1997) using implantable markers. Computational time varied from minutes (Pellizzari et al. 1989; Maguire et al. 1991; Lemoine et al. 1994; Malandain et al. 1994a, 1994b, 1995; Collignon et al. 1995a, 1995b; Hill et al. 1993, 1994; Studholme et al. 1995; Wells et al. 1995, 1996; Hogan et al. 1995; Kruggel et al. 1999), up to hours (van den Elsen et al. 1994; Maintz et al. 1995, 1996b, 1997; Maes et al. 1999). The most used validation approach for this type of registration was the Vanderbilt medical database.

2.2.2.2 Computer Tomography – Positron Emission Tomography. Alpert et al. (1990) performed rigid 3-D transformations in order to register CT to PET using the image's principal axes and the center of gravity, with simulated data used for validation. Accuracy was reported to be 1 mm. Affine registration was also obtained by Maguire et al. (1991).

2.2.2.3 Positron Emission Tomography – Magnetic Resonance. Registrations that use various algorithms can be found in (Pellizzari et al. 1989; Lavalle et al. 1991; Maguire et al. 1991, Mangin et al. 1992; Jiang et al. 1992a, 1992b; van den Elsen et al. 1992; Li et al. 1993; Collignon et al. 1995a; Wells et al. 1995, 1996; Maintz et al. 1995, 1996a, 1997; West et al. 1997; Li et al. 1993; Lemoine et al. 1994; Meyer et al. 1995; Hemler et al. 1995; Hill et al. 1993, 1994; Hill and Hawks 1994; Studholme et al. 1996, 1997; Malandain et al. 1994a, 1994b, 1995; Viola and Wells 1995; Wells et al. 1995, 1996).

Woods et al. (1992, 1993, 1998a, 1998b) described a registration technique, which calculates the ratio of one image to the other on a pixel-to-pixel basis and then

iteratively moves the images relative to one another to minimize the variance of this ratio across pixels. This work remains the most effective algorithm for PET-MR registration. It offers accuracy of 1.7-2.3 mm, demands computational time in the order of minutes and it has been validated with the Vanderbilt medical database. Other studies (Wells et al. 1995, 1996) used controlled motion to validate their algorithm.

2.2.2.4 Single Photon Emission Computed Tomography – Magnetic Resonance. Maguire et al. (1991) used user-identified landmarks and user-identified external markers to perform affine SPECT-MR registration by locally optimizing cross-correlation. Jiang et al. (1992b) used multi-resolution chamfer matching on semi-automatically segmented surfaces. Hogan et al. (1995, 1999) used also feature-based algorithms and used fiducial markers as validation methodology. Nikou et al. (1998) performed the most promising SPECT-MR registration in term of accuracy with a voxel-based algorithm that required processing time up to one hour and used controlled motion simulations to validate their work.

2.2.2.5 Functional Magnetic Resonance – Magnetic Resonance. Kybic et al. (1999) proposed to register the distorted EPI image with a corresponding geometrically correct anatomical MRI image to recover the deformation.

2.2.2.6 Magnetic Resonance - X-Ray. Betting and Feldmar (1995) registered MR to X-ray images (2-D and 3-D) by automatic extraction of contours from MR images followed by projection of them onto the X-ray plane, and minimization of

the contour distance using a variation of the iterative closest point (ICP) algorithm (Besl and McKay, 1992).

2.2.3 Findings

Registration and co-registration algorithms that are most promising in term of accuracy are visualized in the framework of figure 2.1 and summarized as follow:

(i) Registration (within-modality applications): (i.1) CT and X-ray: Maurer et al. (1997) with a fiducial markers approach of claimed accuracy of 500 μm. (i.2) SPECT: Faber and Stokely (1998) with a principal axes based algorithm having sub-voxel accuracy. (i.3) MR: Friston et al. (1995) and Holden et al. (2000) with voxel-based algorithms of claimed accuracy of respectively 100 and 78-122 μm. (i.4) fMR and PET: Friston et al. (1995) with the same voxel-based algorithm (SPM).

(ii) Co-registration (between-modality applications): (ii.1) CT - MR: van den Elsen et al. (1994) and Maurer et al. (1997) with respectively voxel-based and fiducial markers algorithms having sub-voxel accuracy. (ii.2) MR – PET: Woods et al. (1992, 1993, 1998a, 1998b) with a voxel based algorithm of accuracy within 1.7 and 2.3 mm. (ii.3) fMR – MR: Kybic et al. (1999) with a voxel-based algorithm. (ii.4) MR – X-ray: Betting and Feldmar (1995) with a feature-based algorithm. (ii.5) CT - PET: Alpert et al. (1990) with a principal axes algorithm of claimed accuracy of 1 mm.

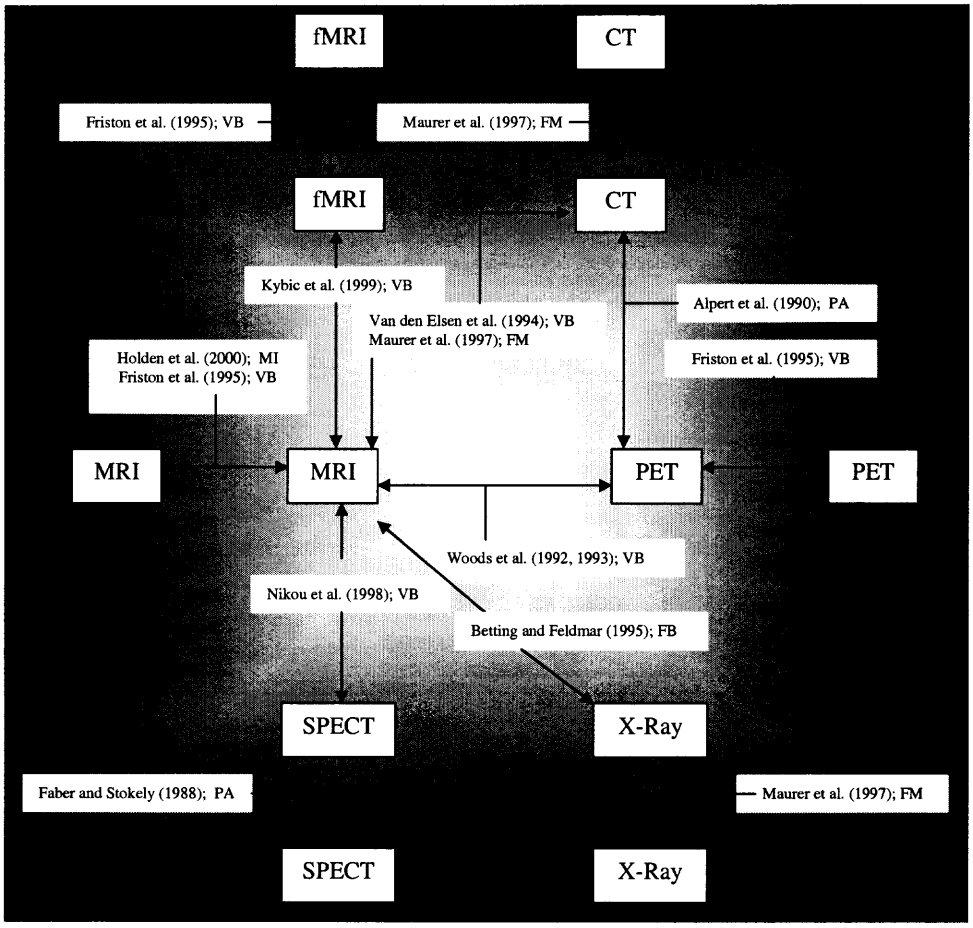

Figure 2.1 A Framework for Brain Image Rigid Registration

For each modality are shown best registration (within-modality) and co-registration (between-modalities) algorithms in term of accuracy. Authors are indicated together with the algorithm typology (FM: fiducial markers; MI: mutual information; VB: voxel-based; FB: feature-based; PA: principal axes).

CHAPTER 3

SCIENTIFIC METHODOLOGY

3.1 Motivation

This work starts from the fact recognized in literature, that fiducial markers technique for brain image registration present a clear disadvantage. If the fiducial markers are affixed to the subject's head, then either for single or multiple recording sessions they can be localized at different positions, and this completely obscures the assumption on the basis of which the methodology works. Precisely, when markers are affixed and a single recording session is performed on a single subject, because of the skin movement they will be imaged at different locations. If, on the other hand, there are multiple recording sessions on a single subject, then it is very difficult, almost impossible, to place the markers at the same location on the subject's head. Maurer et al. (1997) reported methodologies that rely on markers that are screwed on the subject's head.

However, this solution even offering high accuracy is not always the most practical. This is for two reasons. First, it is unreal to screw markers in case of brain imaging that is done for research purpose. Second, this methodology needs to have an automatic algorithm that allow markers localization into the brain images such that any registration algorithms that is applied, know the marker location such to perform reliably and precisely image matching. Another question of interest in the development of fiducial markers techniques is the determination of the sufficient number of markers. The question steam from the fact that any registration

algorithms that for purpose of image matching uses fiducial markers, need to have them in a sufficient number such that a head coordinate system can be built.

The other methodology that was incorporated in the automatic algorithm is that of the moment-based/principal-axes transformation method. The advantage offered by this methodology is that of simplicity of implementation and speed of computation. The disadvantage is that it requires prior segmentation of brain images. Segmentation can be obtained simply by roughly setting a threshold into the brain image. But in such a case, results of the registration algorithm would not be robust, since changing threshold of segmentation would also change registration performance.

It is then preferable to apply an algorithm that it is based on principal axes but does not require threshold segmentation of brain images. Also, it is highly valuable to devise a registration algorithm that is computationally fast. Some current state of the art algorithms based on maximization of mutual information require long and expensive optimization processes, and also that the algorithm is initialized close to the desired solution. Predictably, in the near future, resolution of brain images will increase due to the increasing need, both in research and diagnostic applications, to extract more information about the functional activation of the human brain during task performance. Finer images resolution would certainly facilitate the study of brain functions, also make available to the physician finer detail about information processing in the human brain. Thus, even though speed of computation will increase, it is fare to assume that registration algorithms that are dependent on optimization processes would not always be practical, considering the massive

computation they demand. In view of such possibility, algorithms like the one that has been developed in this dissertation, could serve to the purpose of finding the trade-off between accuracy and speed of computation.

3.2 Research Methods

This chapter explains in detail what the present research consisted of, what are the advantages of the computer based system that has been developed and how it advances the present state of the art in the field of fMRI registration. This research aimed to merge together two state of the art methodologies for brain image rigid registration. They are: (i) fiducial markers and (ii) moment-based/principal-axes. An automatic technique has been developed that incorporates the two methodologies such to obtain a new method with the advantages of the two and to find a trade-off between accuracy and computational demand of a registration algorithm. The new technique has been implemented into a fully automatic computer based system provided with a graphical user interface. The use of a simulated dataset to test the algorithm furnished a "proof of concept" of the efficacy of the alignment program.

Testing has been extended to real data such to provide accuracy figures that are realistic in the real world setting. Thus, this research required efforts under both scientific and technology domains. Science was required to understand characterize and combine the two methodologies reported in literature, such to derive the new one: AUTOALIGN. Also, in devising new mathematical formulations that give solution to issues related to the implementation of ideas that constitute the new

methodology. Technological effort was required to implement into software and test all of the procedures of which the method is composed of. This required mastery and command of computer programming languages such as Matlab, OpenGL and ANSI C.

3.3 Scientific Approach

It is now explained in detail what the present research consisted of. First of all, this research has developed software tools that can be used to visualize the content of specific files containing brain images acquired through functional Magnetic Resonance Imaging (fMRI). To visualize the images is helpful for two simple reasons. First is that through visualization, a considerable amount of information is provided to the physician. In the specific case of image registration, it is also possible for the physician to directly inspect the image and see (in some cases) the head motion present into them. Second, after registration is desirable to visually inspect the images such to check for registration accuracy. OpenGL was used to write software routines that allow visualizing the content of files containing brain images obtained with fMRI. OpenGL is a sub-class of libraries of the C language, specially designed for graphical applications.

Since this research handled three dimensional brain images, and since it is intended to develop applications that furnish the most of the available visual information, the human brain has been visualized in three 2D composite views. They are called: Axial, Sagittal and Coronal views. The user is allowed to slide interactively by the use of keyboard each of the brain slides in the three views.

Also, the computer-based system (AUTOALIGN) has been implemented on an SGI Origin 2400, which is provided with high hardware acceleration for graphic renderings. Thus, both high rendering and computational speed feature the graphical routines.

The software system is provided with a Graphical User Interface (GUI), which code is written in Matlab. There are several reasons why Matlab is preferred to other software environments for the development of the GUI. Matlab offers plenty of flexibility combined with features that ease operations like calling programs and passing parameters to them. Also, Matlab is preferable because each of the other programs written either in ANSI C or OpenGL is completely independent from the GUI. What is visible to the user is the GUI, through which, some basic parameters relevant to the format of the brain images to process, are given as input to both ANSI C and OpenGL programs. These programs are called through simple UNIX commands that are easily interpreted by Matlab. Independence between GUI and programs is a feature that is more difficult to achieve with software environments like Visual C++.

Together with software for visualization, this research has developed a novel registration algorithm, which, as anticipated earlier was obtained by merging together two state of the art methodologies and also incorporated advantages of the two. The first question that needs to be addressed is then: "how many fiducial markers are needed in order to build a head coordinate system for purpose of image matching." The answer this research furnishes is: "three fiducial markers are enough". The reason is that because of the physical constraints of the human head,

which is attached to the neck, subjects can make head rotations that are less than ninety degrees. In mathematical terms, this implies that the equations of the planes of the head coordinate system can be univocally determined with sets of three equations even though there are four unknown coefficients for each plane. Detailed explanation of the solution that this research has adopted and proposed is reported later in this chapter.

Given the number of markers that are sufficient to build the head coordinate system, the first step of the algorithm is that of localizing them automatically into the brain images. This way, disadvantages of the current techniques, due to the practice of affixing or screwing markers, are overcome. The steps necessary to localize the markers are described as follow. First a gradient of the brain image is extracted. The effect of convolving the brain image with a third order gradient is that of finding the zero-crossing points into the images. This process results into the determination of the actual boundary of the subject's head. If markers would be affixed or screwed, they would be located at the boundary of the subject's head. Thus to have localized the boundary of the subject's head is equivalent to having a subset of voxels where the actual markers should be localized. In other words, it is like assuming that the fiducial markers are at the borderline of the human head.

Second, the algorithm needs to identify the principal axes of the subject's head. As reported earlier, moment-based approaches needs prior segmentation before computing the principal axes. In this research, such limitation is overcome by employing a method that weights the inertia components with the voxel's intensity. This is considered when computing the values of the tensors of inertia. The latter

are determined by extracting the eigenvectors of the symmetric inertia matrix. This is accomplished by employing the Jacobi algorithm (Demmel, 1997). A software routine that implements the Jacobi algorithm has been developed in ANSI C and incorporated into the software system. Incorporating into the computation all of the voxels of the image, also those that are not representing parts of the subject's head, allows avoiding pre-processing in term of threshold segmentation. Those pixels outside the head are likely to have intensity values almost close to zero, and thus cancel out unnecessary information.

The algorithm then uses principal axes of the human head, to localize markers at the outer surface. The following method has been used. The brain image is scanned departing from the center of gravity, along two directions identified by two of the eigenvectors of inertia. The markers are assumed to be those reference points that are found along the eigenvectors of inertia, at the intersection with the human head boundary. The latter, as mentioned earlier, is found through the extraction of the gradient of the brain image. To find the markers, the algorithm evaluates all of the voxels that are along the directions of the eigenvectors of inertia. From them, a subset of is derived that satisfies the condition of being a local maximum. A local maximum is defined as that voxel for which the intensity is greater or equal to the subsequent ten voxels on the eigenvector. From this subset of pixels, identified by the algorithm, the right (left) marker corresponds with that voxel that has the larger (smaller) index value in the volume, and at the same time its intensity is above a given threshold.

Once found the three markers are found automatically, the algorithm proceeds with the computation of the head coordinate system. This research has proposed a straightforward methodology based on computational geometry, to compute the unit vectors of the head coordinate system on the basis of only three points. The contribution of the methodology is that it was shown it is possible to find the four unknown coefficients of the mathematical equation of a plane in 3D, by only three parameters. This allowed for each plane, to write a linear system of three equations. The fourth equation is derived from the physical constraints of the human head. It is impossible for the head to make rotations larger than ninety degrees because of the fact that the head is constrained to the neck. Therefore, the physical restraint constitutes the fourth mathematical constraint that is needed.

Having the mathematical expression of the equations of the head coordinate system, any given images can be registered to a reference image by matching the axes. This implies to find the three rotation angles (pitch, roll and yaw) and the three coordinates of the center of gravity of the brain. To find the three rotation angles, computational geometry was employed. Precisely, rotation about the Z-axis can be derived computing angles between the X and Y-axes of reference and test head coordinate system. Similarly, rotation about X and Y-axes is derived computing angles between Y and Z-axes, and X and Z-axes respectively.

Once the six rigid-body parameters are found, the brain volume needs to be aligned to the reference. To do so, two basic operations are necessary. One is the application of the rigid-body transformation to the grid of voxels such to obtain a new grid. The other operation is that of the interpolation. It consists of estimation

of the voxel's intensity at the location that is placed in between the original grid. This is achieved by a simple tri-linear procedure. Similarly, also the Statistical Parametric Mapping (SPM99) adopts this interpolation scheme (Friston et al. 1995). To apply both rigid-body transformation and tri-linear interpolation, code has been developed and incorporated into the AUTOALIGN system.

To derive the algorithm as a combination of state of the art methodologies required a preliminary study aimed to implement and test the theoretical basis of our method. The preliminary study has been conducted during previous research (Ciulla 2000; Ciulla and Deek 2001a). The moment-based/principal-axes transformation method has been developed as a separate computer based system (EIGEN). It served the purpose of reproducing and testing the theory reported by Alpert et al. (1990). Investigation of the principal axes method started from a two-dimensional brain image in which controlled artificial motion has been applied. Then, implementation has been extended to the three dimensional case (Ciulla 2000). During a preliminary part of the study, the Jacobi algorithm has been reproduced and implemented into software for the extraction of the eigenvectors of a symmetric matrix. The matrix in question is that of the inertia as reported by Alpert et al. (1990). Results of the implementation of the Jacobi algorithm have been compared (Ciulla 2000) to those obtainable with the same dataset by professional software packages such as Matlab and Splus5.

During the preliminary study, a variant in the form of the tensor-based function as reported by Faber and Stokely (1988) has been developed as a separate computer based system (Ciulla 2000). This furnished the basis of development for the

construction of the inertia matrix that incorporates the pixel's intensity such to derive an alternative methodology capable to avoid pre-processing in term of segmentation. Thus, the Jacobi algorithm has been employed to extract eigenvectors from the inertia matrix derived by voxel's intensity. The final stage of the preliminary study consisted of the development and implementation of a fiducial markers based approach called ALIGN (Ciulla 2000; Ciulla and Deek 2001a). It has been demonstrated the efficiency of the mathematics explained in the method section for the determination of a head coordinate system from three fiducial markers only. The ALIGN system simulated what happens in practice when markers are affixed or screwed into the subject's head. Particularly, markers were artificially introduced into the brain volume and later selected manually by the user. This way, it was simulated what an automatic algorithm should be capable to achieve in order to localize markers into the brain volume. Results of registration have been compared across the three modalities of the preliminary study and each methodology has been provided with its separate graphical user interface. After the study was completed (Ciulla and Deek 2001a), the present research has pipelined above methodologies such to create a novel and fully automatic method (AUTOALIGN). This required development of software routines for the computation of gradient images, and an algorithm for the automatic localization of fiducial markers by means of tensors of inertia.

3.4 Technological Effort

AUTOALIGN system is organized in two main panels: (i) Two fMRI Scans and (ii) All fMRI Scans. The first is a section devoted to visualization and alignment of a couple of fMRI volumes. This panel requires more manual interaction of the user with the graphical interface. The user is able to choose reference and test volumes, set the required pixel's resolution and size, and perform alignment by activating four different programs. They are: (i) visualization and localization of markers; (ii) computation of the head coordinate system; (iii) computation of alignment parameters and (iv) interpolation / re-display of brain volumes. The second panel of the computer-based system has been developed for the alignment of entire fMRI time series. This panel requires minimal user interaction so that a set of brain volumes can be aligned to the reference, by means of a program that is mostly independent from the user. The options of the program are the same as those of the first section of the system. The four programs mentioned above are incorporated in a larger and single routine, and there is no visual display during computation. At the end of the process, the user can chose which image to visualize, or can even see the difference image between the reference and the test volumes, such to check if motion artifacts are still present even after alignment. With respect to the Automatic Image Registration (AIR3.08), AUTOALIGN offers the user non-indifferent functionality in term of capability to automatically process an entire fMRI time series. Similarly, the Statistical Parametric Mapping offers such functionality.

3.5 Testing and Validation

The approach that this research adopted in order to test performance of AUTOALIGN software system is explained as follow. The idea used to test the alignment algorithm bases itself on brain image volumes in which, a simulated controlled and artificial motion has been introduced. Therefore, this research has developed also software routines that can be used to simulate motion in sample fMRI images. This was accomplished (Ciulla 2000) developing another computer based system capable to compute the six rigid-body motion parameters on the basis of the user request (ROTRA) and use them to calculate the new grid coordinates of the new artificial volume. ROTRA (Ciulla 2000) has an interface similar to the other GUIs developed to implement the methods and serve as theoretical basis for the development of AUTOALIGN system.

Having capability to produce artificial volumes for which head motion is known a-priori, leads to accuracy in evaluation of the registration performances of the algorithm. The deviation of the actual performance from the desired performance is then computed. The desired performance is known because of the simulations. Also, algorithm's performance was compared to that of the Statistical Parametric Mapping (SPM99) and the Automatic Image Registration (AIR3.08). They are software packages with established accuracy and currently used by the research community. With respect to those, AUTOALIGN is capable to express registration accuracy estimation also in cases in which the motion is not known. Volumes with simulated motion serve the purpose of estimating the accuracy of the system.

Later, validation has been extended to brain images for which the motion is not known. Particularly, AUTOALIGN performance has been investigated with 64 (x res.) x 64 (y res.) x 21 (z res.) and 64 (x res.) x 64 (y res.) x 16 (z res.) fMRI time series. For those cases in which the head motion is not known, AUTOALIGN performs automatically estimation of alignment accuracy. This is achieved as follow; having for both reference and test volume, after alignment, the position of the fiducial markers with respect to the origin of the head coordinate system, it is possible by means of 3D Euclidean distances to compute misalignment values at the markers' location. Misalignment values consist of the location mismatch between markers of the two volumes, after the registration has been done. Markers are placed farthest away from the centroid of alignment because they are localized at the outer-most surface of the head. Theoretically, after registration, if the mismatch is not zero, then a misalignment exists and it is the measure of the maximum misalignment. This is so because the maximum misalignment is measured at the points that are farthest away from the centroid of alignment (Fitzpatrick et al., 1998).

3.6 Contributions

The main advantage of AUTOALIGN software system is that of searching for a trade-off between accuracy and computational time for the problem of alignment of fMRI time series. This was accomplished by merging two state of the art methodologies. To achieve this purpose, novel solutions were given to research

questions posed in literature and thus, the following contributions were given to advance the state of the art.

(i) A new methodology for fMRI alignment that is accurate and fast (independent on optimization processes) at the same time. This constitutes a non indifferent advantage in cases of large brain volumes (high resolution). AUTOALIGN performs well in terms of accuracy with low resolutions (64 x 64 x 16) brain volumes.

(ii) To have shown mathematically that only three points are sufficient to build a coordinate system in the case of the human head. The method constitutes a particular case of the larger mathematical framework on point-based registration made by (Fitzpatrick et al. 1998a). An algorithm was derived and implemented in software by the ANSI C programming language.

(iii) An automatic and reliable approach to localize reference points into the brain images. This overcomes the limitation of affixing/screwing fiducials (Maurer et al. 1997). For this issue this research has furnished both theoretical and practical solutions. It is proposed that fiducial markers can be automatically localized into brain images by means of tensors of inertia. This overcomes limitations that arise if markers are either affixed or screwed to the patient's head. Implementation has also involved us into the formulation of a procedure capable to select markers between subsets of voxels located along the directions identified by the tensors of inertia.

(iv) A novel solution to the problem of reliably determining the axis of minor resolution (64 x 64 x 21) for Moment-based registration. This overcomes the

limitation posed by Moment-Based approaches (Faber and Stokely, 1988) for brain volumes with coarse resolution.

(v) To have demonstrated though AUTOALIGN the feasibility of fiducial based registration in fMRI. This is a novelty in the field.

(vi) To have shown how to avoid threshold segmentation of brain images. In this regard, it is proposed here that voxel's intensities are taken into account in the computation of the inertia matrix of the brain images. Precisely, by weighting the voxel's coordinates with the intensity, all of those constituting the brain image can be included in the computation, such that those outside the brain will cancel themselves out because of their negligible intensity values.

(vi) To have shown how to keep AUTOALIGN algorithm fast such that, for fine resolutions, computation time does not increase dramatically. The answer to this question is in devising a registration algorithm which computational time is independent from different degrees of translation and rotation. Also, it is recommendable to use an interpolation scheme like the tri-liner function such to achieve sub-voxel accuracy in intensity correction and at the same time an acceptable computational demand.

3.7 Head Motion Simulation

Parameters that describe the six degrees of freedom of the head in a 3D volume are three angles: pitch (rotation about the X-axis), roll (rotation about the Y-axis), yaw (rotation about the Z-axis); and three coordinates x, y and z of the origin of the head coordinate system. In all of the cases: principal axes transformation method,

tensor-based method and 3-fiducial markers method; the coordinates of the origin of the head coordinate system are those of the center of mass of the brain.

Either given eigenvectors or tensors of the symmetric inertia matrix or given the unit vectors of the head coordinate system, for both reference volume and test volume, it is possible to compute the three angles (pitch, yaw and roll) applying the following procedure. The yaw angle can be found on the basis of the angle between X-axes and Y-axes (on the XY plane) of the head coordinate system. Particularly, since both eigenvectors and unit vectors are orthogonal, angles between X-axes and between Y-axes will be averaged. Similarly, pitch and roll angles can be found averaging respectively angles between Y-axes and Z-axes, and X-axes and Z-axes. Once the three angles (pitch, yaw and roll) and the three coordinates (x, y and z) of the origin of the head coordinate system are known, the rigid-body transformation can be computed and applied to the test volume with respect to the center of gravity of the brain (origin of head coordinate system).

3.8 Head Coordinate System of the 3-Fiducial Markers Technique

This method is presented for two reasons: One is that, the method itself is simple because based only on 3-fiduciary markers, which under some assumptions, are enough to cover the six degree of freedom in a 3D volume. The other is that, such a method is applicable to cross-modality registration (Maurer et al. 1997). The method requires that the origin be at the midpoint between the ear's markers. The construction of the head coordinate system takes the following form. Let $P_1 = (x_1, y_1, z_1)$, $P_2 = (x_2, y_2, z_2)$ and $P_3 = (x_3, y_3, z_3)$ be respectively the left ear, right ear and

nose fiduciary markers. Let $A_{XY} * x + B_{XY} * y + C_{XY} * z + D_{XY} = 0$ be the equation of plane XY as passing through the three fiduciary points. The values of the coefficients of plane XY can be computed as:

$$A_{XY} = \begin{vmatrix} (y_2 - y_1) & (z_2 - z_1) \\ (y_3 - y_1) & (z_3 - z_1) \end{vmatrix} \quad (3.1)$$

$$B_{XY} = - \begin{vmatrix} (x_2 - x_1) & (z_2 - z_1) \\ (x_3 - x_1) & (z_3 - z_1) \end{vmatrix} \quad (3.2)$$

$$C_{XY} = \begin{vmatrix} (x_2 - x_1) & (y_2 - y_1) \\ (x_3 - x_1) & (y_3 - y_1) \end{vmatrix} \quad (3.3)$$

$$D_{XY} = - (y_1 * B_{XY}) - (x_1 * A_{XY}) - (z_1 * C_{XY}) \quad (3.4)$$

Where the mid-point between the ears is stored as the origin $P_0 = (x_0, y_0, z_0)$ of the head coordinate system. Let $A_{ZY} * x + B_{ZY} * y + C_{ZY} * z + D_{ZY} = 0$ be the equation of plane ZY found by the constraints that it must be perpendicular to plane XY and it must pass through the origin P_0 of the coordinate system and through the nose P_3. Let $A_{ZX} * x + B_{ZX} * y + C_{ZX} * z + D_{ZX} = 0$ be the equation of plane ZX found by the constraints that it must be perpendicular to plane XY and plane ZY and at the same time must pass through the origin P_0 of the coordinate system. The likely assumption that the human brain cannot make rotations bigger than 90-degrees ensures that one of the coefficients of both planes ZY and ZX is equal to one. The constraints ensure a unique solution of the problem. This amounts to demanding

that the axis of the coordinate system cannot make an angle bigger than 90-degrees with the axis of the fixed coordinate system. Therefore the problem of finding a plane can be solved with three constraints even though there are four unknown coefficients. The values of the coefficients of plane ZY can be computed as follows:

$$A_{ZY} = 1 \tag{3.5}$$

$$B_{ZY} = delta_1 / delta \tag{3.6}$$

$$C_{ZY} = delta_2 / delta \tag{3.7}$$

$$D_{ZY} = delta_3 / delta \tag{3.8}$$

Where:

$$delta = B_{XY} * det_1 - C_{XY} * det_2 \tag{3.9}$$

$$delta_1 = -A_{XY} * det_1 - C_{XY} * det_3 \tag{3.10}$$

$$delta_2 = B_{XY} * det_3 - A_{XY} * det_2 \tag{3.11}$$

$$delta_3 = B_{XY} * det_4 + C_{XY} * det_5 - A_{XY} * det_6 \tag{3.12}$$

$$det_1 = \begin{vmatrix} z_0 & 1 \\ z_3 & 1 \end{vmatrix} \tag{3.13}$$

$$det_2 = \begin{vmatrix} y_0 & 1 \\ y_3 & 1 \end{vmatrix} \tag{3.14}$$

$$det_3 = \begin{vmatrix} -x_0 & 1 \\ -x_3 & 1 \end{vmatrix} \quad (3.15)$$

$$det_4 = \begin{vmatrix} z_0 & -x_0 \\ z_3 & -x_3 \end{vmatrix} \quad (3.16)$$

$$det_5 = \begin{vmatrix} y_0 & -x_0 \\ y_3 & -x_3 \end{vmatrix} \quad (3.17)$$

$$det_6 = \begin{vmatrix} y_0 & z_0 \\ y_3 & z_3 \end{vmatrix} \quad (3.18)$$

The values of the coefficients of plane ZX can be computed as follows:

$$A_{ZX} = delta_1 / delta \quad (3.19)$$

$$B_{ZX} = 1 \quad (3.20)$$

$$C_{ZX} = delta_2 / delta \quad (3.21)$$

$$D_{ZX} = delta_3 / delta \quad (3.22)$$

Where:

$$delta = \begin{vmatrix} A_{XY} & C_{XY} \\ A_{ZY} & C_{ZY} \end{vmatrix} \quad (3.23)$$

$$delta_1 = \begin{vmatrix} -B_{XY} & C_{XY} \\ -B_{ZY} & C_{ZY} \end{vmatrix} \quad (3.24)$$

$$delta_2 = \begin{vmatrix} A_{XY} & -B_{XY} \\ A_{ZY} & -B_{ZY} \end{vmatrix} \quad (3.25)$$

$$delta_3 = x_0 * det_1 - z_0 * det_2 - y_0 * det_3 \quad (3.26)$$

$$det_1 = \begin{vmatrix} C_{XY} & -B_{XY} \\ C_{ZY} & -B_{ZY} \end{vmatrix} \quad (3.27)$$

$$det_2 = \begin{vmatrix} A_{XY} & -B_{XY} \\ A_{ZY} & -B_{ZY} \end{vmatrix} \quad (3.28)$$

$$det_3 = \begin{vmatrix} A_{XY} & C_{XY} \\ A_{ZY} & C_{ZY} \end{vmatrix} \quad (3.29)$$

3.9 The AUTOALIGN Technique

The principal axes transformation method (Alpert et al. 1990) relies on the use of a threshold T to select the pixels above a given arbitrary intensity. The use of the threshold aims to select only those pixels relevant to the brain for the computation of the inertia matrix. This implies that changing the value of the threshold would accordingly change the alignment performance of the method, since the numerical values of the symmetric inertia matrix are computed on the basis of the coordinates of the pixels above the arbitrary threshold. To make the method more robust, a technique was utilized that cancels out the pixels outside the brain weighting the pixel coordinates with their intensities. The formulas used are reported as follows:

$$I_{xx} = [\ \textstyle\sum_i\ (\ x_i - \alpha\ )^2 * f\ (p_i)\ /\ \sum_i f\ (p_i)\ ] \qquad (3.30)$$

$$I_{yy} = [\ \textstyle\sum_i\ (\ y_i - \beta\ )^2 * f\ (p_i)\ /\ \sum_i f\ (p_i)\ ] \qquad (3.31)$$

$$I_{zz} = [\ \textstyle\sum_i\ (\ z_i - \gamma\ )^2 * f\ (p_i)\ /\ \sum_i f\ (p_i)\ ] \qquad (3.32)$$

$$I_{xy} = I_{yx} = [\ \textstyle\sum_i\ (\ x_i - \alpha\ ) * (\ y_i - \beta\ ) * f\ (p_i)\ /\ \sum_i f\ (p_i)\ ] \qquad (3.33)$$

$$I_{yz} = I_{zy} = [\ \textstyle\sum_i\ (\ y_i - \beta\ ) * (\ z_i - \gamma\ ) * f\ (p_i)\ /\ \sum_i f\ (p_i)\ ] \qquad (3.34)$$

$$I_{zx} = I_{xz} = [\ \textstyle\sum_i\ (\ z_i - \gamma\ ) * (\ x_i - \alpha\ ) * f\ (p_i)\ /\ \sum_i f\ (p_i)\ ] \qquad (3.35)$$

Where α, β and γ are respectively the values of x, y and z coordinates of the center of gravity of the brain; and $f\ (p_i)$ is the value of the i^{th} pixel's intensity.

Any fiduciary markers methods, to become fully automatic, require that an algorithm accurately localizes markers and that their shape and consistency is such to be detected by the imaging modality. Therefore, considering that there is

evidence that marker techniques offer accurate registration results (Maurer et al. 1997) we devised an algorithm that, on the basis of the directions identified by the principal axes transformation method finds automatically three points on the subject's head that can be adopted as markers. As we have seen in the previous section, three markers are enough to determine a coordinate system by which the position of the head can be uniquely featured into the scanning volume.

Thus, the method to localize the markers works in four steps: *(i)* the symmetric inertia matrix is obtained weighting the voxel's coordinates with their intensity; *(ii)* the eigenvectors of the inertia matrix are computed and identify the principal axes of the brain; *(iii)* A third order gradient of the image is computed in order to identify the borderline between the outer surface of the head and the pixels outside; *(iv)* Departing from the center of gravity of the head, the image is scanned along the X and Y directions identified by the principal axes in order to find the markers at the intersection between the two principal axes and the outer surface of the head. Two markers at the right and left ear locations are found scanning along the X direction. The marker at the nose location is found scanning along the Y direction.

Extracting the gradient of the image furnished the brain's edges and made possible to find the markers at the borderline between its outer surface and the pixels outside the head. To find the markers at the intersection of the head's outer surface and the two principal axes is equivalent to the practice of affixing them to the subject's head but present the advantage of accurate and automatic localization.

3.10 AUTOALIGN Registration Algorithm

3.10.1 Extraction of the Tensors of Inertia

Formulas used to extract the tensors of inertia of the brain volume were given earlier (Ciulla and Deek 2001a). The Jacobi-algorithm (Demmel 1997) allowed computing the eigenvectors (e_x, f_x, g_x; e_y, f_y, g_y; e_z, f_z, g_z) of the inertia matrix:

$$\Omega = \begin{vmatrix} I_{xx} & I_{xy} & I_{xz} \\ I_{yx} & I_{yy} & I_{yz} \\ I_{zx} & I_{zy} & I_{zz} \end{vmatrix} \tag{3.36}$$

3.10.2 Localization of Fiducial Markers

Given the physical constraints of the subject's head, three fiducial markers are sufficient to build a head coordinate system. Since affixing or screwing markers might be unpractical, it has been shown that fiducial markers can be found on the directions of two of the tensors of inertia of the brain volume (Ciulla and Deek 2001a). To localize the three fiducial markers, the algorithm performs the following steps: (i) the gradient of the brain image is computed in order to identify the outermost surface of the subject's head. The X and Y components of the gradient, respectively Δ_x and Δ_y, are computed convolving the brain image Γ with:

$$G_x = \begin{vmatrix} -1.0 & -2.0 & -1.0 \\ 0.0 & 0.0 & 0.0 \\ 1.0 & 2.0 & 1.0 \end{vmatrix} \tag{3.37}$$

$$G_y = \begin{vmatrix} 1.0 & 0.0 & -1.0 \\ 2.0 & 0.0 & -2.0 \\ 1.0 & 0.0 & -1.0 \end{vmatrix} \quad (3.38)$$

The gradient image is obtained by:

$$G = [(\Delta_x * \Delta_x) + (\Delta_y * \Delta_y)]^{1/2} \quad (3.39)$$

$$\Delta_x = G_x \times \Gamma \quad (3.40)$$

$$\Delta_y = G_y \times \Gamma \quad (3.41)$$

(ii) Departing from the origin of the head coordinate system ($P_0 = [x_0, y_0, z_0]$), the algorithm scans the gradient image along directions identified by two of the tensors of inertia (X and Y) such to localize three points at the intersection between the tensors and the head boundary. The three points to be adopted as markers are called the "left ear" ($P_1 = [x_1, y_1, z_1]$), "right ear", ($P_2 = [x_2, y_2, z_2]$) and "nose" ($P_3 = [x_3, y_3, z_3]$). Let xres and yres be respectively the X and Y resolution of the brain volume. To search for the "left ear" marker with k = 0...n and i = x_0...n, let

$$i_k = ((y_0 / (1+ f_x)) * xres + ((i - k) / e_x)) + ((z_0 / (1+ g_x)) * yres * xres) \quad (3.42)$$

be n+1 sets of (x_0-n) voxels where our marker is located; where e_x, f_x and g_x are respectively the x, y and z components of the X tensor of inertia. If the value $f(i_k)$ of the intensity of the i_k voxel is greater or equal to each of the preceding $f(i_j)$ (with j = 1...n), then the i_k voxel is assumed as potential left ear marker. Thus, a subset of at most (x_0-n) potential left ear markers is derived from the (n+1)*(x_0-n) voxels.

The "left ear" marker will be that voxel i_k of the subset for which i is the smallest in value and at the same time the intensity $f(i_k)$ is greater than a threshold TH. Thus, the coordinates of the "left ear" marker will be:

$$x_1 = (i_k / e_x) \tag{3.43}$$

$$y_1 = (y_0 / (1+ f_x)) \tag{3.44}$$

$$z_1 = (z_0 / (1 + g_x)) \tag{3.45}$$

Similarly, to search for the "right ear" marker with $k = 0\ldots n$ and $i = x_0\ldots(xres-n)$:

$$i_k = ((y_0 / (1 - f_x)) * xres + ((i + k) / e_x)) + ((z_0 / (1 - g_x)) * yres * xres) \tag{3.46}$$

are n+1 sets of $(xres-x_0-n)$ voxels where the marker is located. A subset of at most $(xres-x_0-n)$ potential right ear markers is derived from the i_k voxels considering only those for which the value of the intensity $f(i_k)$ is greater or equal to each of the subsequent $f(i_j)$ (with $j = 1\ldots n$). The "right ear" marker will then be that voxel i_k of the subset for which i is the greatest in value and at the same time the intensity $f(i_k)$ is greater than TH. The coordinates of the "right ear" marker will be:

$$x_2 = (i_k / e_x) \tag{3.47}$$

$$y_2 = (y_0 / (1 - f_x)) \tag{3.48}$$

$$z_2 = (z_0 / (1 - g_x)) \tag{3.49}$$

Similarly, for the "nose" marker with $k = 0\ldots n$ and $i = y_0\ldots(yres-n)$:

$$i_k = (((i + k) / f_y * xres) + (x_0 / (1 - e_y))) + ((z_0 / (1 - g_y)) * yres * xres) \tag{3.50}$$

The scalars e_y, f_y and g_y are respectively x, y and z component of the Y tensor of inertia. The coordinates of the "nose" marker will be:

$$x_3 = (x_0 / (1 - e_y)) \tag{3.51}$$

$$y_3 = (i_k / f_y) \tag{3.52}$$

$$z_3 = (z_0 / (1 - g_y)) \tag{3.53}$$

Once the three markers are found into the reference volume, they can be reproduced into each of the test volumes of the series. This is done by simply using equations (3.43)-(3.45), (3.47)-(3.49) and (3.51)-(3.53) with values of $P_0 = [x_0, y_0, z_0]$ and e_x, f_x, g_x, e_y, f_y, g_y extracted from the test volumes and thus independent from any thresholds. As for i_k, its numerical value in each test volumes is the same found into the reference volume. This approach increases the reliability of localization across brain images.

3.10.3 Construction of the Head Coordinate System

Let α be the XY plane of equation $A_{XY} * x + B_{XY} * y + C_{XY} * z + D_{XY} = 0$ ($P_1 \in \alpha$, $P_2 \in \alpha$, $P_3 \in \alpha$), β be the ZY plane of equation $A_{ZY} * x + B_{ZY} * y + C_{ZY} * z + D_{ZY} = 0$ ($\beta \perp \alpha$ and $P_0 \in \beta$, $P_3 \in \beta$) and γ be the ZX plane of equation $A_{ZX} * x + B_{ZX} * y + C_{ZX} * z + D_{ZX} = 0$ ($\gamma \perp \alpha$, $\gamma \perp \beta$ and $P_0 \in \gamma$). The coefficients of α, β and γ are found as illustrated earlier (Ciulla and Deek 2001a) and the unit vectors (l_x, m_x, n_x; l_y, m_y, n_y; l_z, m_z, n_z) of the head coordinate system can be computed as follow:

$$l_z = \begin{vmatrix} B_{ZY} & B_{ZX} \\ C_{ZY} & C_{ZX} \end{vmatrix} \tag{3.54}$$

$$m_z = -\begin{vmatrix} A_{ZY} & A_{ZX} \\ C_{ZY} & C_{ZX} \end{vmatrix} \tag{3.55}$$

$$n_z = \begin{vmatrix} A_{ZY} & A_{ZX} \\ B_{ZY} & B_{ZX} \end{vmatrix} \tag{3.56}$$

$$l_y = \begin{vmatrix} B_{XY} & B_{ZY} \\ C_{XY} & C_{ZY} \end{vmatrix} \tag{3.57}$$

$$m_y = -\begin{vmatrix} A_{XY} & A_{ZY} \\ C_{XY} & C_{ZY} \end{vmatrix} \tag{3.58}$$

$$n_y = \begin{vmatrix} A_{XY} & A_{ZY} \\ B_{XY} & B_{ZY} \end{vmatrix} \tag{3.59}$$

$$l_x = \begin{vmatrix} m_y & m_z \\ n_y & n_z \end{vmatrix} \tag{3.60}$$

$$m_x = -\begin{vmatrix} l_y & l_z \\ n_y & n_z \end{vmatrix} \tag{3.61}$$

$$n_x = \begin{vmatrix} l_y & l_z \\ m_y & m_z \end{vmatrix} \tag{3.62}$$

3.10.4 Determination of the Rigid-Body Transformation

Given that X and Y axes of the head coordinate system are orthogonal, rotations ψ_r and ψ_a about the Z axis of reference (r) and test (a) brain images can be computed as:

$$\cos \psi_r = l_{xr} / [(l_{xr} * l_{xr}) + (m_{xr} * m_{xr})]^{½} \tag{3.63}$$

$$\cos \psi_a = l_{xa} / [(l_{xa} * l_{xa}) + (m_{xa} * m_{xa})]^{½} \tag{3.64}$$

$$\sin \psi_r = m_{xr} / [(l_{xr} * l_{xr}) + (m_{xr} * m_{xr})]^{½} \tag{3.65}$$

$$\sin \psi_a = m_{xa} / [(l_{xa} * l_{xa}) + (m_{xa} * m_{xa})]^{½} \tag{3.66}$$

$$\psi_a = \text{atan} (\sin \psi_a / \cos \psi_a) \tag{3.67}$$

$$\psi_r = \text{atan} (\sin \psi_r / \cos \psi_r) \tag{3.68}$$

$$\psi_x = \psi_a - \psi_r \tag{3.69}$$

where l_{xr}, m_{xr}, n_{xr}; l_{xa}, m_{xa}, n_{xa} are the unit vectors of the X axis of the head coordinate system respectively for reference (r) and test (a) brain images and ψ_x is

the rotation about the Z axis to apply to the test image to align the reference image. Rotations ψ_r and ψ_a can also be computed as:

$$\cos \psi_r = l_{yr} / [(l_{yr} * l_{yr}) + (m_{yr} * m_{yr})]^{1/2} \quad (3.70)$$

$$\cos \psi_a = l_{ya} / [(l_{ya} * l_{ya}) + (m_{ya} * m_{ya})]^{1/2} \quad (3.71)$$

$$\sin \psi_r = m_{yr} / [(l_{yr} * l_{yr}) + (m_{yr} * m_{yr})]^{1/2} \quad (3.72)$$

$$\sin \psi_a = m_{ya} / [(l_{ya} * l_{ya}) + (m_{ya} * m_{ya})]^{1/2} \quad (3.73)$$

$$\psi_a = \text{atan} (\sin \psi_a / \cos \psi_a) \quad (3.74)$$

$$\psi_r = \text{atan} (\sin \psi_r / \cos \psi_r) \quad (3.75)$$

$$\psi_y = \psi_a - \psi_r \quad (3.76)$$

The scalars l_{yr}, m_{yr}, n_{yr}; l_{ya}, m_{ya}, n_{ya} are the unit vectors of the Y axis of the head coordinate system respectively for reference (r) and test (a) brain images and ψ_y is the rotation about the Z axis to apply to the test image to align the reference image. The yaw angle ψ is found averaging (3.69) and (3.76):

$$\psi = - (\psi_x + \psi_y) / 2 \quad (3.77)$$

Rotations ϕ_r and ϕ_a about the Y axis of reference (r) and test (a) brain images can be computed using the unit vectors of the X axis:

$$\cos \phi_r = n_{xr} / [(l_{xr} * l_{xr}) + (n_{xr} * n_{xr})]^{1/2} \quad (3.78)$$

$$\cos \phi_a = n_{xa} / [(l_{xa} * l_{xa}) + (n_{xa} * n_{xa})]^{1/2} \quad (3.79)$$

$$\sin \phi_r = l_{xr} / [(l_{xr} * l_{xr}) + (n_{xr} * n_{xr})]^{1/2} \quad (3.80)$$

$$\sin \phi_a = l_{xa} / [(l_{xa} * l_{xa}) + (n_{xa} * n_{xa})]^{1/2} \quad (3.81)$$

$$\phi_a = \text{atan} (\sin \phi_a / \cos \phi_a) \quad (3.82)$$

$$\phi_r = \text{atan} (\sin \phi_r / \cos \phi_r) \quad (3.83)$$

$$\phi_x = \phi_a - \phi_r \quad (3.84)$$

Rotations ϕ_r and ϕ_a can also be computed using the unit vectors of the Z axis:

$$\cos \phi_r = n_{zr} / [(l_{zr} * l_{zr}) + (n_{zr} * n_{zr})]^{½} \quad (3.85)$$

$$\cos \phi_a = n_{za} / [(l_{za} * l_{za}) + (n_{za} * n_{za})]^{½} \quad (3.86)$$

$$\sin \phi_r = l_{zr} / [(l_{zr} * l_{zr}) + (n_{zr} * n_{zr})]^{½} \quad (3.87)$$

$$\sin \phi_a = l_{za} / [(l_{za} * l_{za}) + (n_{za} * n_{za})]^{½} \quad (3.88)$$

$$\phi_a = \text{atan} (\sin \phi_a / \cos \phi_a) \quad (3.89)$$

$$\phi_r = \text{atan} (\sin \phi_r / \cos \phi_r) \quad (3.90)$$

$$\phi_z = \phi_a - \phi_r \quad (3.91)$$

The scalars l_{zr}, m_{zr}, n_{zr}; l_{za}, m_{za}, n_{za} are the unit vectors of the Z axis of the head coordinate system, respectively for reference (r) and test (a) brain images and ϕ_x and ϕ_z are the rotations about the Y axis to apply to the test image to align the reference image. The roll angle ϕ is found averaging (3.84) and (3.91):

$$\phi = (\phi_x + \phi_z) / 2 \quad (3.92)$$

Rotations Θ_r and Θ_a about the X axis of reference (r) and test (a) brain images can be computed using the unit vectors of the Z axis:

$$\cos \Theta_r = m_{zr} / [(m_{zr} * m_{zr}) + (n_{zr} * n_{zr})]^{½} \quad (3.93)$$

$$\cos \Theta_a = m_{za} / [(m_{za} * m_{za}) + (n_{za} * n_{za})]^{½} \quad (3.94)$$

$$\sin \Theta_r = n_{zr} / [(m_{zr} * m_{zr}) + (n_{zr} * n_{zr})]^{½} \quad (3.95)$$

$$\sin \Theta_a = n_{za} / [(m_{za} * m_{za}) + (n_{xa} * n_{xa})]^{½} \quad (3.96)$$

$$\Theta_a = \text{atan} (\sin \Theta_a / \cos \Theta_a) \quad (3.97)$$

$$\Theta_r = \text{atan} (\sin \Theta_r / \cos \Theta_r) \quad (3.98)$$

$$\Theta_z = \Theta_a - \Theta_r \quad (3.99)$$

Rotations Θ_r and Θ_a can also be computed using the unit vectors of the Y axis:

$$\cos \Theta_r = m_{yr} / [(m_{yr} * m_{yr}) + (n_{yr} * n_{yr})]^{½} \quad (3.100)$$

$$\cos \Theta_a = m_{ya} / [(m_{ya} * m_{ya}) + (n_{ya} * n_{ya})]^{½} \quad (3.101)$$

$$\sin \Theta_r = n_{yr} / [(m_{yr} * m_{yr}) + (n_{yr} * n_{yr})]^{½} \quad (3.102)$$

$$\sin \Theta_a = n_{ya} / [(m_{ya} * m_{ya}) + (n_{ya} * n_{ya})]^{½} \quad (3.103)$$

$$\Theta_a = \text{atan} (\sin \Theta_a / \cos \Theta_a) \quad (3.104)$$

$$\Theta_r = \text{atan} (\sin \Theta_r / \cos \Theta_r) \quad (3.105)$$

$$\Theta_y = \Theta_a - \Theta_r \quad (3.106)$$

Angles Θ_z and Θ_y are rotations about the X axis to apply to the test image to align the reference image. The roll angle Θ is found averaging (3.99) and (3.106):

$$\Theta = - (\Theta_y + \Theta_z) / 2 \quad (3.107)$$

The rotation matrix is expressed as:

$$R = \begin{vmatrix} a & b & c \\ d & e & f \\ g & h & l \end{vmatrix} \quad (3.108)$$

where:

$$a = \cos\psi * \cos\phi \quad (3.109)$$

$$b = -\sin\psi * \cos\phi \quad (3.110)$$

$$c = -\sin\phi \quad (3.111)$$

$$d = -(\sin\Theta * \sin\phi * \cos\psi) + (\cos\Theta * \sin\psi) \quad (3.112)$$

$$e = (\sin\psi * \sin\Theta * \sin\phi) + (\cos\Theta * \cos\psi) \quad (3.113)$$

$$f = -\sin\Theta * \cos\phi \quad (3.114)$$

$$g = (\cos\Theta * \sin\phi * \cos\psi) + (\sin\Theta * \sin\psi) \quad (3.115)$$

$$h = -(\sin\psi * \cos\Theta * \sin\phi) + (\sin\Theta * \cos\psi) \quad (3.116)$$

$$l = \cos\Theta * \cos\phi \quad (3.117)$$

and the translation vector is expressed as:

$$T = \begin{vmatrix} \varepsilon_r - \varepsilon_a \\ \lambda_r - \lambda_a \\ \pi_r - \pi_a \end{vmatrix} \quad (3.118)$$

Scalars $\varepsilon_r - \varepsilon_a$, $\lambda_r - \lambda_a$ and $\pi_r - \pi_a$ are respectively the x, y and z difference between coordinates of centers of gravity of reference and test brain images.

3.10.5 Interpolation

Tri-linear interpolation was incorporated into the registration procedure extending the two-dimensional method illustrated by Castleman (1996) to 3D. The eight neighboring voxels are taken into account to determine the intensity value f(X,Y,Z) at any intra-voxel location:

$$f(X,0,0) = x\,[f(1,0,0) - f(0,0,0)] \tag{3.119}$$

$$f(0,Y,0) = y\,[f(0,1,0) - f(0,0,0)] \tag{3.120}$$

$$f(0,0,Z) = z\,[f(0,0,1) - f(0,0,0)] \tag{3.121}$$

$$f(X,1,0) = x\,[f(1,1,0) - f(0,1,0)] \tag{3.122}$$

$$f(0,Y,1) = y\,[f(0,1,1) - f(0,0,1)] \tag{3.123}$$

$$f(1,1,Z) = z\,[f(1,1,1) - f(1,1,0)] \tag{3.124}$$

$$f(1,0,Z) = z\,[f(1,0,1) - f(1,0,0)] \tag{3.125}$$

$$f(0,1,Z) = z\,[f(0,1,1) - f(0,1,0)] \tag{3.126}$$

$$f(X,Y,0) = y\,[f(X,1,0) - f(X,0,0)] \tag{3.127}$$

$$f(Y,Z,0) = z\,[f(0,Y,1) - f(0,Y,0)] \tag{3.128}$$

$$f(Z,X,0) = x\,[f(1,0,Z) - f(0,0,Z)] \tag{3.129}$$

$$f(X,Y,1) = xy\,[f(1,1,Z) - f(0,1,Z)] - xy\,[f(1,0,Z) - f(0,0,Z)] \tag{3.130}$$

$$\begin{aligned} f(X,Y,Z) = {} & f(0,0,0) + x\,[f(1,0,0) - f(0,0,0)] + \\ & y\,[f(0,1,0) - f(0,0,0)] + \\ & z\,[f(0,0,1) - f(0,0,0)] + \\ & xy\,[f(0,0,0) - f(1,0,0) - f(0,1,0) + f(1,1,0)] + \\ & zy\,[f(0,0,0) - f(0,1,0) - f(0,0,1) + f(0,1,1)] + \end{aligned}$$

$$xz\,[f(0,0,0) - f(1,0,0) - f(0,0,1) + f(1,0,1)] +$$

$$xyz\,[f(1,1,1) - f(1,1,0) - f(0,1,1) - f(1,0,1) +$$

$$f(0,0,1) + f(0,1,0) + f(1,0,0) - f(0,0,0)] \qquad (3.131)$$

3.10.6 Accuracy Estimation

According to Fitzpatrick et al. (1998) accuracy of an alignment method based on markers is worst at the locations that are farthest from the centroid of alignment. To measure registration accuracy (A) at the three marker locations, 3D Euclidean distances have been computed as:

$$A = [\,(X^{o}_{MR} - X^{o}_{MA})^2 + (Y^{o}_{MR} - Y^{o}_{MA})^2 + (Z^{o}_{MR} - Z^{o}_{MA})^2\,]^{1/2} \qquad (3.132)$$

where $X^{o}_{MR}\ Y^{o}_{MR}\ Z^{o}_{MR}$ are respectively x, y, and z coordinates of the marker in the reference brain image with respect to the global (O) coordinate system and X^{o}_{MA} $Y^{o}_{MA}\ Z^{o}_{MA}$ are those of the same marker in the test brain image after alignment is performed:

$$\begin{vmatrix} X^{o}_{MA} \\ Y^{o}_{MA} \\ Z^{o}_{MA} \end{vmatrix} = R * \begin{vmatrix} X^{H}_{MA} \\ Y^{H}_{MA} \\ Z^{H}_{MA} \end{vmatrix} + \begin{vmatrix} \varepsilon_A \\ \lambda_A \\ \pi_A \end{vmatrix} \qquad (3.133)$$

Scalars $X^{H}_{MA}\ Y^{H}_{MA}\ Z^{H}_{MA}$ are respectively x, y, and z coordinates of the marker in the test brain image with respect to the subject's head coordinate system. Scalars ε_A, λ_A, π_A are coordinates of the center of gravity with respect to the global (O) coordinate system. The rotation matrix is R. Values of accuracy (A) have meaning similar to that of the fiducial registration error (FRE) illustrated by Fitzpatrick et al. (1998) and also express how reliably markers are localized across brain images.

CHAPTER 4

TECHNOLOGY DEVELOPMENT

4.1 General Description of AUTOALIGN Computer Based System

Medical image data obtained with functional Magnetic Resonance Imaging is recorded in multiple scanning periods and is stored to form large image databases. Before any analysis tools can be used in order to extract information about functional human brain activation, fMRI data requires spatial pre-processing in term of registration. Also it requires visualization, thus it is prone to the application of computer based systems that incorporate both data display and algorithmic tools to perform spatial pre-processing procedures.

In recent years, emphasis has been placed on developing computer systems, which make effective use of data in various forms, such as image graphics, video sequences, and other scientific or medical data. Recent approaches that adopted to develop image database systems, have generally fallen into one of the following two classifications: (i) databases with no image understanding capabilities or (ii) vision systems which store images in a basic image depository (Bach et al. 1993). Figure 4.1 shows the architectural framework of visual information systems. It is visible from the picture that two different domains need to be filled: (i) query system and (ii) computer vision system. This implies that the search initiated by the query does not have to be restricted to alphanumeric summaries of the images, but it has to go beyond in the interpretation and understanding of the images. Computer Vision System needs to be included to give visualization properties to the system

and also has to communicate with the image understanding routines, such to furnish the appropriate answer to the user in the form of images.

On the other hand, as figure 4.2 shows, databases rely mainly on alphanumeric summaries of the images, which are used to satisfy queries, and determine the resulting images (Chang et al. 1988). These systems provide query mechanisms that are similar to traditional databases. They lack of any property to accurately interpret image data. Computer vision systems address more specifically both image interpretation and understanding. However, these types of systems are intended for vision or research. They do not provide emphasis on specific database processes such as querying (Bach et al. 1993).

An architectural framework of brain image registration systems is given in figure 4.3. The GUI is the only portion of the system that the user can see and can directly interact with. The Computer Vision System is constituted by the set of routines that allows visualization of the image content, before and after processing. The Computer Vision System feeds back visual information to the user and also it serves the purpose of initializing the registration system according to the user request. The Registration System allows spatial processing. It constitutes the core of the registration algorithm, and directly interacts with the Image Database, also furnishing information back to the computer vision system for post processing visualization.

One of this dissertation's aims has been to build a computer-based system with the intent to combine together an image registration algorithm with a computer

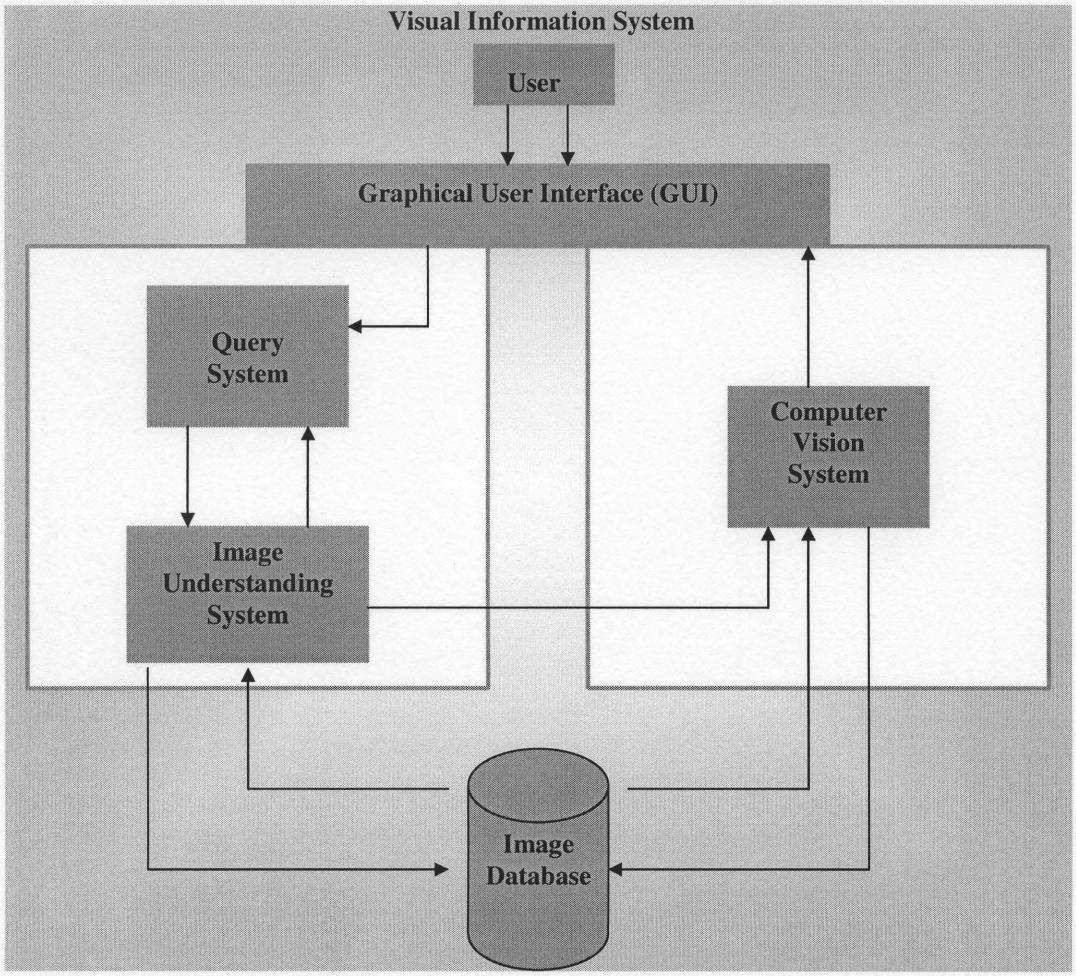

Figure 4.1 The Architectural Framework of a Visual Information System

It is by filling two different domains that state of the art visual information systems can be developed. The first domain is filled by the query system that incorporates the characteristics of a classical information system. In addition, the system needs the Image Understanding subsystem to be the interface between the query system and the Image database (knowledge provided by Bach et al. 1993).

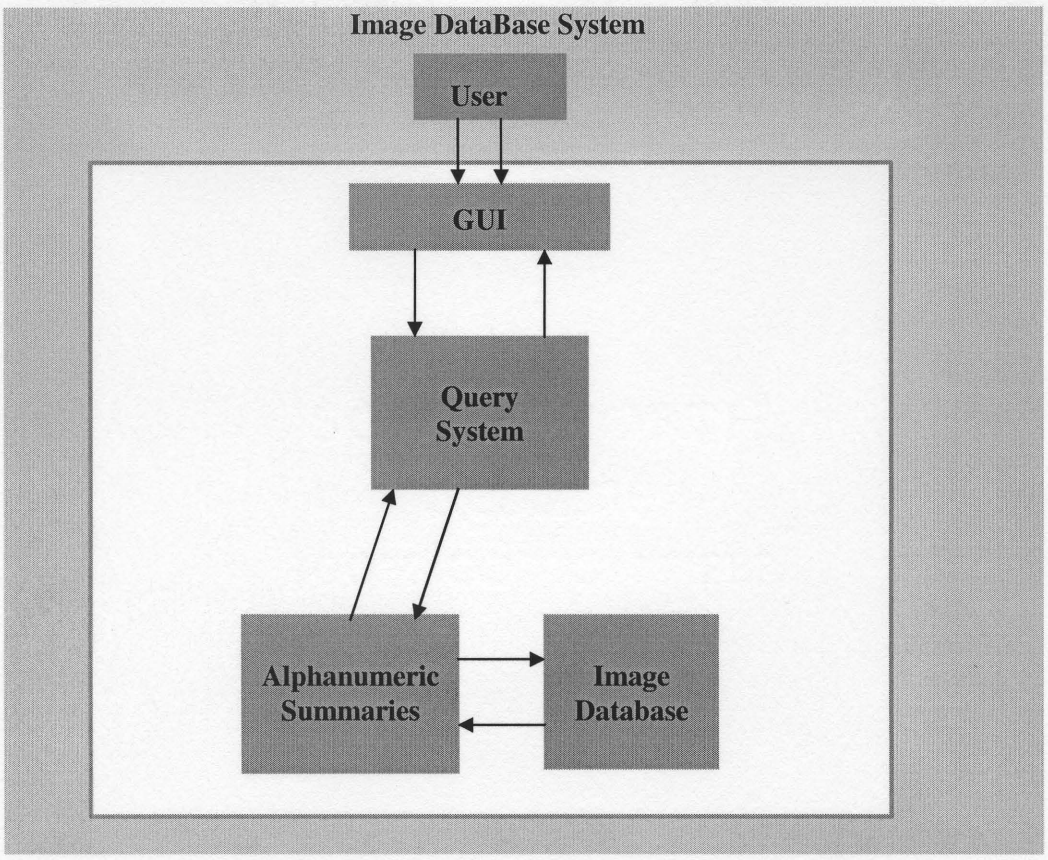

Figure 4.2 Architectural Framework of an Image Database System

The components of this type of systems are: (i) The Graphical User Interface; (ii) The Query System; (iii) Alphanumeric Summaries; and (iv) The Image Database. As suggested by the picture, components of this type of systems, recall the more traditional text based information systems. As a matter of fact, research done on image database systems achieved development of systems that perform image selection mainly relying on alphanumeric summaries of the images. However, visual systems handling images needs to have query mechanisms capable to accurately interpret and retrieve complex image data (knowledge provided by Bach et al. 1993).

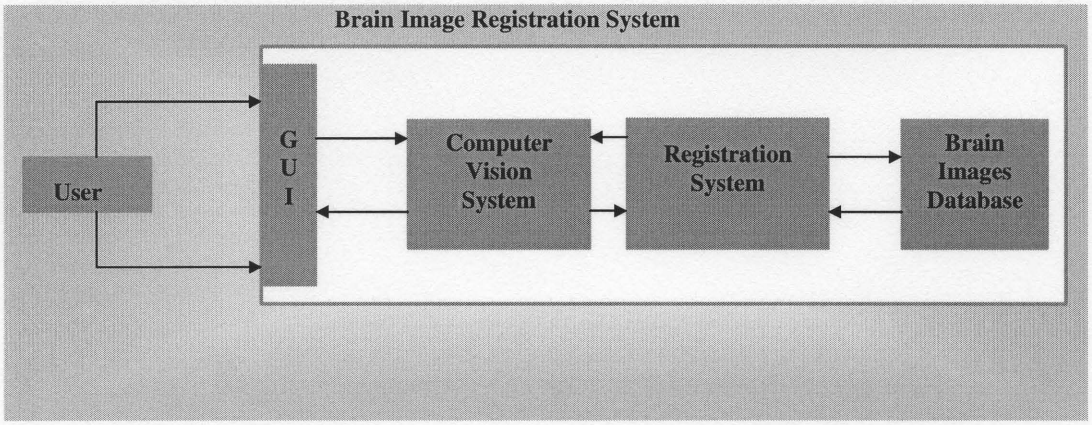

Figure 4.3 Architectural Framework of a Computer Based System for Brain Image Registration

According to the top level framework given in figure 4.1, a visual information system that incorporates vision capabilities together with image processing and understanding subsystems, can be classified in the subclass of Computer Vision Systems (Bach et al. 1993). The picture illustrates the components of the system: (i) Graphical User Interface (GUI); (ii) Computer Vision System; (iii) Registration System and (iv) Brain Image Database.

vision system. The computer based system falls in the second category mentioned above (i.e. vision systems with image understanding capabilities).

The system has been provided with a Graphical User Interface and has been implemented using three software environments: Matlab, OpenGL and ANSI C; and its architectural diagram is illustrated in figure 4.4. Matlab has been used in order to build the GUI (Graphical User Interface). The user through the GUI initiates both visual displays, consisting of graphical applications and computational routines. Communication between the graphic applications and the computational routines are achieved through exchange of information contained into files stored in the local system. The user receives feedback of both visual and numerical nature together with information relative to the alignment parameters that are stored into output files. Interactive graphic applications were used to visualize fMRI data and were developed with OpenGL. ANSI C has been used to write routines performing mathematical computations of the registration algorithm.

Figure 4.5 shows the GUI of the AUTOALIGN software system. The GUI controls the X, Y and Z resolution of the brain image. The "Display Info" button allows the user to get information on how to set X, Y and Z resolution, while the "DataType" option allows the user to choose the format of the brain image to process. The "Display Scan" button activates a program that displays three composite 2D views (Plane, Sagittal and Coronal Sections), which can be sliced interactively by the keyboard. Also, it computes the gradient of the image; the eigenvectors of inertia corresponding to the principal axes, and it finds the three fiducial markers on which the registration algorithm is based. The "Unit Vectors"

button computes the unit vectors of the head coordinate system. The "Align Scan" button aligns the test brain image to the reference one. The "Reference Scan" is specified in the GUI as a file name containing the unit vectors of the reference brain image. Once the computation is performed, the "ReDisplay" button re-displays the scan that has been aligned to the reference. The "Align All" button allows aligning an entire fMRI time series to the reference image. Finally the "Diff. Image" button displays, after alignment, difference images between reference and aligned volumes.

AUTOALIGN contains both visualization and image processing capabilities typical of a computer vision system. As mentioned in the previous section, computer based systems of this kind that were developed earlier were: (i) Statistical Parametric Mapping (SPM99) and (ii) Automatic Image Registration (AIR3.08). For what concerns a comparison AUTOALIGN with the above two, it can be said in term of functionality AUTOALIGN, like AIR3.08, focuses on the registration issue, while SPM99 is also widely used for data analysis. Also, in SPM99, the realignment component is part of a set of options aimed to various spatial pre-processing operations. SPM99 provides to the user also with operations like normalization, smoothing and segmentation of brain images. AIR3.08 is prone to the automatic registration of couple of volumes only. AUTOALIGN and SPM99, on the other hand, are capable to align entire fMRI time series.

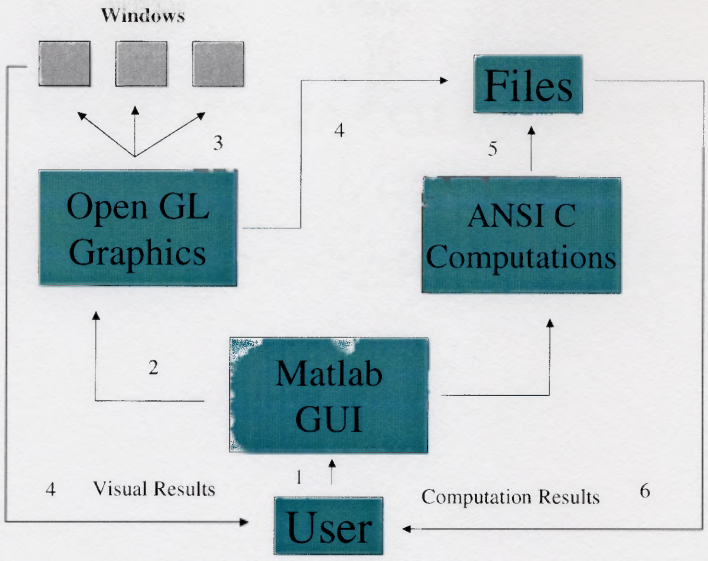

Figure 4.4 Architectural Diagram of AUTOALIGN Computer Based System for Brain Image Registration

The picture illustrates system-user interactions and internal functions of the AUTOALIGN computer program. The user communicates with the Matlab GUI, and can interact with the OpenGL graphic applications through the use of both mouse and keyboard. The ANSI C modules of the system communicate with each other through files stored in the working directory. Both text and visual feedback is provided to the user, plus output files containing results of the realignment algorithm.

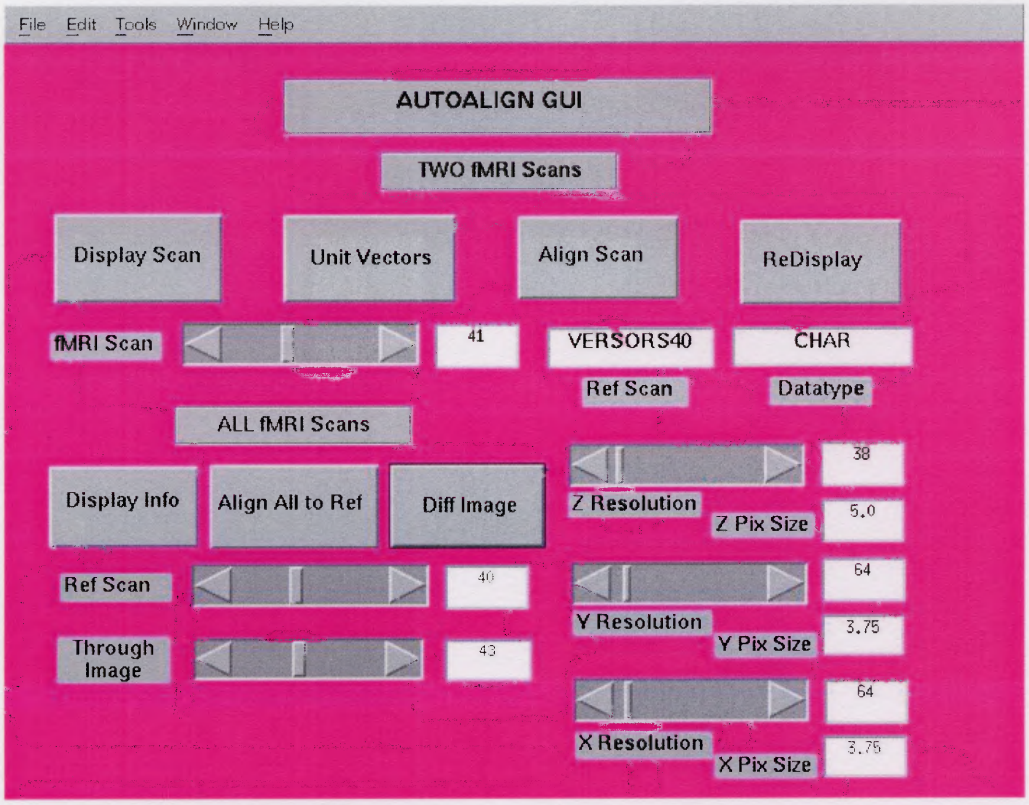

Figure 4.5 AUTOALIGN Graphical User Interface (GUI)

Each button is connected to a separate module. Each module receives information consisting of the program's parameters from both slides and edit boxes. Brain images in several different data formats (unsigned char, int, float and double) can be automatically processed. The GUI's panel is divided in two main sections. The upper section (Two fMRI Scans) is designed to assist the alignment of a couple of volumes, while the lower section (All fMRI Scans) is designed to align automatically, without any user interactions, an entire fMRI time series. While the former allows re-display of brain volumes after registration, the latter allows the user to display difference images between reference and test volumes after tri-linear interpolation has been applied.

4.2 Detailed Description

4.2.1 Generally Object Oriented

In this paragraph it is given a description of the computer-based system that has been developed. In order to apply object-oriented methodologies to the design of a computer-based system, a flow chart needs to be derived that contains objects whose behavior is described by attributes. According to object orientation methodologies, an object (and its behavior) is described by a set of attributes. Under such a methodology an object can be depicted by the following attributes: Inputs, Outputs, Limiting factors / Controls (e.g. Constraints) and Resources (Ranki 1994). In the following, AUTOALIGN will be decomposed in diagrams. In figure 4.6 AUTOALIGN is shown at its top level by using an approach that determines meaningful objects and organizes them such that the data flow and processes' layout becomes Object Oriented (OO). The approach was conceptually re-adapted from Ranki (1994). Each box identifies an object and each side of the box has a particular meaning. The left side of the box is for inputs, the right side of the box is for outputs, the topside is for constraints and the bottom side is for mechanisms (resources). Inputs are transformed into outputs, controls constrain or dictate the conditions under which transformations occur and mechanisms (resources) describe how the function is accomplished (Ranki 1994). The same OO approach can be used to generalize and describe the full activity and structural organization of the software at the highest layer. Stratifying the chart in layers can give insights on how the internal and external activities of the AUTOALIGN software are

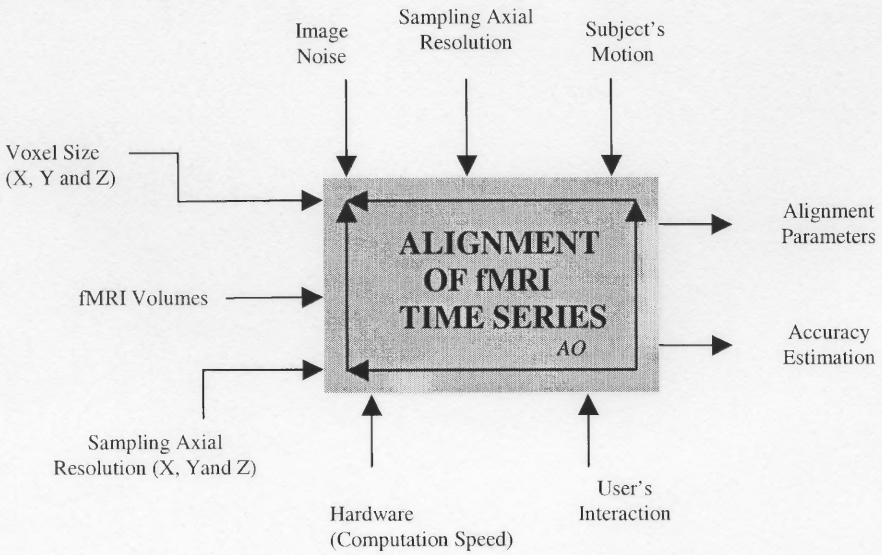

Figure 4.6 AUTOALIGN Level 0 Diagram

The purpose is to spatially register fMRI time series and to correct for intensities at sub-voxel accuracy. The view-point is the user.

developed. Thus, AUTOALIGN can be thought as having several layers hierarchically structured below the one shown in Figure 4.6 and for which there is another stratification that comprises the other relevant data flow and functions of the computer program (conceptually re-adapted from Ranki, 1994). AUTOALIGN data description, which is relevant to, inputs, outputs, resources and controls, furnishes other information relevant to the specific meaning of each of the entries of the diagram and it is given in Appendix A.

Figure 4.7 illustrates data flow between the programs that constitute the first part (two fMRI scans) of the AUTOALIGN computer based system. Each of the objects represents a button in the Graphical User Interface. The "Display Button" object takes as inputs, voxel's size and sampling axial resolution, from the options of the GUI. The program performs several computations and offers both visual and numerical displays. Results of this program are saved interactively by the user in a file that contains numerical values of the three fiducial markers' coordinates that are found automatically by the algorithm. The "Unit Vectors" object receives as input the output of "Display Scan" and automatically computes the axes and the origin of the head coordinate system. On the basis of the head coordinate system of the reference volume, the "Align Scan" button computes pitch, roll and yaw angles and the misalignment vector of the origin. Later, after alignment is performed, the "ReDisplay" object displays the original brain volume. Figure 4.8 illustrates the "All fMRI Scans" section, which is at the same level of the "two fMRI Scans" section. This diagram shows the fully automatic part of the system devoted to the alignment of entire fMRI time series. The "Display Info" object reads from a

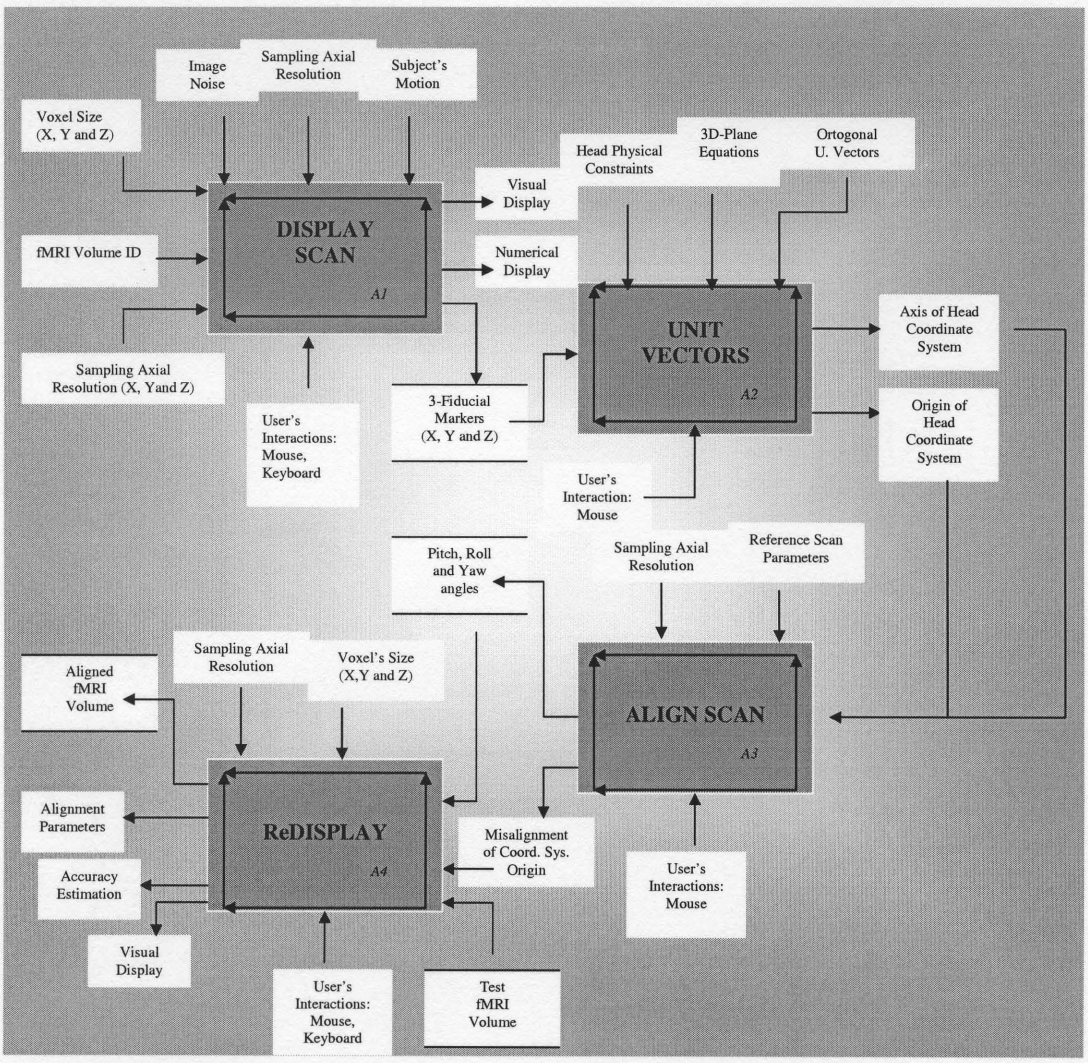

Figure 4.7 AUTOALIGN Level 1 Diagram (Two fMRI Scans)

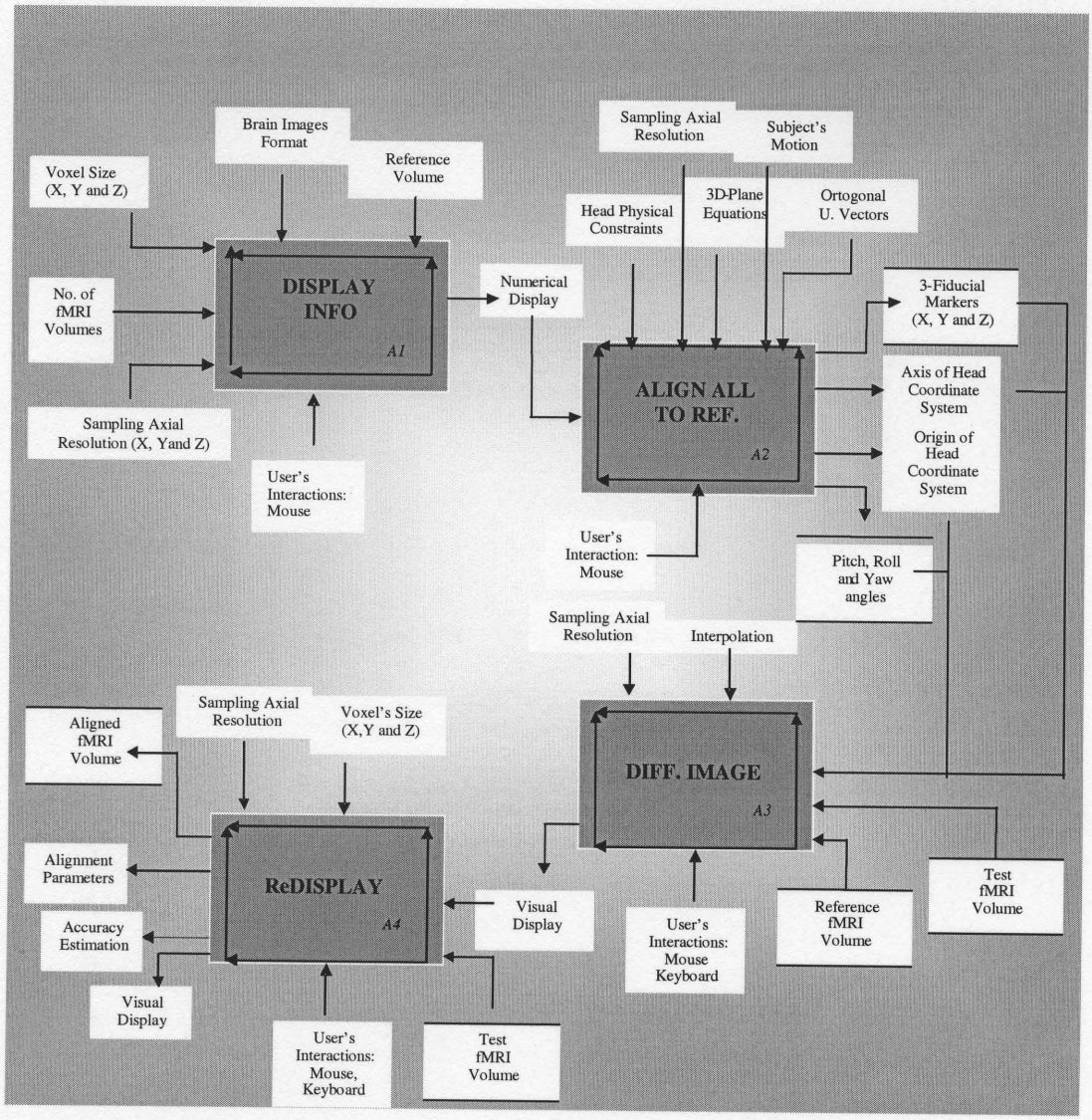

Figure 4.8 AUTOALIGN Level 2 Diagram (All fMRI Scans)

standard header, data relevant to the format of the brain images and produces numerical display. The "Align All to Ref." object is a large routine that incorporates into one, all of the programs of the "two fMRI Scans" section. The "Diff. Image" object computes the difference image between reference and test volumes. The "ReDisplay" object function as shown in figure 4.8.

Figure 4.9 shows details of decomposition of the data flow between routines that constitute the "Display Scan" object. The latter is constituted by the following objects. There is a "Load fMRI data" object which is an ANSI C routine. It receives an fMRI volume as input and produces the equivalent analog data as output. The "Compute Gradient" object incorporates a simple convolution operator that transforms the original brain volume into a gradient volume, thus identifying the zero-crossing points of the image. The "Compute Inertia" object also receives the brain image in analog format (0-255) from the "Load fMRI Data" object and computes the inertia matrix. The latter is fed to the "Compute Eigenvect." object, which extracts, by the Jacobi algorithm (Demmel 1997), eigenvectors corresponding to the eigenvalues of the inertia matrix. Finally, the "Find Markers" object finds automatically three fiducial markers at the intersections of two of the tensors of inertia (eigenvectors) with the head boundary found by the "Compute Gradient" object. At the end of the process, the program saves the information about the fiducial markers into an output file.

Figure 4.10 also shows details of what constitute the "Unit Vectors" object. It is an assembly of three objects, which in turn implements three steps of the algorithm used to determine unit vectors of the head coordinate system of the brain

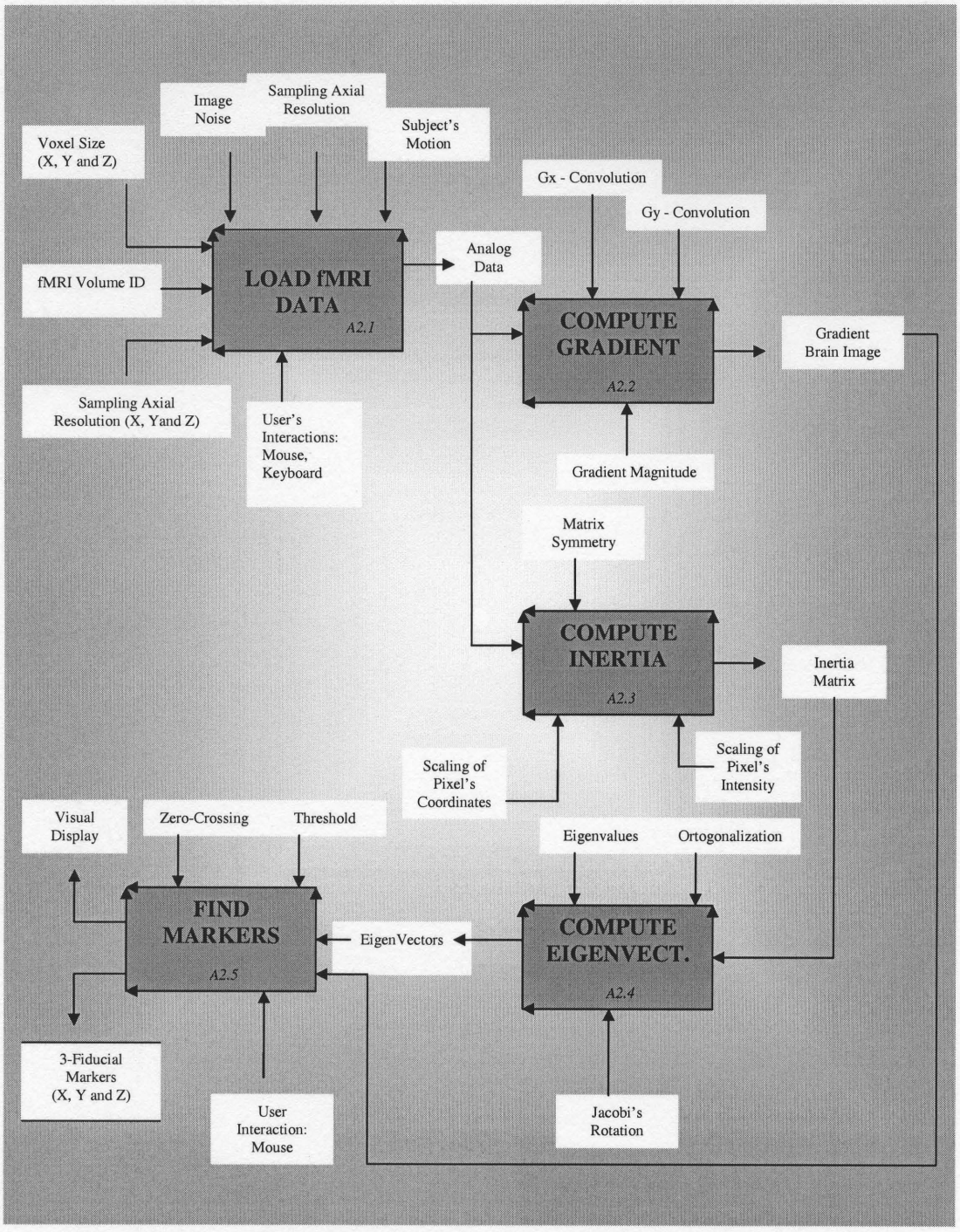

Figure 4.9 AUTOALIGN Level 2 Diagram (Display Scan)

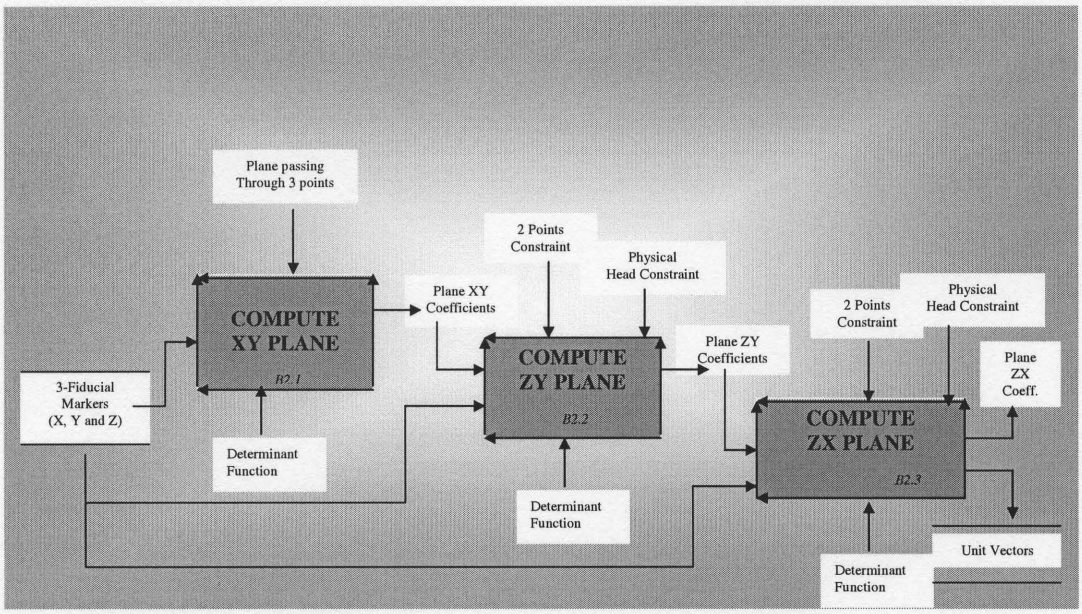

Figure 4.10 AUTOALIGN Level 2 Diagram (Unit Vectors)

volume. The "Compute XY Plane" object writes the equation of a plane passing through three fiducial markers. The "Compute ZY Plane" writes the equation of a plane that is perpendicular to the XY plane and passes through the center of gravity and the "nose" marker. The "Compute ZX Plane" writes the equation of a plane that is perpendicular to the previous two (XY and ZY) planes and passes through the center of gravity of the brain.

Figure 4.11 illustrates the objects that constitute the "Align Scan" object. The "Compute R. Matrix" object takes as input the unit vectors of both reference and test images. It computes the rotation matrix, which incorporates the pitch, roll and yaw rotations about the three axes of the coordinate system. The "Compute T. Vector" object is a simple routine that computes the misalignment vector between the centers of gravity of two brain images. Finally, the "Compute New Coord." object applies the rigid-body transformation to the original grid of voxels, thus obtains coordinate values of the new grid. At the end of the process the rotation-translation matrix is saved into an output file.

Figure 4.12 shows details of the data flow between the objects that compose the "ReDisplay" object. The "Load fMRI Data" object receives as input the test brain image, and transforms it into analog representation. The "Apply Transf." object receives the analog brain image from the "Load fMRI Data" object, also reads the rotation-translation matrix from the file stored in the working directory, and finally obtains the new grid coordinate values. The latter are fed to the "Interpolate" object, which is performs the calculation of the pixel's intensity at the

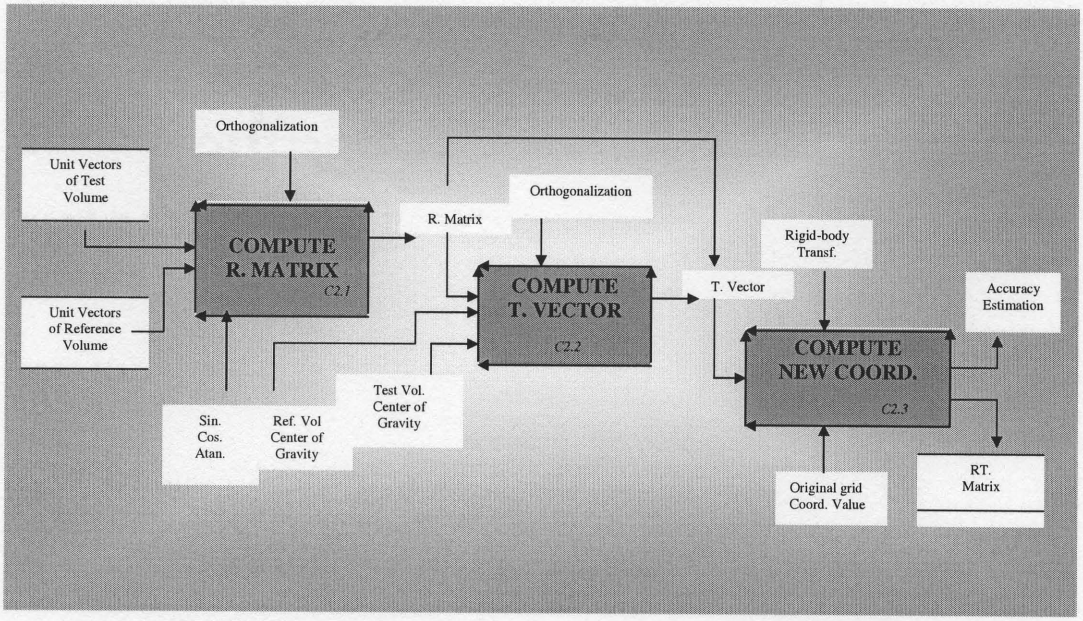

Figure 4.11 AUTOALIGN Level 2 Diagram (Align Scan)

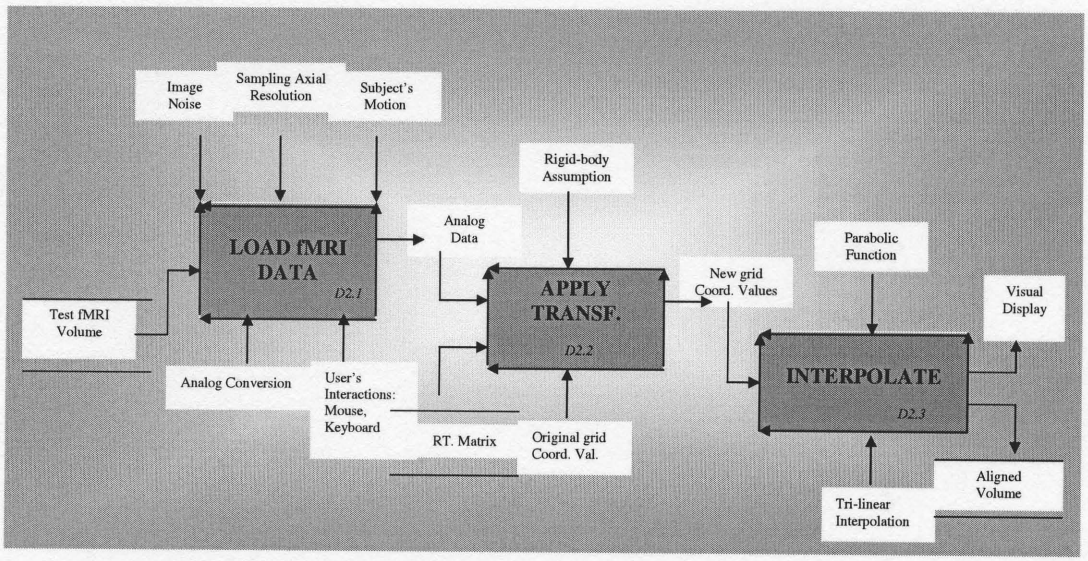

Figure 4.12 AUTOALIGN Level 2 Diagram (ReDisplay)

new grid's coordinates by a 3D extension of the tri-linear interpolation scheme described by Castleman (1996). Finally, the "Interpolate" object furnishes aligned brain volumes and save them into output files.

Figure 4.13 shows in finer decomposition the objects of "Diff. Image". The "Load fMRI Data" object inputs two brain volumes and convert them into analog (0-255) scale. The "Diff. Image" object returns the difference image to the visual display.

Finally, figure 4.14 illustrates with finer detail objects constituting the "Align All to Ref." Object. The "Load fMRI Data" object works as above. The "Find Markers" object automatically locates three fiducial markers and feed data to the "Compute Planes" object, which is basically a routine comprising of the three objects of figure 4.10. Finally, the "Compute Transf." and the "Interp." objects, which respectively compute the new grid's coordinates, alignment parameters and accuracy coefficients, complete the process. Also, numerical display is given to the user for each of the test volumes that are aligned to the reference.

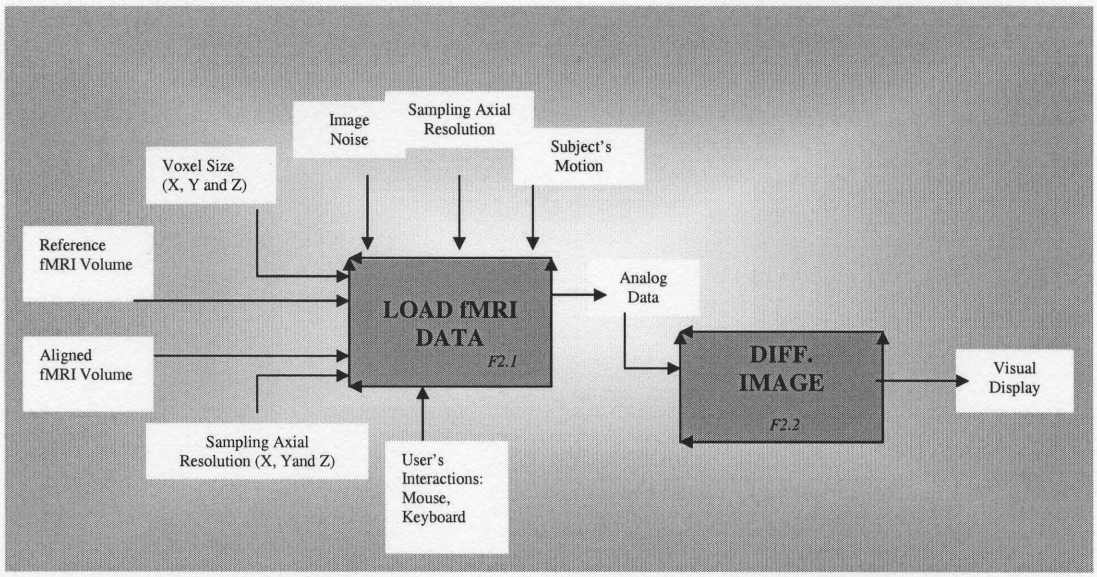

Figure 4.13 AUTOALIGN Level 2 Diagram (Diff. Image)

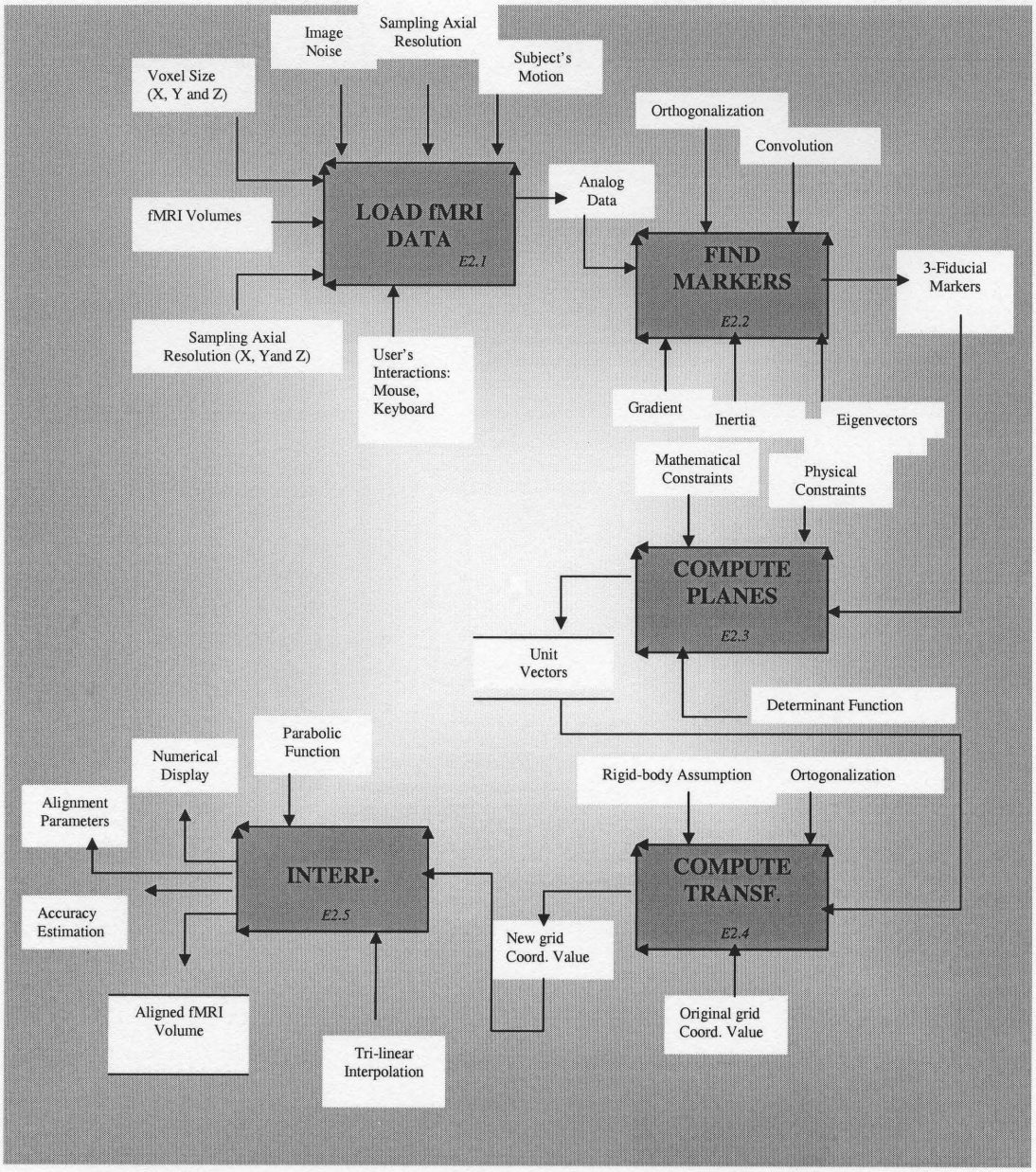

Figure 4.14 AUTOALIGN Level 2 Diagram (Align All to Ref.)

4.2.2 Structure Chart Based

In the present paragraph, a structure chart description of the AUTOALIGN computer based system is given. Figure 4.15 shows the top-level structure chart of the AUTOALIGN software system. Consistently with the representation given earlier, the system is composed of two main parts: (i) "Two fMRI Scans" used to align a couple of fMRI volumes and (ii) "All fMRI Scans" used to align an entire fMRI time series. As figure 4.16 shows, the system is provided with input routine, which accept values from the user such that brain volumes can be loaded consistently with their format. The system also incorporates output routines that save into files values of accuracy coefficients and alignment parameters for each of the brain volumes.

Figure 4.17 shows the structure chart of the "Two fMRI Scans" portion of the system, exactly one layer down. Data flow across the four modules such that from the original brain volumes: (i) three fiducial markers are found; (ii) axes of the head coordinate system are derived; (iii) three angles of rotation are retrieved together with misalignment values of the origin of the coordinate system and (iv) alignment parameters are saved together with accuracy coefficients. A new (aligned) brain volume is produced. Figure 4.18 shows the structure chart organization of the "Display Scan" module. The first operation that is performed is that of loading the brain image. The diagram offers a detailed description of the operations performed by the program in order to find the three fiducial markers. Particularly the gradient is computed, the inertia matrix is extracted, the eigenvectors are found and finally,

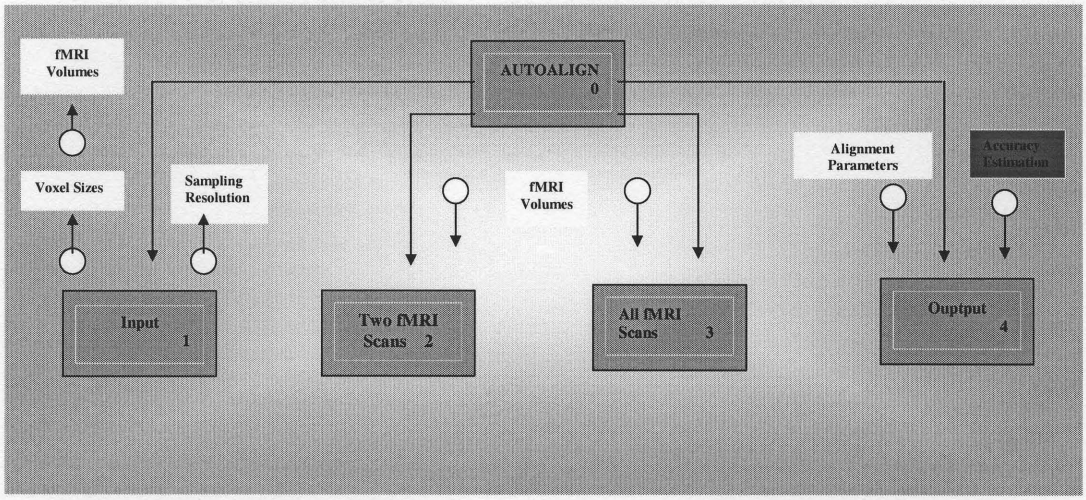

Figure 4.15 AUTOALIGN Structure Chart Level 0

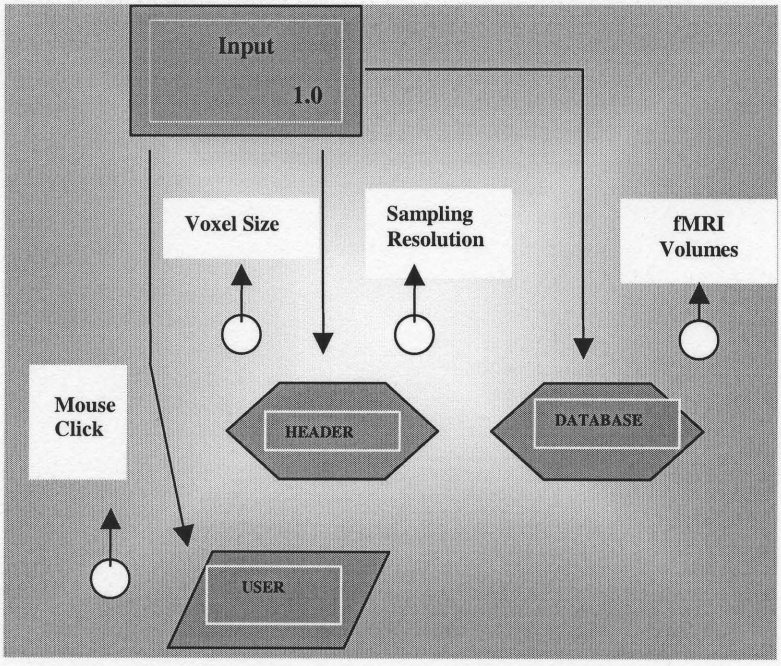

Figure 4.16 AUTOALIGN Structure Chart level 0: Input

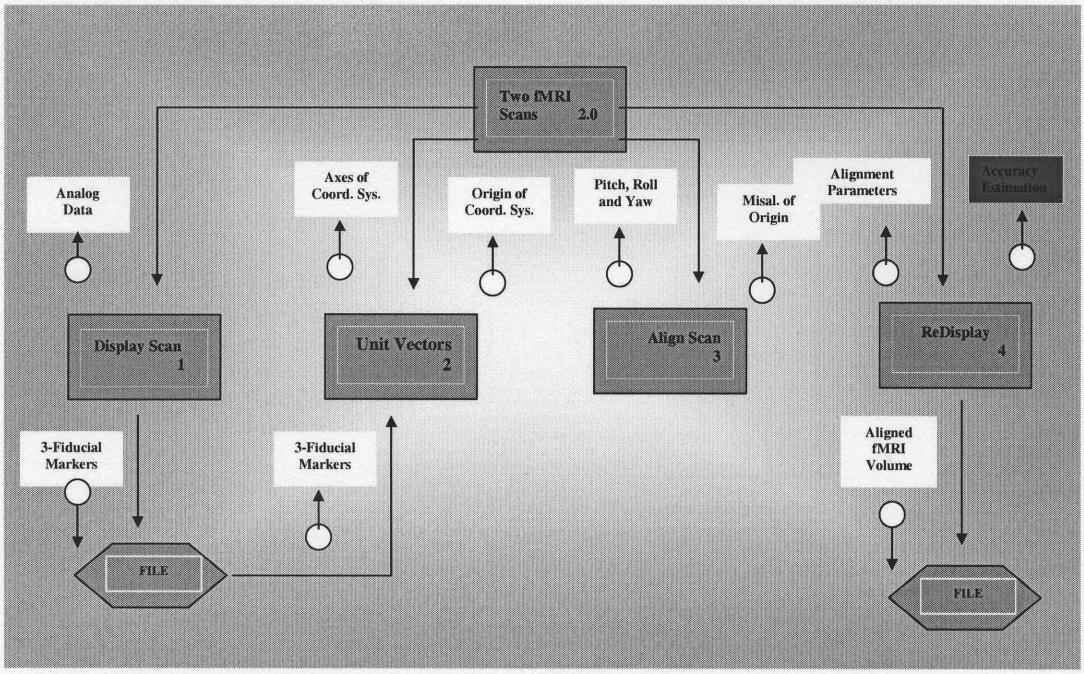

Figure 4.17 AUTOALIGN Structure Chart Level 1: Two fMRI Scans

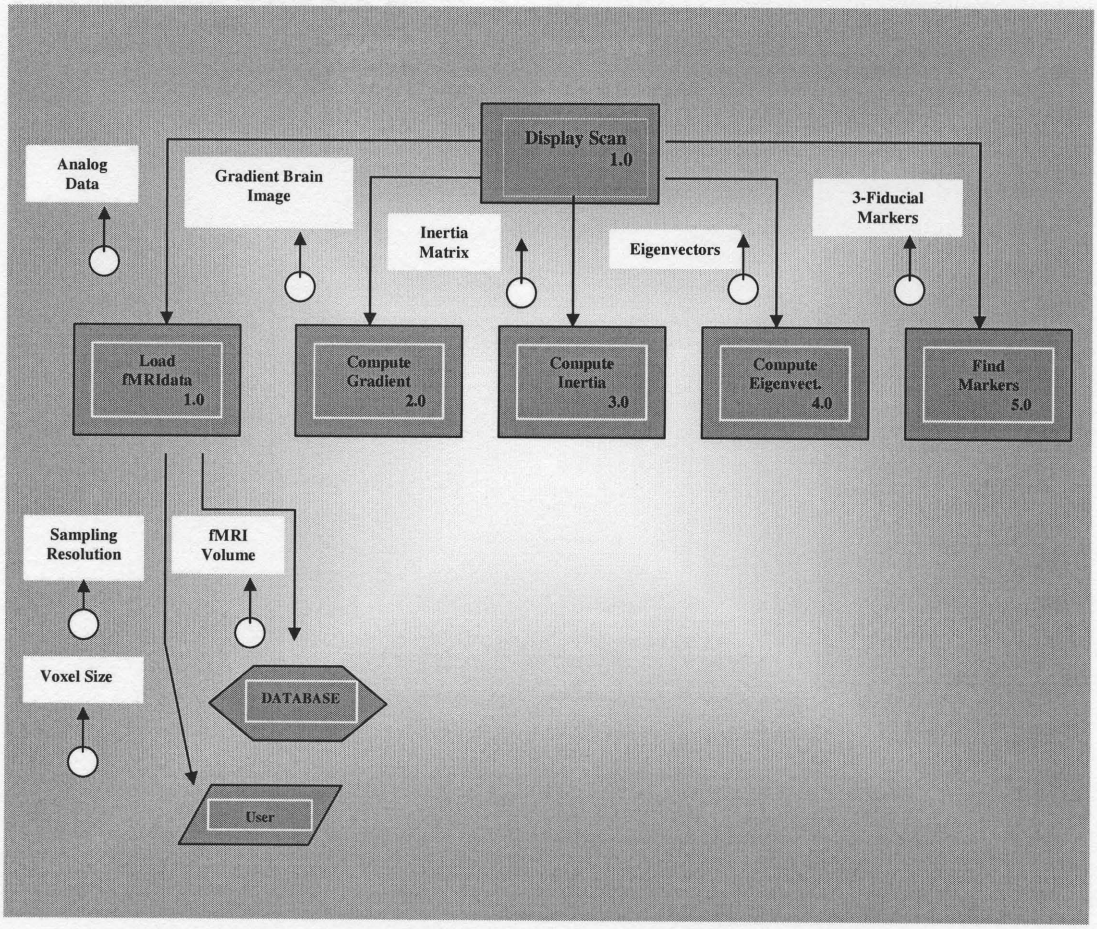

Figure 4.18 AUTOALIGN Structure Chart Level 2: Display Scan

markers are localized. This program reads data both from the user and from the database containing the brain images.

Figure 4.19 shows the data flow of the program used to derive the unit vectors of the head coordinate system from the three fiducial markers. Three different modules compute the three planes of the coordinate system, consistently with what has been shown in figure 4.10. Both input and output operations are performed automatically from and to files placed in the working directory. Figure 4.20 shows the organization of the "Align Scan" module. There are three sub-modules, two of which dedicated to the computation of rotation-translation matrix, and one devoted to the calculation of new grid values. At the end of the process, the rotation-translation matrix is saved into a file and the estimation of alignment accuracy is given as a display to the user.

Figure 4.21 shows the data flow of the "ReDisplay" module. First the brain image is loaded and converted into analog (0-255) scale, then the transformation is applied and the value of the intensity at the new grid coordinates is found by tri-linear interpolation. Finally, the aligned volume is displayed to the user and saved into a file. Figure 4.22 illustrates the structure chart of the "All fMRI Scans" section of the AUTOALIGN software system that is used to align an entire fMRI time series to a reference brain volume. The user reads information about the format of the brain volumes from a standard header file. This produces a numerical display that is used by the user to fix the values of the options of the graphical user interface. The "Align All to Ref." button activates a fully automatic program

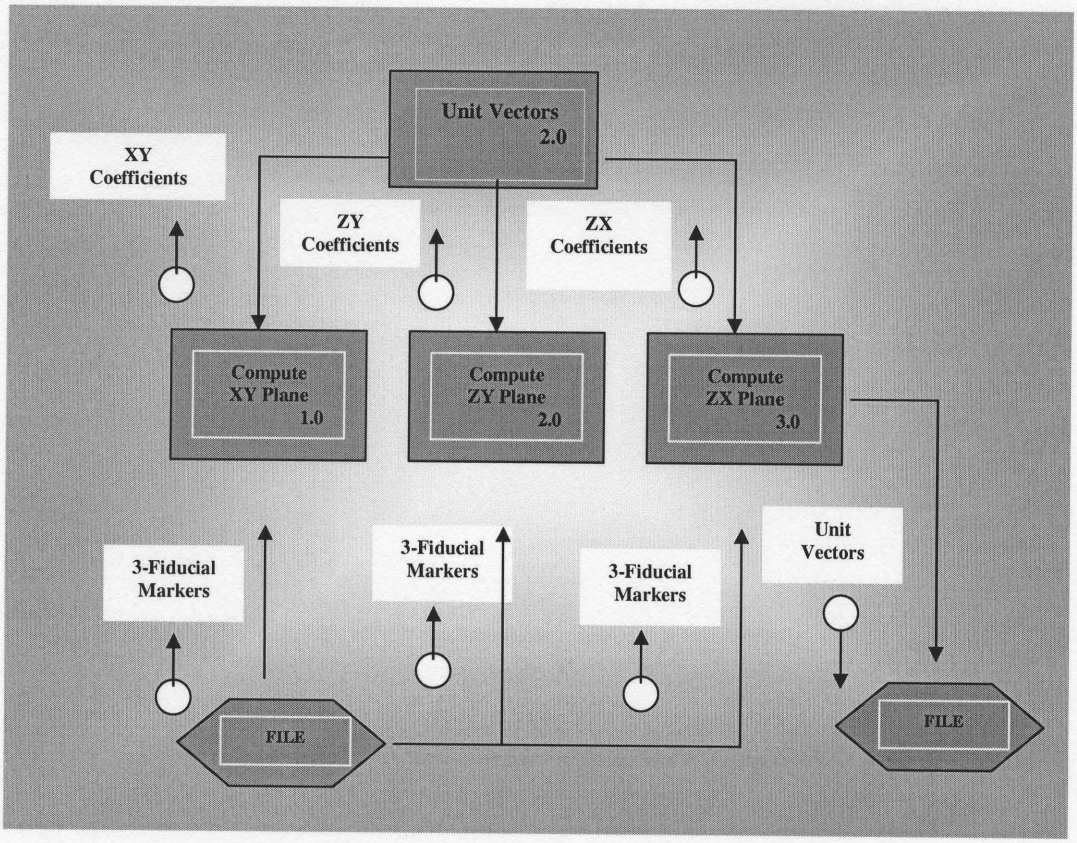

Figure 4.19 AUTOALIGN Structure Chart Level 2: Unit Vectors

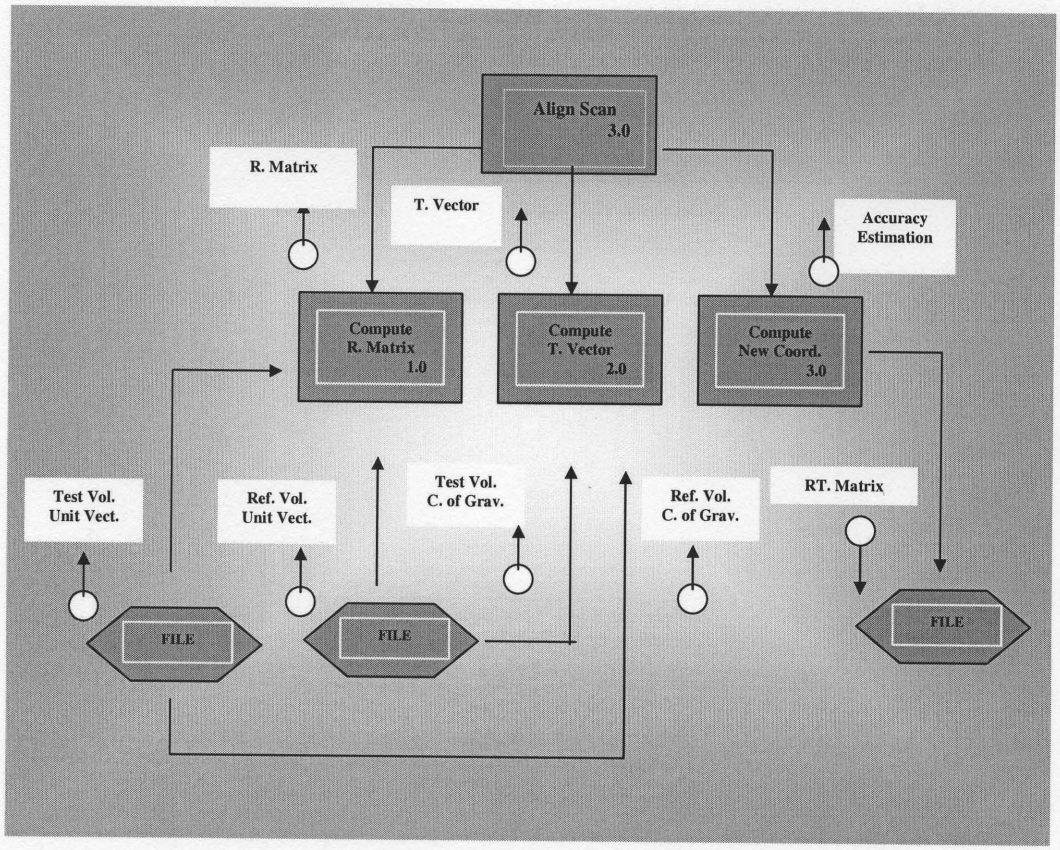

Figure 4.20 AUTOALIGN Structure Chart Level 2: Align Scan

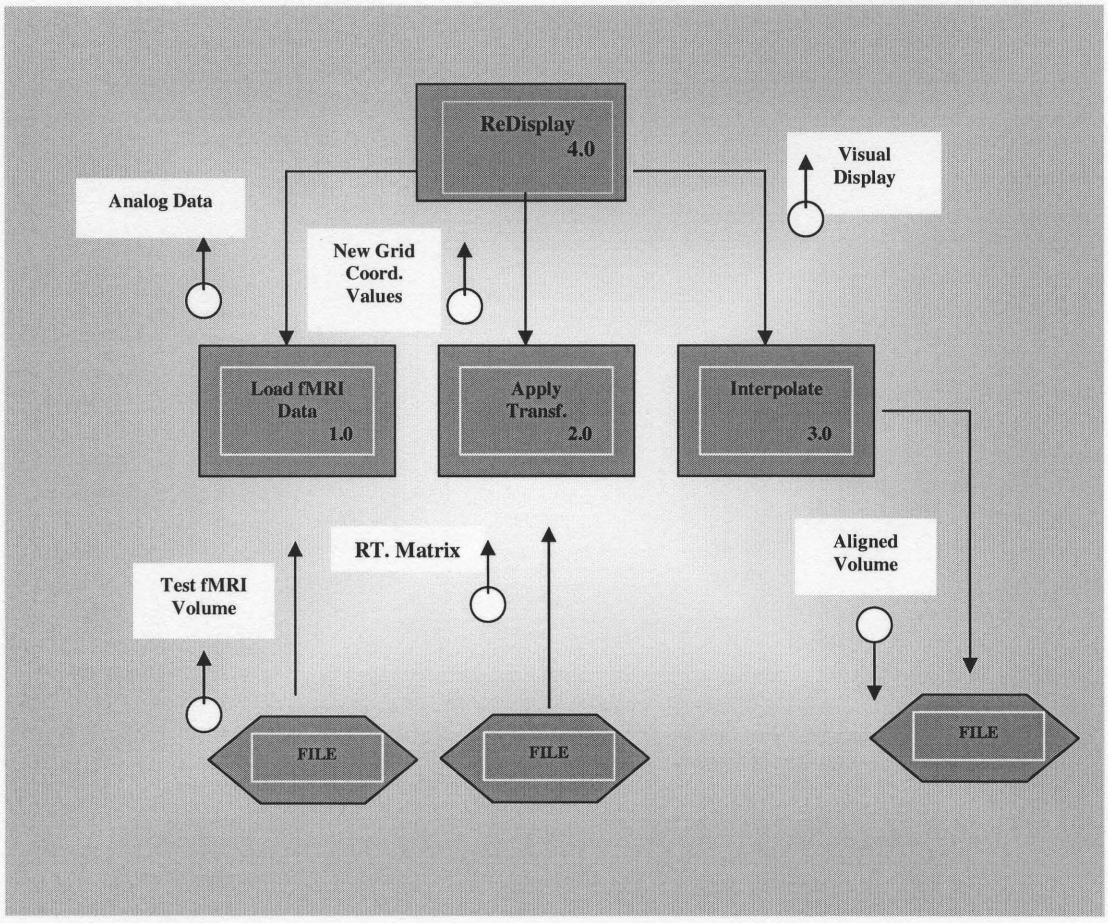

Figure 4.21 AUTOALIGN Structure Chart Level 2: Re-Display

written in ANSI C at the end of which, are found: (i) three fiducial markers; (ii) axes and origin of the head coordinate system and (iii) three rotation angles (pitch, roll and yaw). At the end of the alignment process the user chose any brain images to compute the difference between itself and the reference image and display such difference in three 2D composite views. This operation allows the user to check into the difference image for residual artifacts that might be present after the alignment process.

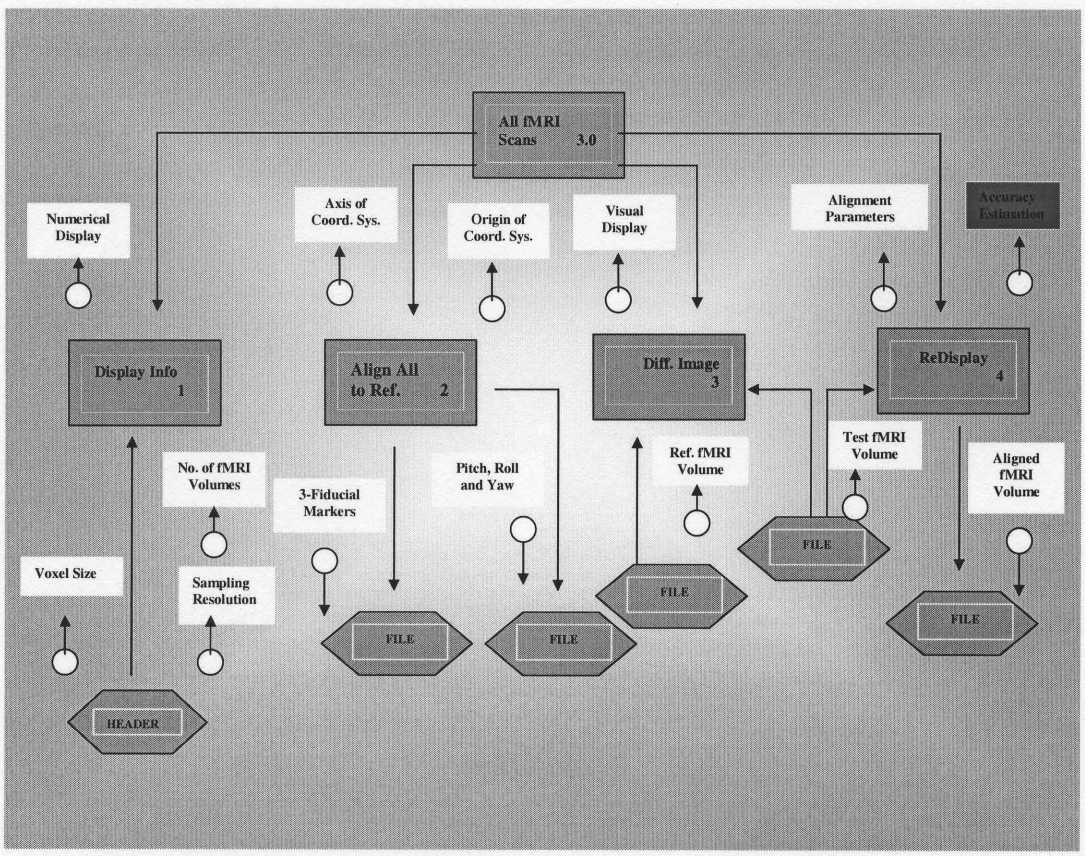

Figure 4.22 AUTOALIGN Structure Chart Level 1: All fMRI Scans

Alternatively, the user chose any brain volumes to display as it is after alignment. The program outputs both accuracy coefficients and alignment parameters in two different files.

Figure 4.23 shows details of the data flow of the "Align All to Ref." button. Data is loaded according to the user instructions. Then, markers are automatically found and fed to the routine that computes three planes of the head coordinate system. This process involves application of several routines, each of which has been illustrated in figure 4.14. The unit vectors are saved into a file that is later read by another routine, which, purpose is to compute the rigid-body transformation. Finally, a routine is activated that interpolate the brain image at the location of the new grid coordinates and save the aligned fMRI volume into an output file. The format of this file is the same as that of the original brain images. Figure 4.24 shows how the "Diff. Image" module functions. Two fMRI scans, respectively the reference and the test volume after alignment, are read and converted into analog scale. Finally, a difference image is displayed for the user to see. Figure 4.25 gives an idea of the output data of the AUTOALIGN software system. It consists, as previously mentioned, of two different output files, one containing the accuracy coefficients and the other containing the alignment parameters.

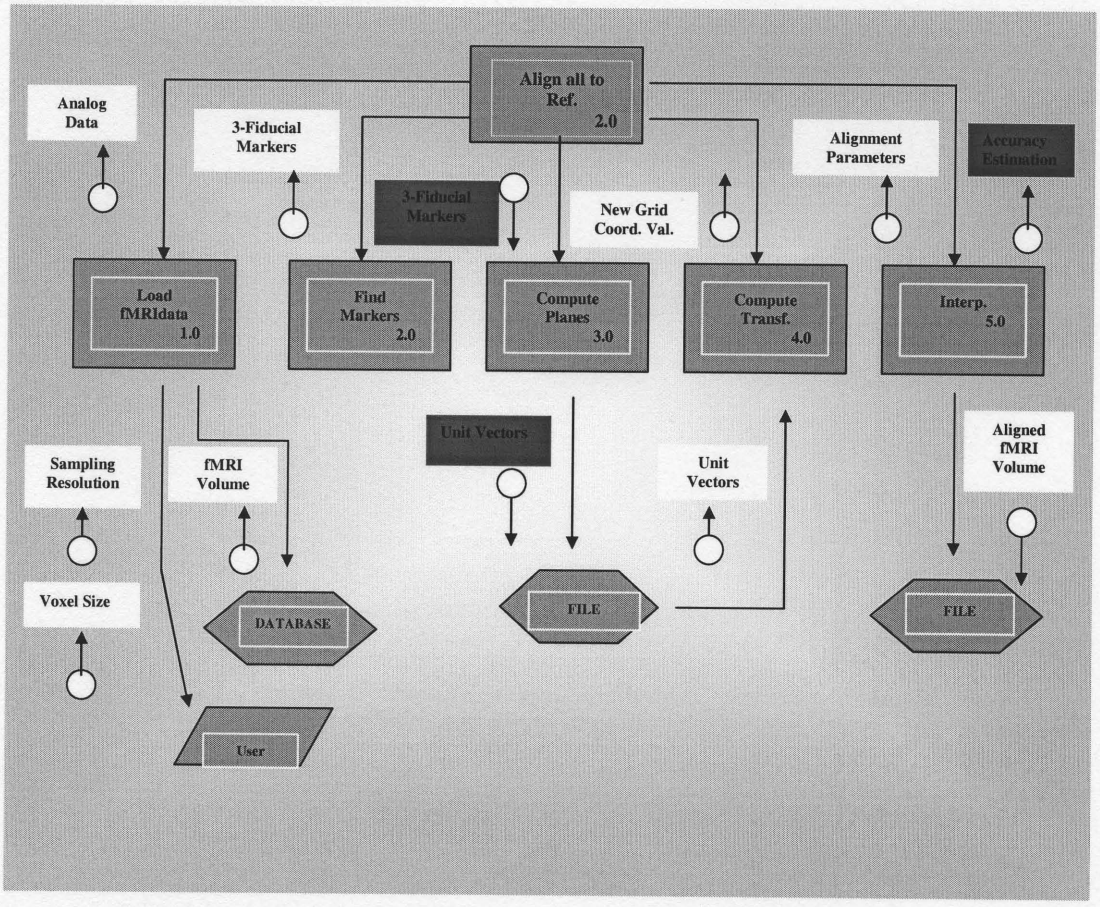

Figure 4.23 AUTOALIGN Structure Chart Level 2: Align All to Ref

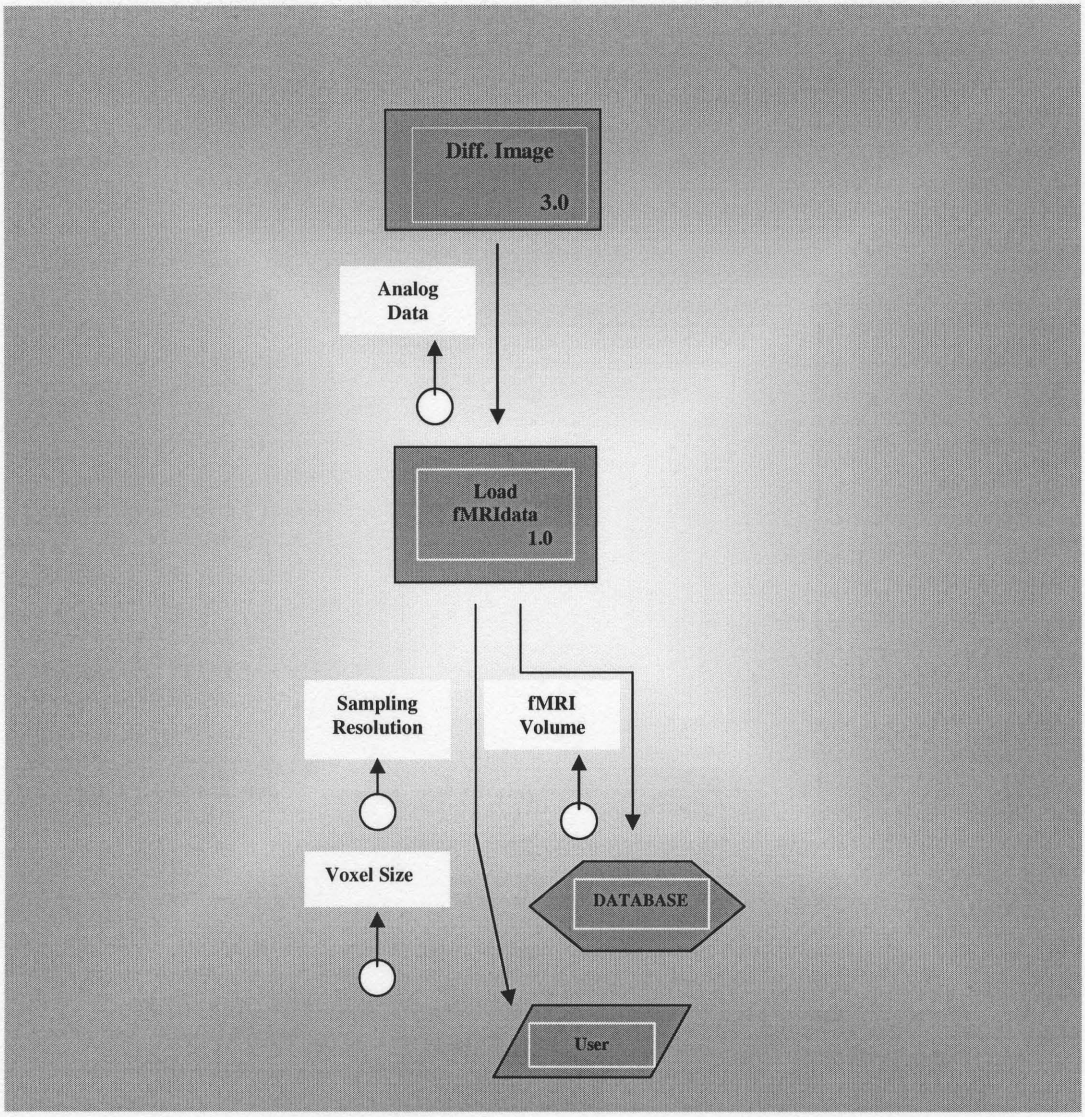

Figure 4.24 AUTOALIGN Structure Chart Level 2: Diff. Image

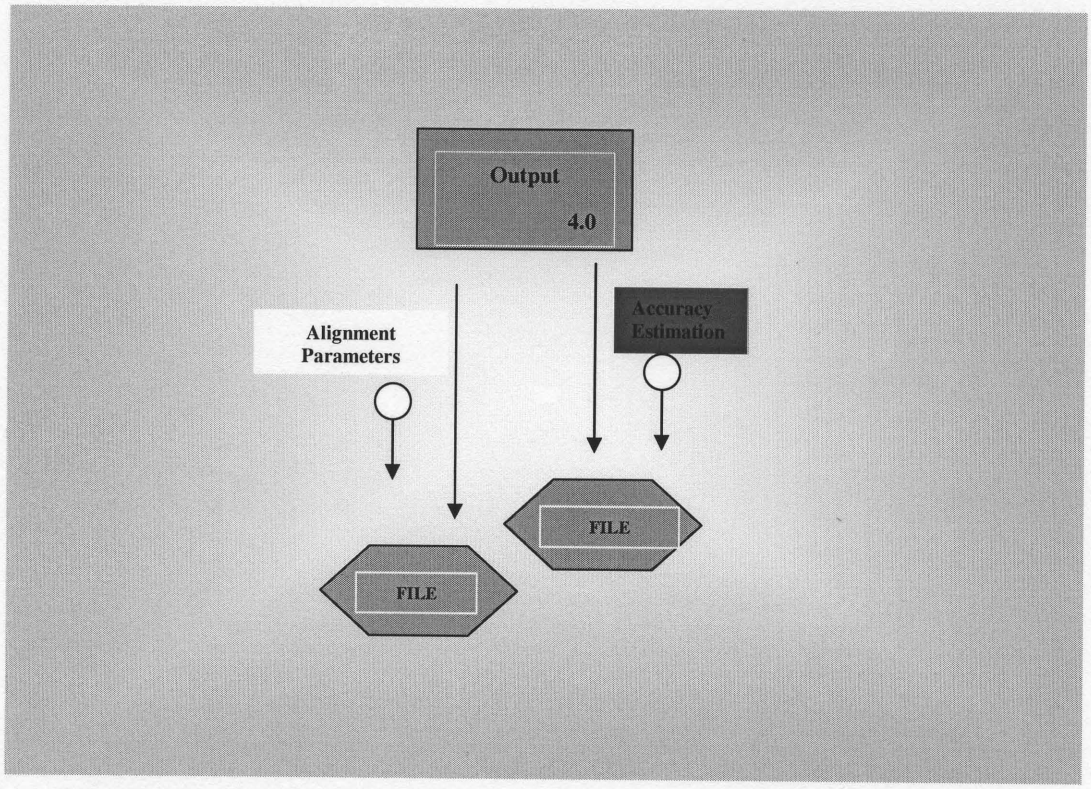

Figure 4.25 AUTOALIGN Structure Chart Level 1: Output

CHAPTER 5

METHODOLOGY VALIDATION

This chapter reports on performance assessment of the AUTOALIGN registration algorithm developed to align functional Magnetic Resonance Images time series (fMRI). Performance of the algorithm was preliminarily assessed by fMR brain images in which controlled motion has been simulated. Further experimentation has been conducted with real fMRI time series. Rigid-body transformations were retrieved automatically and the value of motion parameters compared to those obtained with the Statistical Parametric Mapping (SPM99) and the Automatic Image Registration (AIR 3.08). Further tests relevant to reliability assessment of the technique underlying AUTOALIGN algorithm are reported in Appendix B.

5.1 Preliminary Analysis with Simulated Data

A set of preliminary experiments was performed with a T2*-weighted Magnetic Resonance (MR) volume having sampling resolution of 64 (3.75 mm), 64 (3.75 mm) and 28 (5.00 mm) respectively in the x, y and z directions. Data was obtained by a G.E. 1.5 T Signa Scanner by echo planar imaging (EPI). The aim of the experiments was to test how AUTOALIGN estimated motion parameters. fMRI data were used in which simulated motion was artificially introduced. Rotations at steps of 0.2° in the [-3°, 3°] range for pitch, roll and yaw angles were simulated. Also, in another experimental session, translations at steps of 0.2 voxels in the range [-3; 3] were simulated. The same data was used to perform experiments with

the Statistical Parametric Mapping (SPM99) and Automatic Image Registration (AIR3.08).

Figure 5.1 shows a sample of the three 2D composite views of an original fMRI volume (a) and the same after rotations of 1.8° have been applied simultaneously about the three axes (b). For the images shown in figure 5.1, figure 5.2 shows the gradient images together with the three fiducial markers locations (white) found automatically as described in the previous section. Figure 5.3 shows the plot estimation results of pitch, roll and yaw for AUTOALIGN (a), SPM99 (b) and AIR3.08 (c) with the same dataset. Estimations (black) are displayed versus an ideal line (white) within the [-3°, 3°] range. The "amis" values were computed as the average of the sum of the absolute differences between desired values and the obtained performance:

$$amis = \sum_i | x_i - E(x_i) | / n \qquad (5.1)$$

where x_i and $E(x_i)$ are respectively the i^{th} actual performance and desired performance ($i = 1 \ldots n$ and $n = 30$).

AUTOALIGN results presented here were obtained after an improvement was made in the estimation of the yaw angle with respect to the version presented earlier (Ciulla and Deek, 2001a). The "amis" values are average Euclidean metrics measuring average misalignment expressed in millimeters and degrees respectively for x, y, z and pitch, roll, yaw. AUTOALIGN "amis" values obtained in the experimental session aimed to estimate traslational movements alone were 0.22, 0.22 and 0.43, respectively along x, y and z direction. Figure 5.4 shows difference

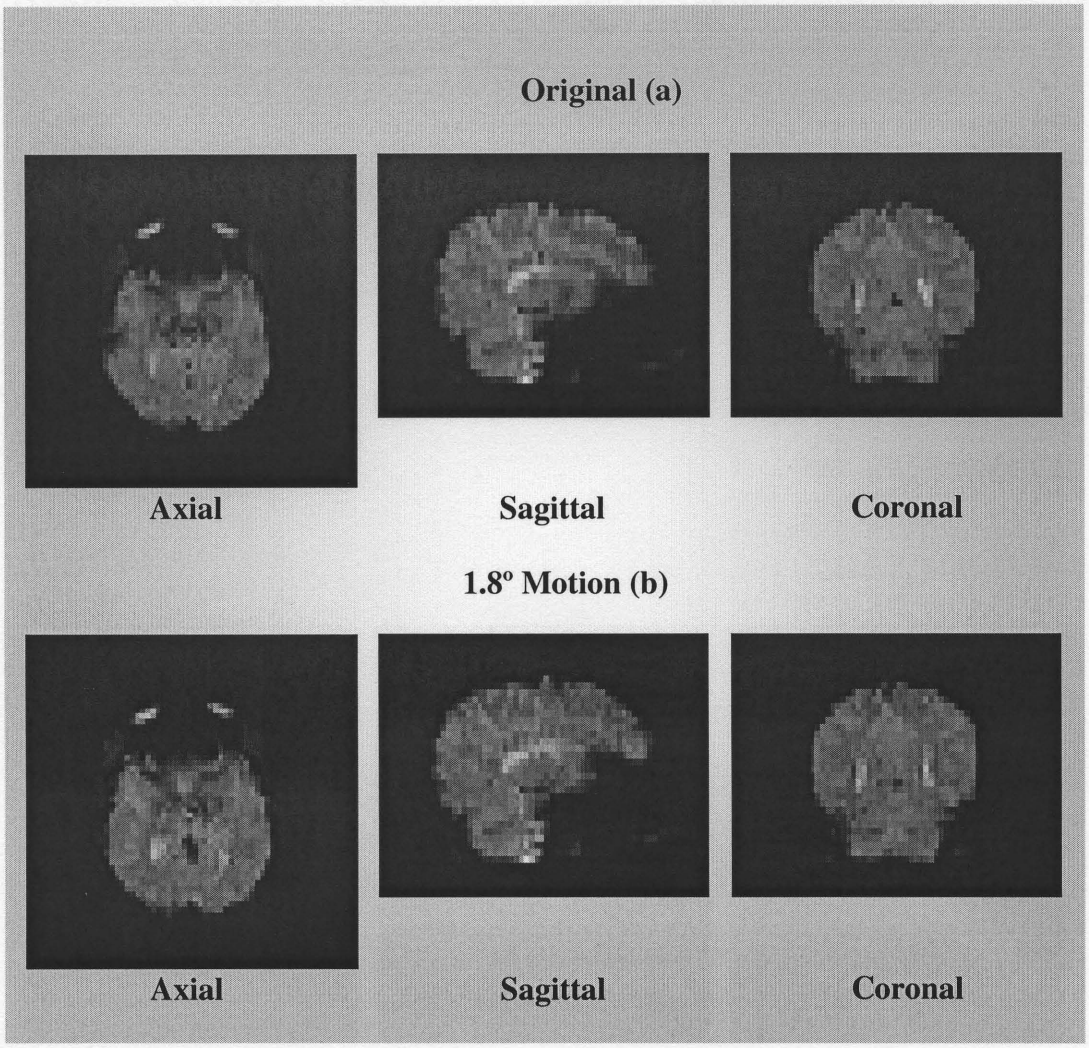

Figure 5.1 Functional MRI Data Shown in three 2D Composite Views (Axial, Sagittal and Coronal)

An original fMRI (a) and the same after a rotation of 1.8 deg about the three axes (pitch, roll and yaw) has been simulated (b) (artificial volume).

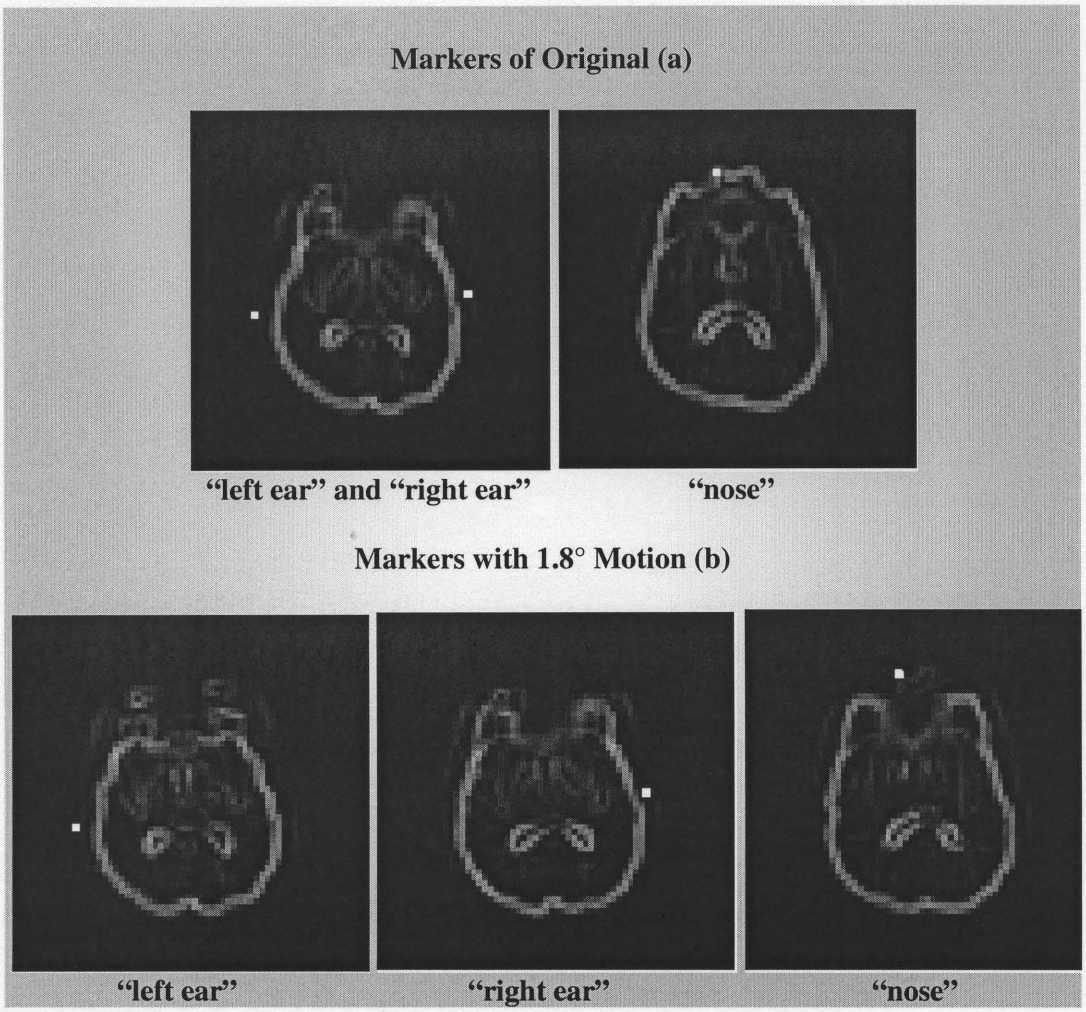

Figure 5.2 Location of Fiducial Markers into the Artificial fMRI

The three fiducial markers (white) were found automatically by AUTOALIGN in the original fMRI (a) and the artificial volume (b).

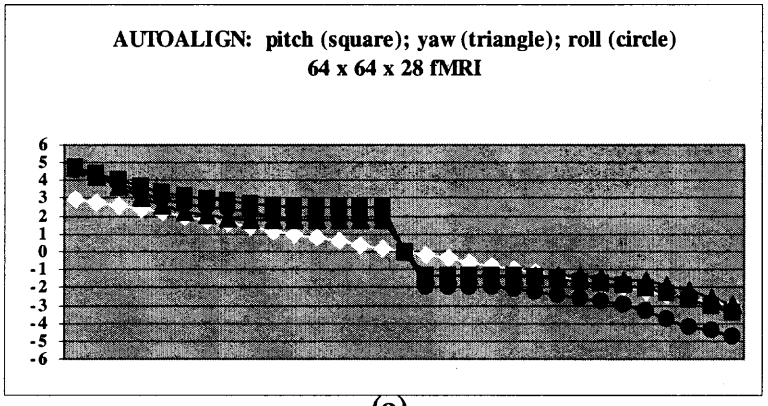

(a)

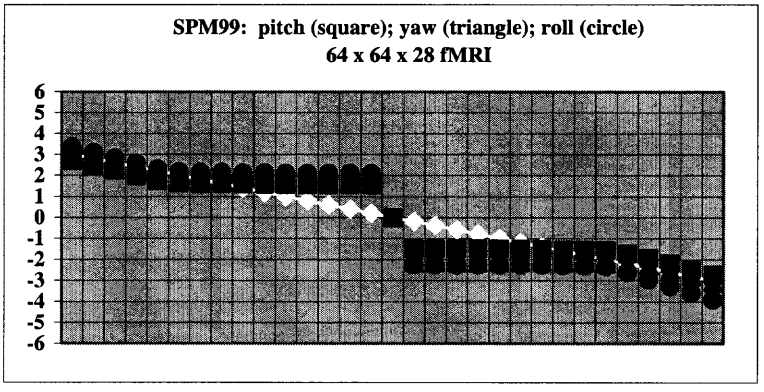

(b)

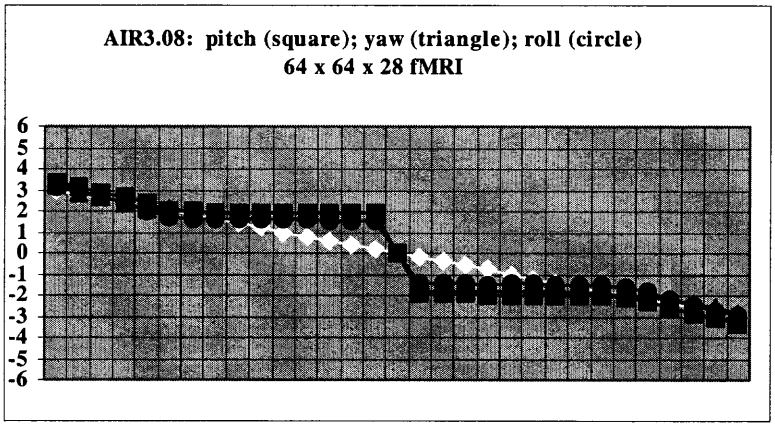

(c)

	"amis" pitch	*"amis" roll*	*"amis" yaw*
AUTOALIGN	*1.55*	*1.23*	*0.96*
SPM99	*1.79*	*0.75*	*0.91*
AIR3.08	*1.44*	*0.418*	*0.58*

(d)

Figure 5.3 Preliminary Analysis

Plot of estimation results of pitch, roll and yaw angles for the artificial fMRI volumes in which motion was simulated at steps of 0.2° in the [-3°, 3°] range; AUTOALIGN (a), SPM99 (b), AIR3.08 (c). For this set of experiments, the average misalignment ("amis") was computed as the average of the sum of absolute differences between desired values (white line) and actual estimations (black lines). Values are shown in (d) and units are in deg. AUTOALIGN overestimation of angles > |2.5°|, relatively to SPM99 and AIR3.08, might be attributable to a different reaction of the algorithm to the interpolation necessary to produce the fMRI volumes.

images between original, as presented in figure 5.1a, and aligned, after tri-linear interpolation has been applied. Difference images were not exactly equal to zero showing that motion artifacts are still present even after alignment (Grootoonk et al. 2000) and that majority of spuriousness are placed along the brain edges (Freire and Mangin 2001).

5.2 Validation with Real fMRI Time Series

Three fMRI time series consisting of 56, 45 and 55 scans each, which for simplicity were called 1st, 2nd and 3rd, were collected with sampling axial resolution of 64 (3.75 mm), 64 (3.75 mm) and 21 (5.00 mm) respectively in the x, y and z directions. These were axial BOLD (Blood Oxygen Level Dependent) MR images acquired with a G.E. 1.5 T Signa Scanner; pulse sequence: echo planar (EPI); TR (Time to Repetition): 4000 msec; TE (Time to Echo): 60 msec; FOV (Field of View): 240 mm. Also, eight time series of 50 scans each with sampling axial resolution of 64 x 64 x 16 (8.00 mm) were used for experimentation. For simplicity they were called exp1-01, exp-02, exp-04, exp-05, exp-06, exp-07, exp-08 and exp-09. These were BOLD MR images acquired with a MAGNETOM VISION Siemens 1.5 T scanner; pulse sequence type: asymmetric spin echo; TR = 2.68 msec, TE = 37.0 msec and FOV = 240 mm (Buckner et al. 2000).

Figures 5.5 and 5.6 show the plot of registration parameters (pitch, roll, yaw in fig. 5.5 and x, y, z in fig. 5.6) estimated by AUTOALIGN (a), SPM99 (b) and AIR3.08 (c) with the 3rd time series consisting of 55 scans. For this set of

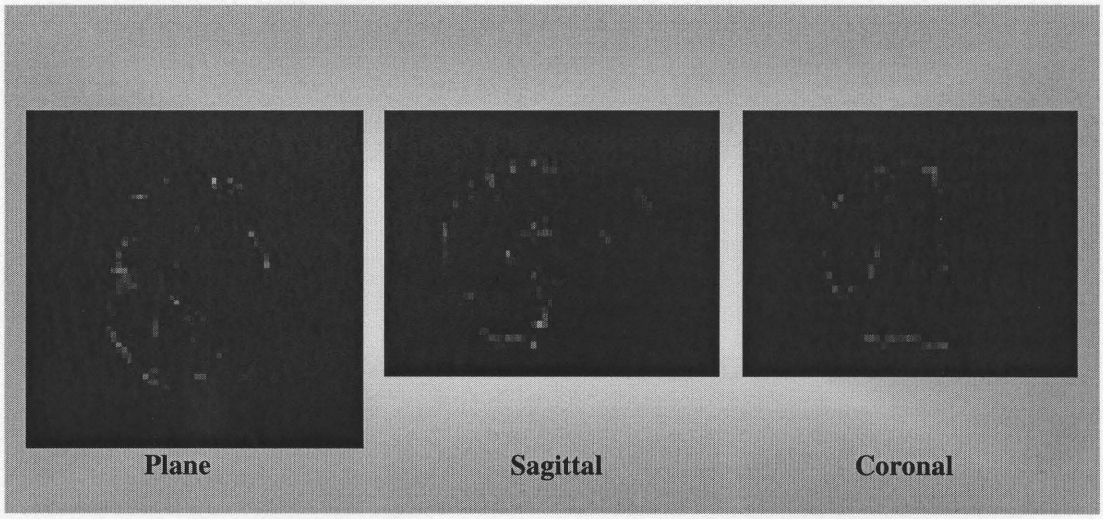

Figure 5.4 fMR Difference Images

They were computed subtracting from the original (shown in figure 5.1a), the corresponding aligned images obtained after AUTOALIGN motion parameter estimation and intensity correction (triliner interpolation).

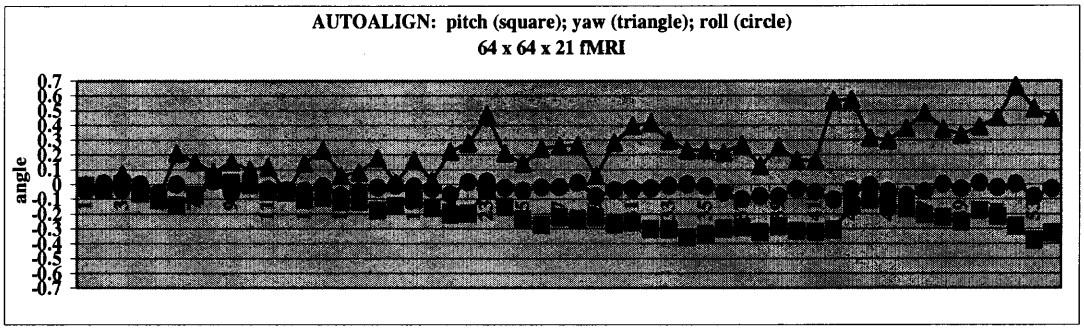

(a)

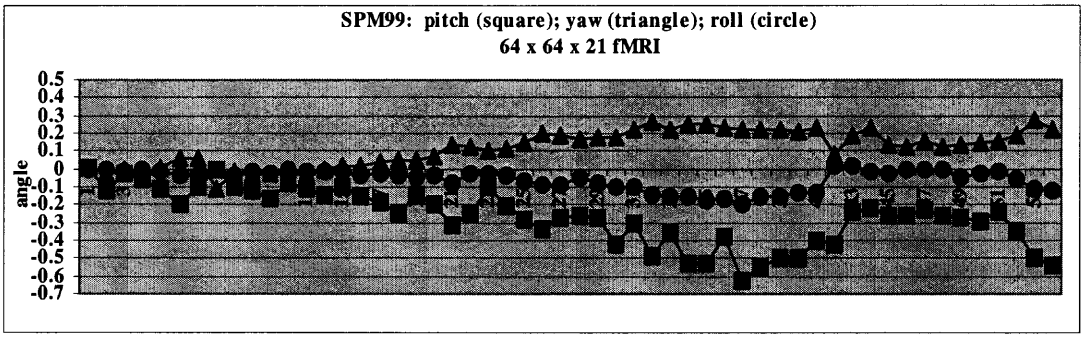

(b)

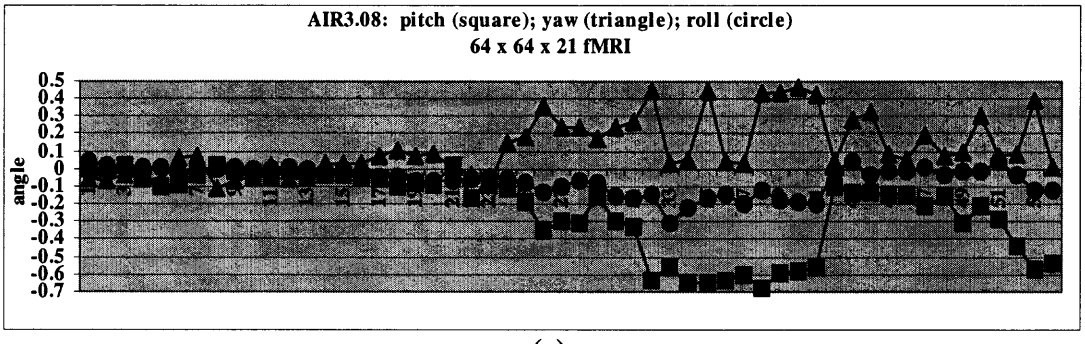

(c)

Figure. 5.5 Angles Estimation Plot with Real fMRI Data

AUTOALIGN (a), SPM99 (b) and AIR3.08 (c) estimations of pitch (■), yaw (▲) and roll (●) angles (units are in deg), with an fMRI time series consisting of 55 scans.

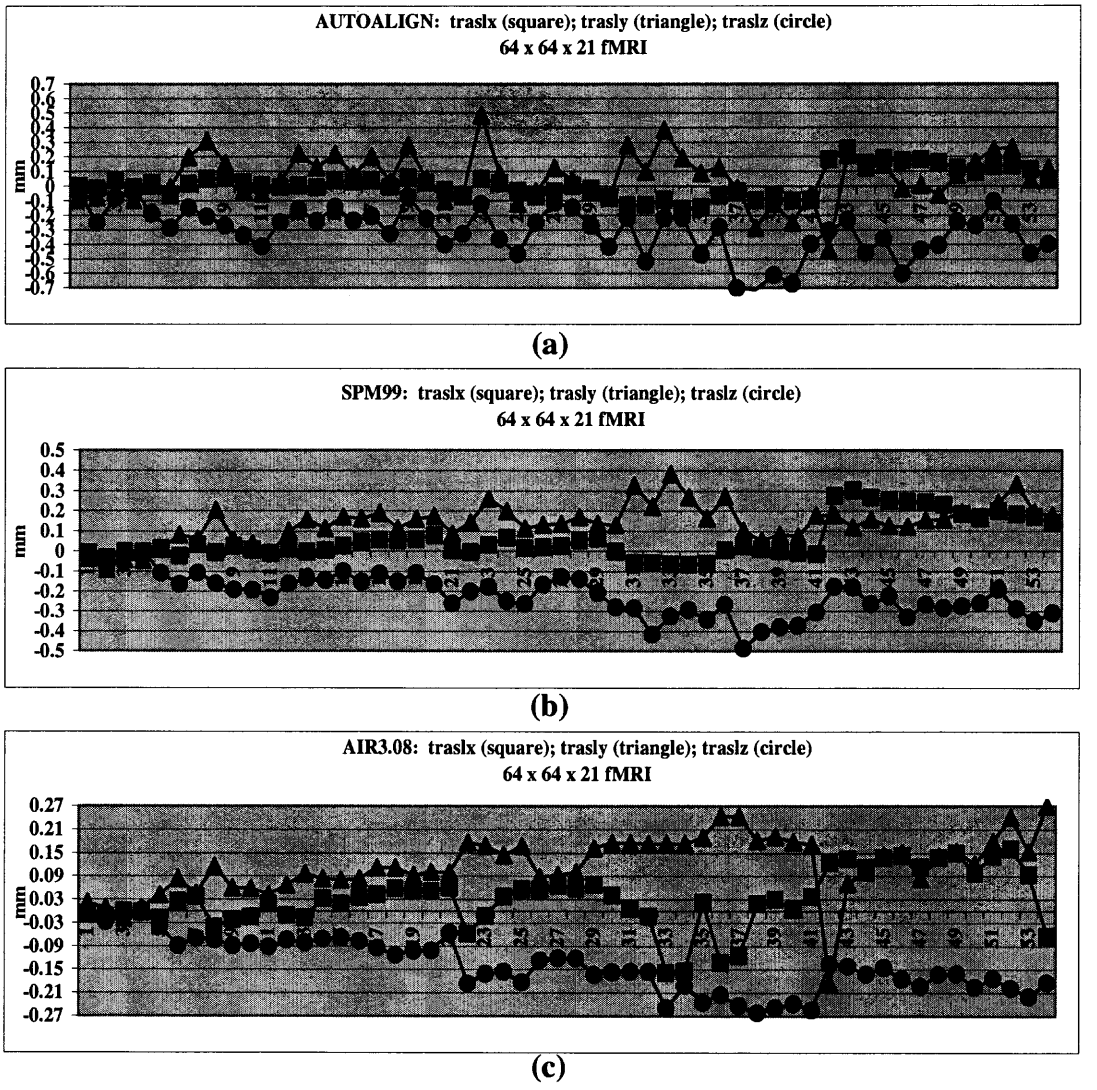

Fig. 5.6 Translation Estimation Plot with Real fMRI Data

AUTOALIGN (a), SPM99 (b) and AIR3.08 (c) estimates of translational movements along the three major axis: traslx (■), trasly (▲) and traslz (●) (units are in millimeters), with an fMRI time series consisting of 55 scans.

Table 5.1 "Amis" Values

They were computed for couple of techniques to estimate the average motion estimation discrepancy expressed in degrees (pitch, roll and yaw) or millimeters (x, y and z). Results are relevant to fMRI time series consisting of 56 (1st), 45 (2nd), 55 (3rd) and 50 (exp1-01, 02, 04-09).

Performance Comparison						
	fMRI 64 x 64 x 21					
AUTOALIGN / SPM99	***x***	***y***	***z***	***pitch***	***roll***	***yaw***
1st	0.03	0.057	0.081	0.126	0.033	0.11
2nd	0.043	0.138	0.087	0.076	0.071	0.181
3rd	0.051	0.105	0.105	0.085	0.049	0.143
	fMRI 64 x 64 x 16					
exp1-01	0.046	0.094	0.118	0.057	0.199	0.091
exp1-02	0.031	0.056	0.097	0.059	0.031	0.09
exp1-04	0.008	0.057	0.034	0.022	0.048	0.046
exp1-05	0.01	0.023	0.071	0.038	0.029	0.087
exp1-06	0.016	0.037	0.05	0.042	0.02	0.17
exp1-07	0.039	0.094	0.036	0.022	0.058	0.074
exp1-08	0.018	0.062	0.038	0.067	0.068	0.058
exp1-09	0.037	0.098	0.148	0.443	0.086	0.325
	fMRI 64 x 64 x 21					
SPM99 / AIR3.08	***x***	***y***	***z***	***pitch***	***roll***	***yaw***
1st	0.045	0.065	0.045	0.044	0.014	0.136
2nd	0.07	0.05	0.032	0.05	0.037	0.061
3rd	0.058	0.07	0.076	0.093	0.037	0.101
	fMRI 64 x 64 x 16					
exp1-01	0.063	0.207	0.063	0.037	0.1	0.026
exp1-02	0.02	0.119	0.034	0.036	0.058	0.055
exp1-04	0.036	0.035	0.045	0.027	0.061	0.013
exp1-05	0.01	0.156	0.034	0.021	0.037	0.026
exp1-06	0.02	0.058	0.025	0.064	0.057	0.015
exp1-07	0.027	0.189	0.02	0.089	0.071	0.064
exp1-08	0.021	0.112	0.023	0.045	0.046	0.017
exp1-09	0.069	0.128	0.207	0.099	0.043	0.065
	fMRI 64 x 64 x 21					
AUTOALIGN / AIR3.08	***x***	***y***	***z***	***pitch***	***roll***	***yaw***
1st	0.045	0.107	0.046	0.156	0.029	0.118
2nd	0.051	0.148	0.112	0.101	0.057	0.229
3rd	0.06	0.144	0.171	0.104	0.078	0.19
	fMRI 64 x 64 x 16					
exp1-01	0.105	0.296	0.172	0.067	0.135	0.09
exp1-02	0.032	0.086	0.093	0.087	0.053	0.095
exp1-04	0.039	0.058	0.076	0.038	0.039	0.043
exp1-05	0.016	0.163	0.047	0.034	0.033	0.079
exp1-06	0.023	0.034	0.068	0.053	0.067	0.178
exp1-07	0.024	0.112	0.033	0.082	0.081	0.108
exp1-08	0.022	0.141	0.05	0.039	0.059	0.07
exp1-09	0.092	0.191	0.16	0.509	0.085	0.357

experiments, "amis" was computed taking into consideration motion parameters estimated by couple of algorithms (e.g. AUTOALIGN / SPM99) and revealed minimal differences across algorithms (order of μm) suggesting reliable and consistent results. Values of "amis" relevant to the eleven time series are shown in table 5.1.

Table 5.2 AUTOALIGN Accuracy Average Values

They were computed across fMRI scans of time series, after alignment.

	A av. ("right ear")	*A av. ("left ear")*	*A av. ("nose")*
1st	*0.131*	*0.133*	*0.216*
2nd	*0.126*	*0.162*	*0.272*
exp1-01	*0.145*	*0.150*	*0.481*
exp1-02	*0.061*	*0.055*	*0.241*
exp1-04	*0.123*	*0.092*	*0.100*
exp1-05	*0.047*	*0.057*	*0.295*
exp1-06	*0.122*	*0.069*	*0.152*
exp1-07	*0.133*	*0.07*	*0.305*
exp1-09	*0.161*	*0.200*	*0.697*

Figure 5.7 shows the plot AUTOALIGN's registration accuracy (A) computed for exp1-08 (a) and 3rd (b). It expresses the measure of worst alignment (Fitzpatrick et al. 1998) and was obtained at the location of the fiducial markers ("right ear", "left ear" and "nose"). Accuracy values across the eleven fMRI time series varied between 0.015 and 0.508 mm ("right ear"), 0.028 and 0.463 mm ("left ear"), 0.08

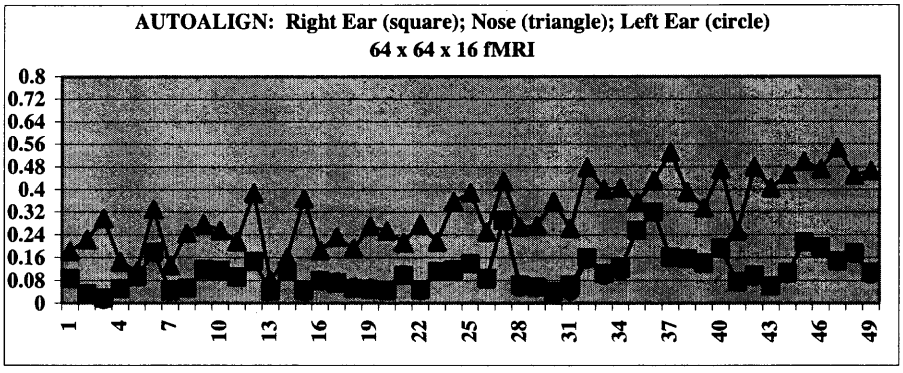

(a)

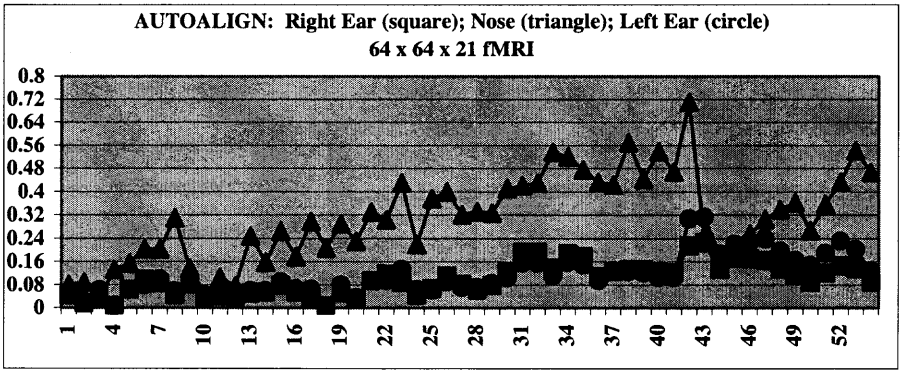

(b)

	A av. ("right ear")	*A av. ("left ear")*	*A av. ("nose")*
exp1-08 (a)	*0.110*	*0.109*	*0.319*
3rd (b)	*0.09*	*0.114*	*0.311*

(c)

Figure 5.7 Plot of Registration Accuracy after AUTOALIGN Motion Correction Data for 50 (a) and 55 (b) fMRI scans. Accuracy is measured in millimeters at the location of the three fiducial markers ("right ear", "left ear" and "nose"), which are the outmost locations with respect with the centroid of alignment and is given as average value across time series (c).

and 1.2 mm ("nose"). Average values across series are reported in figure 5.7c and table 5.2 respectively for exp1-08, 3rd and 1st, 2nd, exp1-01, 02, 04-07, 09. Computational time spent by the three algorithms in order to perform registration and re-slicing of 55 scans was approximately 3 min. (AUTOALIGN), 7 min. (SPM99) and 15 min. (AIR3.08).

Figure 5.8 shows a sample of three axial slices of exp1-02, respectively belonging to reference volume (a) and test volume after AUTOALIGN alignment and trilinear interpolation (b). Figure 5.9 shows gradient images and the three fiducial markers' location (white) as found automatically by AUTOALIGN, respectively for reference (a) and test (b) volumes (prior to alignment) where slices shown in figs. 4a and 4b were respectively contained. Figure 5.10 shows difference images between reference, as presented in fig. 5.8a and test after alignment and trilinear interpolation, as presented in fig. 5.8b. Motion parameters were estimated to be: -0.0187, 0.1275 and 0.064 millimeters respectively for x,y and z; and 0.023, 0.029 and 0.309 deg respectively for pitch, roll and yaw.

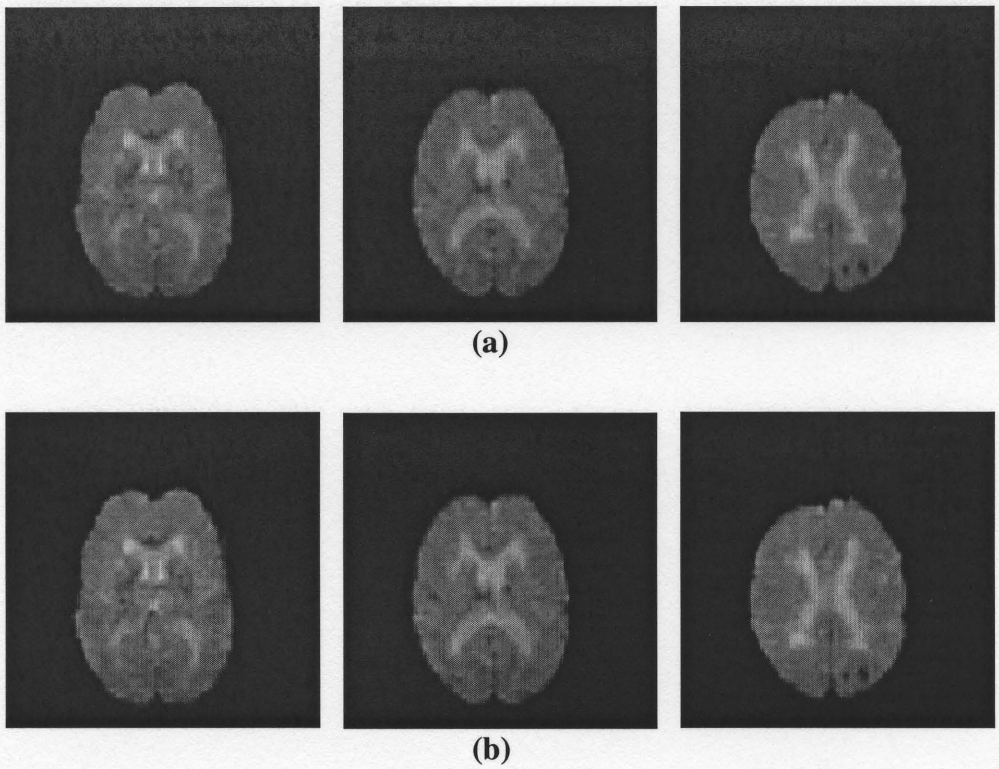

Figure 5.8 Brain Images Before and After AUTOALIGN Alignment

Axial slices of reference (a), and realigned (b) fMRI brain volumes belonging to exp1-02.

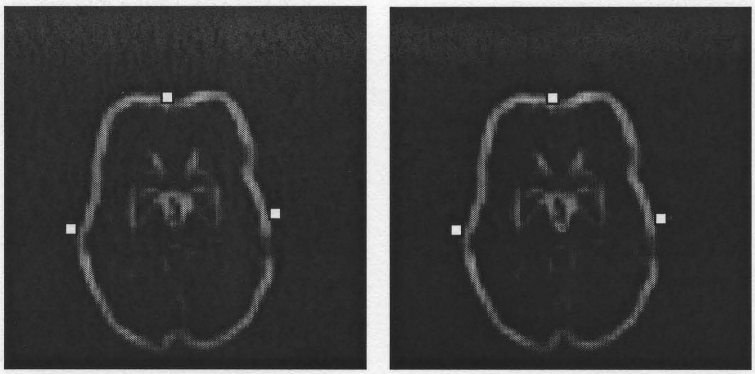

(a) (b)

Figure 5.9 Location of the Three Fiducial Markers into the Real fMRI

Markers (white) were found automatically by AUTOALIGN in reference (a) and test (b) fMRI brain volumes of exp1-02. The volumes were those containing the axial slices shown respectively in figs. 5.8a and 5.8b.

Figure 5.10 Difference Images Obtained with Real fMR

They were computed subtracting from the reference slices shown in fig. 5.8a, those obtained after AUTOALIGN motion correction and trilinear interpolation (shown in fig. 5.8b). Motion related effects are visible.

5.3 Robustness to Noise

A set of experiments was conducted in order to investigate the robustness of AUTOALIGN to noise. The aim was to artificially reproduce changes in signal intensity that might arise during fMRI recordings due to local inhomogeneities of the magnetic field. Twenty brain scans of a 64 x 64 x 28 (x, y and z) time series, previously aligned by SPM99, were used and for each of them the following procedure was adopted in order to simulate noise. Within a cube of 10 x 10 x 10 voxels, placed at the same location in all volumes, each intensity was increased of a random quantity such that the resulting value incorporated 2%, 4%, 8%, 16% and 32% of noise signal.

Thus, for each of above noise levels, artificial time series were produced and aligned to the reference scan. The no-noise condition consisted of the time series aligned by SPM99 for which no manipulation of signal intensity was done and for which motion parameters after alignment were assumed to be equal to zero across scans. Motion parameter values (x, y, z, pitch, roll and yaw), in the noise-condition, were averaged across a time series to show how differently were estimated with respect to the no-noise condition (aligned data). By doing so, it was possible to isolate the effect of random changes in signal intensity on the alignment results and to keep constant other variables like location of intensity changes and head motion.

These experiments were also extended to SPM99 and AIR3.08 and for the three algorithms it was found that performance decreases exponentially with increasing noise level, with AIR3.08 and SPM99 being more robust than AUTOALIGN. Figure 5.11 shows the plot of average values, across time series, of

estimated motion parameters, versus increasing noise levels (2^N; N=1, 2, 3, 4, 5).

This behavior can be understood considering that computation of the tensors of inertia implies using the full image-information content, which gives AUTOALIGN characteristics of an intrinsic registration algorithm, but reduces intensity values to scalars and vectors, thus making the algorithm more sensitive to noise than SPM99 and AIR3.08 are.

However, better robustness to noise can be obtained simply by making the algorithm's feature extraction (vectors and scalars) less dependent on the voxel's intensity. In this regard, an experimental session was performed with the same fMRI and the eigenvectors of inertia were extracted assuming the mass of each voxel as unitary. The formulas used were reported in Ciulla and Deek (2001) as (1) through (9). Though this approach introduces another kind of instability due to the threshold (T) used for segmentation, it shows higher robustness to noise, given that an optimal value of T is chosen. On the other hand, extracting the eigenvectors of inertia considering the voxels' mass equal to the signal intensity, as reported by Ciulla and Deek (2001) in equations (39) – (44), might be preferred in cases of high quality fMRI recording (e.g. relatively low noise images). Figure 5.11d displays the results obtained assuming unitary mass for each voxel (AUTOALIGN-EIGEN with T=10) and shows approximately an 86% (1-0.24/1.8) increase in robustness to noise with respect to the original method (figure 5.11a).

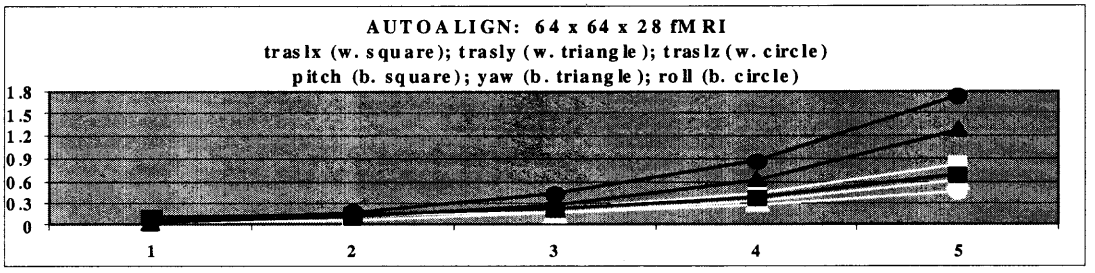

(a)

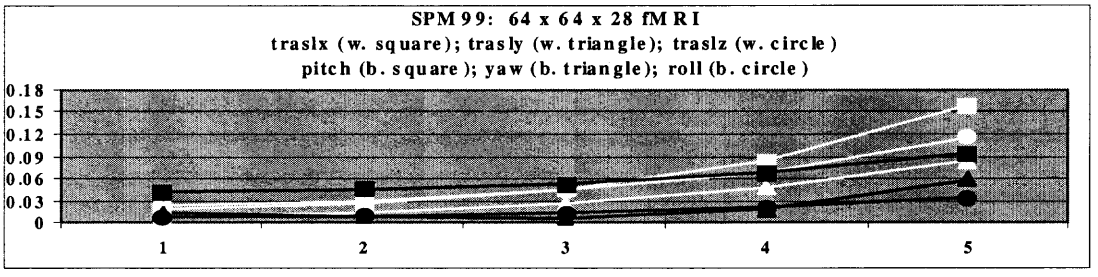

(b)

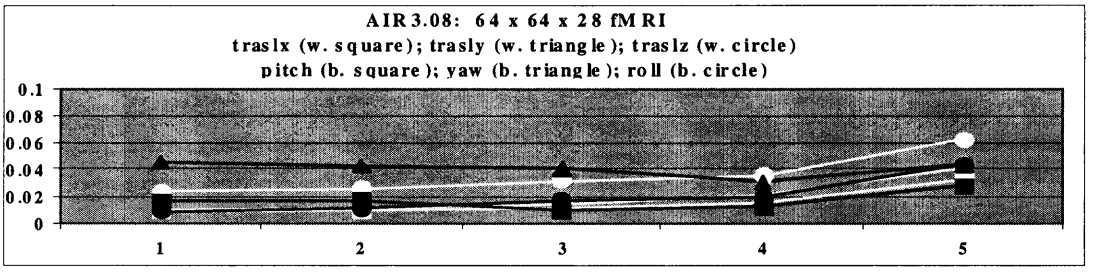

(c)

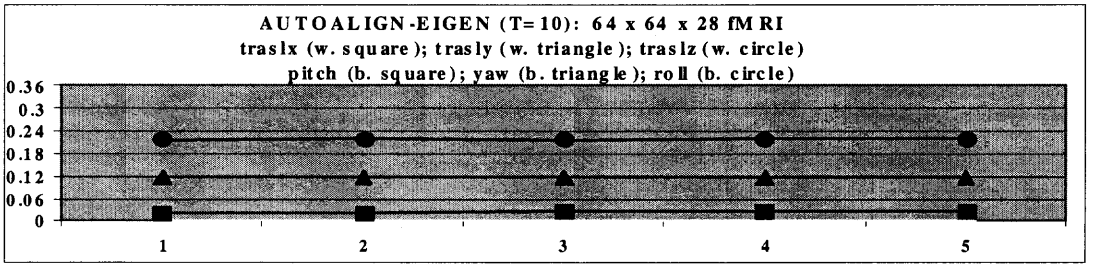

(d)

Figure 5.11 Plot of Average Values of Estimated Motion Parameters Versus Noise Level (2^N where N=1, 2, 3, 4, 5)

AUTOALIGN (a), SPM99 (b), AIR3.08 (c) and AUTOALIGN-EIGEN (d). For each of pitch (■), yaw (▲), roll (●), traslx (white square), trasly (white triangle) and traslz (white circle), values were computed as differences between noise and no-noise conditions. Units are in deg and millimeters.

5.4 Reliability of the Three Points Method

As this research shows, given the physical constraints of the human head, three points are enough to determine a coordinate system for matching purpose. Also, it can be observed that the approach proposed here to identify the direction of the axis of minor resolution of the head coordinate system works better than the tensor-based method proposed by Faber and Stokely (1988). A pre-aligned (SPM99) 64 x 64 x 28 fMRI time series consisting of 68 scans was sub-sampled in the Z-direction (minor resolution) such to obtain volumes with 25, 22, 18 and 14 slices.

By using aligned data, it was possible to isolate the effect of sub-sampling on the determination of the Z-direction of the head coordinate system. Across 68 scans, average values of the unit vectors of the Z-direction were obtained for each sub-sampled time series with two approaches: (i) Z-eigenvector of the volume's inertia matrix (Faber and Stokely 1988) and (ii) Z-axis found as perpendicular to the XY plane (Ciulla and Deek 2001a).

The XY plane is obtained on the basis of X and Y inertia tensors of the volume. The Z-direction needs to be orthogonal to the XY plane and this is assumed to be the ideal condition. For both Z-eigenvector and Z-axis, the average value of the unit vectors obtained with the sub-sampled volume was subtracted from the average value of the unit vectors obtained with 28 slices. Therefore, difference values between original (28 slices) and sub-sampled volume unit vector averages were obtained for volumes having 25, 22, 18 and 14 slices.

Figure 5.12 shows the bar plot of such difference values for unit vectors in the

x (a), y (b) and z (c) directions. They increase with decreasing resolution in both Z-eigenvector (e_z, f_z, g_z; white) and Z-axis (l_z, m_z, n_z; black), but more for the former than the latter, suggesting that worse alignment would be obtained if the Z-eigenvector was employed instead of the Z-axis as Z-direction of the head coordinate system. These results indicate that the estimation of the Z-eigenvector from the inertia matrix degrades with decreasing resolution more than that of the Z-axis. This fact agrees with the work of Faber and Stokely (1988) that described loss of performance with coarser sampling axial resolution and suggests that the three points technique (Ciulla and Deek 2001a) is more reliable in identifying the Z-direction along the axis of minor resolution.

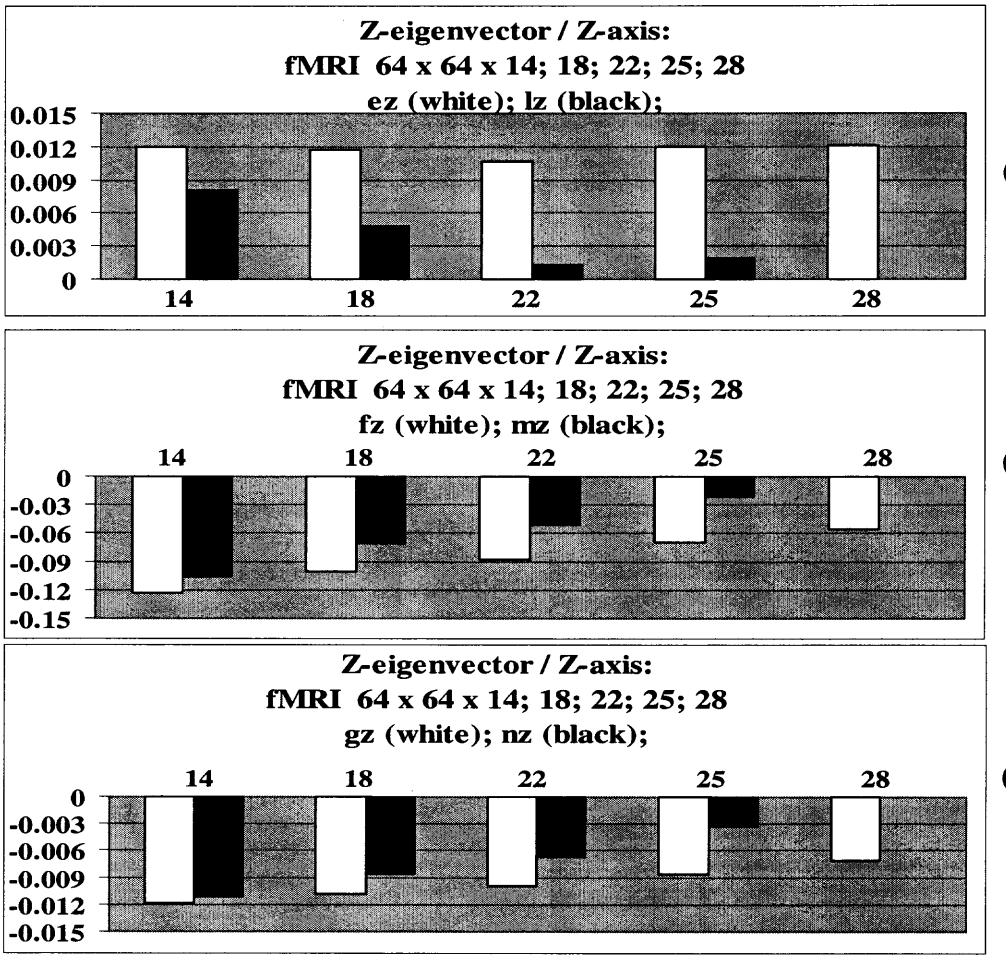

Figure 5.12 Bar Plot of Average Difference Values between Unit Vectors of Z-eigenvector (white) and Z-axis (black)

Values were obtained across time series consisting of 68 fMRI scans. Differences were obtained subtracting from the value of the unit vectors obtained with the 28 slices volume those computed respectively with sub-sampled volumes having 14, 18, 22 and 25 slices. e_z, f_z, g_z (white) and l_z, m_z, n_z (black) were obtained respectively (i) extracting the Z-eigenvector of the inertia matrix and (ii) computing the Z-axis with the three points technique of the AUTOALIGN algorithm.

5.5 Performance Comparison with Existing Algorithms

In this section, presented is a comparative evaluation of performance characteristics based on data presented in chapter 2, that was collected from the literature and that is relevant to established registration algorithms. For each of the algorithms, three factors were considered: (i) accuracy; (ii) computational time and (iii) resolution. Values of these factors are reported in tables 5.3, 5.4 and 5.5 and were scaled to the range [0 1] in order to compute a performance coefficient in the following form:

$$P = (1-\alpha) * (1-\tau) * (1-\rho) \qquad (5.2)$$

Small values of accuracy (α), computational time (τ) and resolution (ρ); all tend to increase P. Thus, a high value of performance coefficient (P) represents a weighted index of high accuracy (small α), short computational time (small τ) and small resolution (ρ). The choice of this formula was motivated by the fact that in general, registration algorithms needs to be as much accurate as possible, computationally fast and that small resolution pose limitations to high values of accuracy. Therefore, a performance coefficient in this form wants to reward algorithms capable to reach high accuracy of alignment of small resolution brain volumes, with low computational cost. Tables 5.3, 5.4 and 5.5 show results obtained computing the P value for each modality and group algorithms in (i) voxel-based and maximization of mutual information (table 5.3); (ii) surface (feature, anatomical landmark, segmentation) based (table 5.4) and (iii) fiducial markers and moment-based algorithms (table 5.5). Though the present approach proposes an index aimed to measure performance of a registration algorithm, any comparative evaluation of performance across algorithms needs to be based on

same brain volumes and same registration (e.g. MRI) or co-registration problem (e.g. CT-MR). An excellent example of this type is constituted by the work of West et al. (1997).

Table 5.3 Performance Coefficient (P) of VB and MMI Approaches

Author	*Modality*	*Accuracy*	*Time*	*Resolution*	*Method*	*Perf. (P)*
Van den Elsen et al. (1994)	CT-MR	(Med. Val. Ref. to GS) 1.6 mm	1-2 hours	512 x 512 x (28;34) 256 x 256 x (20;26)	VB	0.2343
Friston et al. (1995)	fMRI PET MRI	100 μm	Order of minutes	64 x 64 x 5.0 mm 256 x 256 x 118 128 x 128 x 43	VB	0.9969 0.4649 0.9872
Woods et al. (1993)	PET-MR	(Med. Val. Ref. to GS) 2.3 mm	20 - 30 min	512 x 512 x (28;34) 256 x 256 x (20;26)	VB	0.5162
Woods et al. (1998a, 1998b)	MRI	< 2.00 mm < 0.5 mm	26 - 323 sec. 2.8 - 13 min	128 x 128 x 15		0.5817 0.8089
Woods et al. (1992)	PET	< 1.745 mm	3 – 6 min	128 x 128 x 15	VB	0.6926
Collignon et al. (1995a, 1995b)	CT-MR PET-MR	(Med. Val. Ref. to GS) 1.5 mm 3.6 mm	10-30 min	512 x 512 x (28;34) 256 x 256 x (20;26) 128 x 128 x 15	MMI	0.2908 0.3644
Hill et al. (1993, 1994)	CT-MR PET-MR	(Med. Val. Ref. to GS) 1.2 mm 3.2 mm	20 min	512 x 512 x (28;34) 256 x 256 x (20;26) 128 x 128 x 15	MMI	0.3001 0.3850
Maes et al. (1999)	CT-MR	0.5-3.1 mm	91-2,597 sec	256 x 256 x 128 512 x 512 x 48	MMI	0.1117

Table 5.4 Performance Coefficient (P) of FB, ALB and SB Approaches

Author	*Modality*	*Accuracy*	*Time*	*Resolution*	*Method*	*Perf. (P)*
Maintz et al. (1995, 1996b, 1997)	CT-MR PET-MR	(Med. Val. Ref. to GS) 5.1 mm 3.5 mm	1-12 hours 40 minutes	512 x 512 x (28;34) 256 x 256 x (20;26) 128 x 128 x 15	FB	0.0001 0.3291
Jiang et al. (1992a, 1992b)	CT-MR PET-MR	(Med. Val. Ref. to GS) 5.7 mm 4.0 mm	3-20 min	512 x 512 x (28;34) 256 x 256 x (20;26) 128 x 128 x 15	FB	0.0003 0.2618
Hogan et al. (1995)	CT-MR	0.9-8.0 mm	40 min	0.859 x 0.859 x 1.5 mm 128 x 128 x 96	FB	0.7181
Hill et al. (1991)	MRI CT	< 2 mm	1 min	256 x 256 x 52	FB	0.5069
Maguire et al. (1991)	CT-MR	(Med. Val. Ref. to GS) 3.3 mm	15-30 min	512 x 512 x (28;34) 256 x 256 x (20;26) 128 x 128 x 15	ALB	0.1577
Lemoine et al. (1994)	CT-MR PET-MR	(Med. Val. Ref. to GS) 1.6 mm 4.6 mm	15 min	512 x 512 x (28;34) 256 x 256 x (20;26) 128 x 128 x 15	SB	0.2753 0.1706
Malandain et al. (1994a, 1994b, 1995)	CT-MR PET-MR	(Med. Val. Ref. to GS) 4.3 mm 4.2 mm	3 min 40 sec	512 x 512 x (28;34) 256 x 256 x (20;26) 128 x 128 x 15	SB	0.0956 0.2374
Pellizzari et al. (1989)	CT-MR PET-MR	(Med. Val. Ref. to GS) 2.7 mm 2.9 mm	20 min	512 x 512 x (28;34) 256 x 256 x (20;26) 128 x 128 x 15	SB	0.2000 0.4312

Table 5.5 Performance Coefficient (P) of FIB and MB Approaches

Author	*Modality*	*Accuracy*	*Time*	*Resolution*	*Method*	*Perf. (P)*
Maurer et al. (1997)	X-ray CT MR	0.5 mm (500 μm)	10,000 steps Algorithm. With 87 sec (CT) and 18 sec (MR) as time to find markers (Wang et al. 1996).	512 x 512 x (28-55) 256 x 256 x (26-55)	FIB	0.4128 0.7003
Ciulla and Deek (2001)	fMRI	< 0.697 mm	3 min (55 vol.), 3.27 sec (2 vol.)	64 x 64 x 21	FIB / MB	0.8916
Alpert et al. (1990)	PET MR	1 mm	2 min.	256 x 256 x 63	MB	0.6009

CHAPTER 6

DISCUSSION

6.1 Performance of Algorithms for Brain Image Rigid Registration

Recent investigation (Fitzpatrick et al. 1998a; Fitzpatrick and West 2001; West et al. 2001) has formulated a mathematical basis for assessing accuracy of fiducial-based algorithms and has shown that in order to ensure successful registration, number of markers, markers configuration and localization into the brain images are the issues to be resolved. Earlier, Maurer et al. (1997) devised a bone implanted registration method which uses the algorithm proposed by Wang et al. (1996) in order to automatically localize fiducials and implements the closed-form solution proposed by Arun et al. (1987) in order to fit two three-dimensional point sets. Results of Maurer et al. (1997) could then be assessed with the theory provided by Fitzpatrick et al. (1998a) and used by West et al. (1997) to conduct a comparative evaluation covering registration performance of several classes of algorithms with CT-MR and PET-MR data.

Within the evaluation, results of Maurer et al. (1997) constituted the "gold standard" to which several studies (van den Elsen et al. 1994; Woods et al. 1992, 1993; Collignon et al. 1995a, 1995b; Hill et al. 1993, 1994; Studholme et al. 1995; Hemler et al. 1995; Maintz et al. 1995, 1996b, 1997; Jiang et al. 1992a, 1992b; Maguire et al. 1991; Lemoine et al. 1994; Malandain et al. 1994a, 1994b, 1995; Pellizzari et al. 1989) compared performance of their algorithms. Results of West et al. (1997) indicated that for CT-MR registration several algorithms: voxel-based

(van den Elsen et al. 1994), MMI (Collignon et al. al. (1997) indicated that for CT-MR registration several algorithms: voxel-based (van den Elsen et al. 1994), MMI (Collignon et al. 1995a, 1995b; Hill et al. 1993, 1994 and Studholme et al. 1995), feature-based (Hemler et al. 1995), segmentation-based (Lemoine et al. 1994) cumulated a median accuracy less or equal to 1.6 mm, while for PET-MR registration a median accuracy less or equal to 2.9 mm was obtained with voxel-based (Woods et al. 1993) and segmentation-based (Pellizzari et al. 1989) algorithms.

A subsequent classification made by West et al. (1999) divided registration methods into two groups: volume-based and surface-based. Techniques that use relationships between voxel's intensity to perform registration were classified as volume-based. Techniques that minimize the distance measure between two corresponding surfaces in the images to be matched were classified as surface-based. Concurrently, the evaluation reported by West et al. (1999) was based on results obtained earlier (West et al. 1997) and revealed that volume-based techniques perform with better accuracy than surface-based techniques within CT-MR registrations and give slightly better accuracy within PET-MR registrations.

Accordingly, the literature survey done within this dissertation, confirms the general tendency of voxel-based algorithms to outperform surface-based (e.g. features, anatomical landmarks) and segmentation-based algorithms. Such tendency is found within co-registration problems like CT-MR and PET-MR, as West et al. (1999) reported, but also in within-modality registrations like MRI, fMRI and PET, as supported by results obtained by Friston et al. (1995).

Common denominator in the evaluation of West et al. (1997, 1999) was that for CT-MR registration the most used (van den Elsen et al. 1994; Collignon et al. 1995a, 1995b; Hill et al. 1993, 1994; Studholme et al. 1995; Lemoine et al. 1994) optimization criterion was the Powell method leading to long computational sessions (up to 2 hours). Consistently, another comparative evaluation done by Maes et al. (1999) focused on optimization strategies for multi-resolution mutual information registration and reported that great advantages in term of reduction of computational time, with respect to the Powell method (best suited for single resolution), can be achieved with more efficient iterative processes based on simplex, conjugate-gradient and Levenberg-Marquardt methods, leading to registration performed with sub-voxel accuracy in less than 5 min. The Levenberg-Marquardt method was found to be fast also by other studies (Thevenaz et al. 1998a; and Thevenaz and Unser 2000). Reasonable processing time was reported using the Newton method as optimization strategy (Woods et al. 1993), though the size of PET-MR registration is usually smaller than that of CT-MR registration.

Wells et al. (1995, 1996) suggested that mutual information, as similarity measure derived from joint-entropy, provides some advantages over the latter. Holden et al. (2000), extending previous work (Woods et al. 1998a; Woods 2000a), aimed to an evaluation of voxel similarity measures. Using MR volumes they have shown that measures based on joint-entropy (e.g. mutual information), which do not require assumptions about the form of relationship between voxel's intensity, performed better than those based on correlation (which on the other hand require

linearity of relationship), leading to very high registration performance in terms of accuracy.

In agreement with Woods (2000a), this dissertation suggests that for within-modality registration voxel-based algorithms, other than those based on MMI, the similarity measure that is mostly accompanied by best accuracy (Friston et al. 1995; Hajnal et al. 1995; Nikou et al. 1998) is that based on intensity differences. On the other hand, mutual information remains one of the most successful voxel's similarity measures for inter-modality registration (Hill and Hawkes 2000). Though was reported by Maintz and Viergever (1998) that surface-based techniques are faster than voxel-based algorithms, computational time data shown in tables 2.2 through 2.6 is not prone to such generalization.

Also, while Maintz and Viergever (1998) reported phantom to be the most popular among the validation approaches, this dissertation finds most used both artificial data with controlled motion and images of the Vanderbilt medical database. While phantom validation is more useful for within-modality studies than it is for between-modality, controlled motion can be very useful in order to improve registration performance, but presents the disadvantage of being an approximation of real settings (Woods 2000b). Finally, this dissertation finds that little work (Betting and Feldmar 1995) has been done for MR-X-ray co-registration and suggests that this type of application might require future effort.

6.2 Creation of the AUTOALIGN Technique

Medical image registration algorithms can be divided into two main categories: extrinsic and intrinsic. Extrinsic registration is applicable by means of foreign objects introduced into the imaged space such as fiducial markers methods (Maurer et al. 1997). Intrinsic registration is applicable through the image transformation as generated by the subject such as anatomical landmarks (Cox 1996) or by mutual information (Wells and Viola 1996; Studholme et al. (1996); Maes et al. 1997; Meyer et al. 1997; Studholme et al. 1997; Thevenaz et al. 1998, 2000; Holden et al. 2000) or by principal axes (Faber and Stokely 1988; Alpert et al. 1990). Since extrinsic methods by definition cannot include patient-related image transformation, the nature of the registration transformation is often restricted to being rigid (translations and rotations). Intrinsic registration methods are more prone to handle the assumption of motion that is not governed by rigid-body transformations.

Excellent registration results have been obtained with either two (Dobbins et al. 1993), or four (Arendsen et al. 1991; Bellers et al. 1993) fiducial markers in the case of registration of computed radiography (CR), or more in the case of registration of MRI (Maurer et al. 1997). With automated algorithms, independent from fiducial or anatomical markers, the general factor limiting the overall accuracy is image noise (Althof et al. 1997) and interpolation (Grootoonk et al. 2000).

On the basis of the above findings this dissertation has developed and compared 3-fiducial markers and principal axes transformation algorithms. The

algorithms are based on the assumption that the human brain is subject to rigid motion during different scanning periods. This was also assumed by previous research (Pellizzari et al. 1989; Woods et al. 1992, 1993, 1998a, 1998b). As far as the determination of the head coordinate system, a method was proposed that use two anatomical landmarks (the anterior and the posterior commissure) to build a Talairach-Tournoux coordinate system (Cox 1996). Besl and McKay (1992) showed that the position of the head into the scanning volume might be determined by a set of points.

On the other hand, it has been shown that in order to determine a head coordinate system with high degree of reliability, only 3-fiducial markers are needed. As far as the registration transformation is concerned, methodologies were evaluated on the basis of the assumption that given a reference volume, a unique coordinate transformation can be found, that if applied to the test volume, makes a perfect alignment to the reference volume (Woods et al. 1992, 1993, 1998a, 1998b). To find the coordinate transformation, the inertia matrix of the volumes was computed as illustrated in literature (Alpert et al. 1990) and also 3-fiducial markers were used (Ciulla 2000).

Ciulla and Deek (2001a) obtained good results by the principal axes transformation method with both low-resolution T2*-weighted Magnetic Resonance (MR) and T1-weighted MR images. Also, good results were obtained with high-resolution T1-weighted MR images when the coordinate transformation was retrieved on the basis of the coordinate system identified by the 3-fiducial markers (ALIGN). Even though ALIGN method was tested for mono-modal

images, it is theoretically applicable to cross-modality registration as well as the principal axes methods (EIGEN and AUTOALIGN) provided that the same amount of brain or head are included for image matching. The only constraint of ALIGN is that care must be employed to ensure that the 3-fiducial markers are placed and localized at the same position for each modality.

It has been seen that previous work (Maurer et al. 1997) uses implanted fiducial markers to register couple of volumes and therefore an automated algorithm for the localization of the markers was developed (Wang et al. 1996). On the basis of above knowledge and considering that common practice (e.g. for research or diagnosis) markers cannot be implanted nor accurately placed at the same position all times, a new technique (AUTOALIGN) has been developed that finds automatically 3-fiducial markers and results of registration for low-resolution fMRI have been presented (Ciulla and Deek 2001a). Thus, the ALIGN method assumed only theoretical validity because it showed the accuracy obtainable when the fiducial markers are placed at the same position at all times. AUTOALIGN on the other hand, combines the theoretical basis of EIGEN and ALIGN, and automatically finds three points to be adopted as markers, thus overcoming the limitations of ALIGN and exploiting the accuracy of EIGEN.

AUTOALIGN technique has been derived by merging together the theoretical basis used successfully by Ciulla et al. (1996, 1999) in order to define a head coordinate system, with the work presented by other authors (Faber and Stokely 1988; Alpert et al. 1990; Maurer et al. 1997). The principal axes transformation method provides with the directions along which we can search for the 3-fiducial

markers. However such a method is dependent on an arbitrary threshold to roughly segment the human brain. Therefore, voxel's coordinates were weighted with their intensity so that the method became independent from any arbitrary thresholds. By taking the third order gradient of the fMRI volume, the borderline between head structures and regions of the volume outside the brain has been detected. Scanning along two of the principal axes directions and finding the intersections between those directions and the borderline of the head, furnished 3-fiducial markers.

Results obtained by Ciulla and Deek (2001a) with T2*-weighted Magnetic Resonance (MR) were compared to those obtained by the Statistical Parametric Mapping (SPM99). It was found that: (i) SPM is more reliable than AUTOALIGN in the estimation of small movements [-3°; 3°]; (ii) AUTOALIGN is more reliable than SPM in the estimation of large movements (>5°).

6.3 AUTOALIGN Algorithm

6.3.1 Background

Earlier Ciulla and Deek (2001a) developed a registration method called ALIGN that uses a coordinate system obtained by three non-collinear fiducial markers. Several simulations were performed with both fMRI and MRI data to show how accurate registration results can be if markers are localized at the same position across images. Also another registration method called EIGEN was developed and tested with the same dataset to confirm that fast and reasonably accurate results can be obtained by moment-based approaches.

Thus, in order to devise a new, fast and accurate registration algorithm (AUTOALIGN), accuracy of point-based registration has been merged with the speed of computation of tensor-based registration. The gradient (Maintz et al. 1996b) of the fMRI volume has been used to identify the outermost surface of the head structures, where markers are screwed (Maurer et al. 1997) and localized (Wang et al. 1996). The tensor-based method (Faber and Stokely 1988) has been used to identify directions along which to scan and search for three points to be adopted as fiducial markers. In the present version of the algorithm, trilinear interpolation has been used to perform intensity correction.

6.3.2 Testing and Validation

AUTOALIGN was preliminarily tested with fMR images in which, simulated and controlled motion has been introduced. Simulated motion is a very common intuitive and straightforward validation approach. However, because it is only an approximation of real settings, it does allow inferring an estimate of quantitative accuracy for an algorithm but not to compare algorithms' estimates with each other (Woods 2000). This constitutes a limitation of the testing paradigm and in general it is attributable to the fact that synthetic data reproduce only by approximation factors influencing algorithm's accuracy. Since different algorithms might react differently to these factors, synthetic data contributes to adding another source of variability to the results. Within the preliminary testing performed by this research, a factor that has determined an approximation of reality was the interpolation used to produce (i.e. re-slice) the artificial data.

In the context of validation, AUTOALIGN motion estimates with real fMRI time series were compared to those obtained with the same dataset by the Statistical Parametric Mapping (Friston et al. 1995) and the Automatic Image Registration (Woods et al. 1998a, 1998b), which are among the most used methods of motion correction in functional imaging laboratories. Within this context, above two voxel-based algorithms assumed then the role of reliable gold standard. Therefore, the value constituted by the similarity between the motion estimates of the three algorithms plays in favor of AUTOALIGN, being the latter a less established method.

6.3.3 Robustness to Noise

Contrary to other voxel-based methods (Friston et al. 1995; Woods et al. 1998a, 1998b), AUTOALIGN does not assume any particular relationships between voxel intensities across brain images. However, it makes reduction of intensity values to scalars and vectors, and our simulations show that its performance is affected by noise sensibly more than SPM99 and AIR3.08, which use the full image information content.

Simulations aimed to investigate the effect of noise (e.g. magnetic field inhomogeneity) on the extraction process of similarity measures between brain images (AIR3.08 and SPM99) and scalars and vectors (AUTOALIGN) and were performed by keeping constant variables like head motion and location of signal intensity changes. Similarly, within one of the theoretical models of a mathematical framework aimed to describe magnetic field inhomogeneities, Andersson et al.

(2001) assumed fixed location of signal intensity changes with respect to the scanner.

However, with regard to the model formulated by Andersson et al. (2001), which assumed noise due to inhomogeneities distributed across the entire Field of View, simulations of this research assumed location of intensity changes restricted to a limited region of the FOV. Such location is shown in Figure 6.1. Though such an assumption is theoretical in its nature, it allows investigating behavior of the registration algorithms relatively to a region smaller than the FOV, thus revealing local robustness. It is expectable to have similar but not necessarily same robustness if the region of intensity changes is located somewhere else in the FOV.

AUTOALIGN robustness to noise can be increased by computing the tensors of inertia, used to localize the markers into the brain images, with the assumption that each voxel has unitary mass (Ciulla and Deek 2001a). As the experiments suggest, this solution might be preferred in those cases for which fMRI is not of high quality relatively to noise.

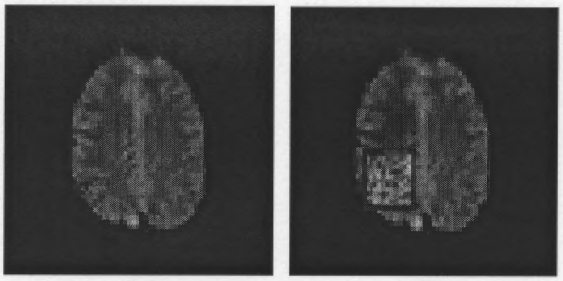

(a) (b)

Figure 6.1 Location of Intensity Changes Used for Noise Simulations (N=5) (a) Original fMRI; (b) Image obtained adding (inside the square) 32% random noise to the intensity values.

6.3.4 The Axis of Minor Resolution

It was known that the tensor-based method is sensitive to low sampling axial resolution (Faber and Stokely 1988). This research performed experimentation, controlling for head motion, to study the effect of lowering resolution on the determination of the Z-axis. The latter was the axis of minor resolution of the brain volumes. It was shown that higher reliability, with respect to the Z-eigenvector, is obtained by using as Z-axis of the head coordinate system the one found on the basis of normality constraints.

6.3.5 AUTOALIGN Point-Based Registration

The issue of finding a point-based rigid transformation between brain images has been fully explored (Fitzpatrick et al. 1998; West et al. 2001) and mathematical formulation has been given to show that accuracy of fiducial-based registration depends on number of markers, their configuration and localization error across images (Fitzpatrick and West 2001).

According to Fitzpatrick et al. (1998), the optimal fiducial configuration is the one for which fiducials are placed at the ellipsoidal isocontours of TRE^2 (Target Registration Error). If more fiducials are added to the configuration, TRE^2 gets smaller only if their root-mean-square distance to the three principal axes of the configuration remains constant. On the basis of such knowledge and considering that at least three non-collinear points are necessary to find the matching transformation (Arun et al. 1987), a simple and straightforward approach to retrieve a head coordinate system has been developed (Ciulla and Deek 2001).

AUTOALIGN uses three fiducials that lie on two of the principal axes of their configuration, and therefore constitutes a practical application in fMRI of a particular case covered by the work of Fitzpatrick et al. (1998). While previous research (Wang et al. 1996) developed a method to localize externally attached markers, this research has used two tensors of inertia to localize automatically points obtained on the basis of the image content. Thus, AUTOALIGN has been given some properties of an intrinsic algorithm, though the matching transformation is found by a point-based approach.

6.3.6 Types of fMRI Motion Related Effects

Friston et al. (1996) made distinction between movement related effects in the fMR images that are function of the subject's head location in the scan of reference and the previous scans (e.g. the spin history effect) and clearly showed that motion related artifacts still exists into the images even if the alignment is ideal (i.e. perfect).

Given the magnitude (4000 msec) of the TR (Time to Repetition) used for data collection of the time series named 1^{st} 2^{nd} and 3^{rd}, motion related effects produced by the spin history excitation can be considered negligible (Grootoonk et al. 2000). On the other hand, for those time series named exp1-01, 02, 04-09, the TR was as short as 2.68 msec (Buckner et al. 2000). Thus, the spin excitation history might have had an effect on the fMR images.

AUTOALIGN motion correction concerned with those effects that are relevant to the subject's head position in the frame of reference. For such motion, the work

presented by Grootoonk et al. (2000) shows that even in case of ideal alignment, artifacts are left into the images and are attributable to the approximate nature of interpolation. Other motion artifacts that are attributable to magnetic field inhomogeneities at different positions in the scanner were studied by Andersson et al. (2001), but were not studied by the present research.

CHAPTER 7

CONCLUSION

7.1 Algorithmic Performance in Brain Image Rigid Registration

Comparison between alignment techniques can be done, within either a registration or a co-registration application (e.g. PET-MR), using exactly the same brain images with all of the algorithms. This requirement is most likely to be satisfied by planned experiments of the type done by West et al. (1997, 1999). Also, to assess performance across algorithms, a reliable reference needs to be adopted. The "gold standard" of Maurer et al. (1997) constitutes an example of this type. Bearing in mind above statements, it can be concluded presenting the general trend that has emerged in this dissertation's literature review. Extrinsic methods based on fiducials have the potential to offer high accuracy for both registration and co-registration applications and also their performance characteristics have been mathematically ascertained (Fitzpatrick et al. 1998a; Fitzpatrick and West 2001; West et al. 2001). Intrinsic algorithms have more limited capacity, than extrinsic methods, the latter being constrained by the type of registration problem. Both voxel-based (e.g. using intensity differences as target function) and mutual information based algorithms outperform surface-based and segmentation-based methods and offer best performance respectively in registration and co-registration applications.

7.2 AUTOALIGN Technique Characteristics

Main aim of this dissertation was to create a new methodology for the alignment of fMRI time series. In this regard, point-based registration was merged with moment/principal axes methodologies. Table 7.1 shows the steps involved in each of the registration methodologies (Faber and Stokely 1988; Alpert et al. 1990; Maurer et al. 1997) from which AUTOALIGN had been derived. Also, it shows differences between methodologies at each step.

Literature shows that point-based registration is more accurate than principal-axes/tensors based registration (Maintz and Viergever 1998). Therefore, "step 3" shown in table 7.1 and used by Maurer et al. (1997) and Ciulla and Deek (2001a) allows, at least potentially, obtaining results superior to those of Faber and Stokely (1988) and Alpert et al. (1990).

In order to free AUTOALIGN from the limitation that arise performing threshold (T) segmentation (pre-processing "step 1" of table 7.1), it is possible to compute the eigenvectors of inertia including all voxels in the volume and considering their mass equal to their intensity. Thus, "step 1" of Faber and Stokely (1988) and Ciulla and Deek (2001a) avoid such limitation with respect to Alpert et al. (1990).

To affix/screw markers (Maurer et al. 1997) is not always practical. Thus, "step 2" of Ciulla and Deek (2001a) and used by AUTOALIGN (table 7.1) serves the purpose of merging the two methodologies: principal-axes/tensors and point-based. The advantages of this fusion are: (i) to exploit accuracy of point-based

registration and speed of computation of moment/principal axes methodologies; (ii) to determine an automatic approach to localize reference points into the brain images without the need of affixing/screwing fiducials which, is surely not free of limitations (Maurer et al. 1997). As far as the threshold (TH) used by AUTOALIGN to locate fiducials, it does not constitute a limitation in terms of reliable localization of markers across brain images because TH is used only for the reference fMRI volume. Similarly, Wang et al. (1996) used a threshold to localize voxels, into the marker-like objects, to candidate as fiducials.

Table 7.1 Methodology Characteristics Used to Create AUTOALIGN

PROCESSING STEPS / AUTHORS	STEP 1 (PRE-PROCESSING)	STEP 2 (FIND MAPPING TRANSFORMATION)	STEP 3 (ALIGNMENT)
Faber and Stokely (1988)	***Include into computat. of Inertia components, all voxels and their intensity (mass = intensity)***	By tensors (moments) as eigenvectors of Inertia matrix	Matching tensors and center of gravity
Alpert el al. (1990);	Include , into computat. of Inertia components only those voxels left after ***threshold (T) segmentation*** (mass = 1).	By tensors (moments) as eigenvectors of Inertia matrix	Matching tensors and center of gravity
Maurer et al. (1997)	Affix / Screw fiducials	By automatically localizing fiducials into brain images	***Point-based matching***
Ciulla and Deek (2001) AUTOALIGN	***Include into computat. of Inertia components, all voxels and their intensity (mass = intensity)***	By intersection of outermost brain surface (found with ***Gradient-edge-finding operator***) and ***tensors***. Fiducials are localized at the intersection by the use of a ***threshold (TH)***	***Point-based matching***

7.3 Performance of AUTOALIGN Algorithm for fMRI

Measurements of average accuracy values, obtained with the real fMRI data used by this dissertation, indicate it to be less than 0.697 mm. Figures 7.1 and 7.2 present plots of across algorithms "amis" values computed from table 5.1 of

chapter 5. For each of the six registration parameters it is assumed that each algorithm's estimate (AUTOALIGN, SPM99 and AIR3.08) does not necessarily constitute the true value of the motion parameter. Three "amis" values of same motion parameter and experimental session, one for each couple of algorithms (e.g. AUTOALIGN/SPM99), constitute a tringle within which, the true value of the motion parameter (e.g. pitch) should be contained. A valid justification to above assertion can be given considering that if three instruments (e.g. algorithms) measure differently the same variable (e.g. motion parameter), then the true value of the variable should lie between the three algorithms' estimate. Triangle's areas are shown in table 7.2; units are μm^2.

Table 7.2 Erone's Triangle Area

$\Delta = [p * (p - \delta_1) * (p - \delta_2) * (p - \delta_3)]^{1/2}$ where p is the semi-perimeter of the triangle formed by three vertices: δ_1 (AA/SPM99), δ_2 (AA/AIR3.08) and δ_3 (SPM99/AIR3.08) "amis" values of table 5.1 for same experiment and motion parameter (e.g. pitch). Units are in μm^2.

Performance Analysis						
	x	*y*	*z*	*pitch*	*roll*	*yaw*
ERONE's Area Δ	*fMRI 64 x 64 x 21*					
1st (56)	636.3961	1563.3992	839.7619	2241.3886	202.5833	6211.1332
2nd (45)	1090.7135	3448.8259	980.8231	1838.042	1049.1841	3815.4705
3rd (55)	1355.6786	3472.6096	2499.6	3744.7692	697.9112	7091.802
	fMRI 64 x 64 x 16					
exp1-01 (50)	757.876	3736.7959	2296.4367	1054.0067	6121.6145	1163.4371
exp1-02 (50)	298.3319	2230.5518	1577.8973	800.3999	815.2055	2418.6773
exp1-04 (50)	138.2604	958.1232	405.3991	291.3313	935.6388	278.4241
exp1-05 (50)	48	1742.6876	680.3235	354.945	457.4846	1013.9822
exp1-06 (50)	156.8182	592.9974	500.1874	1106.5932	529.9057	1102.8803
exp1-07 (50)	319.4683	3854.3065	326.4536	884.212	2006.7287	2309.5227
exp1-08 (50)	175.4592	3360.3896	416.6665	845.2385	1335.02	381.9174
exp1-09 (50)	1135.3326	5697.0645	11782.6689	17466.8594	1778.7006	9602.5312

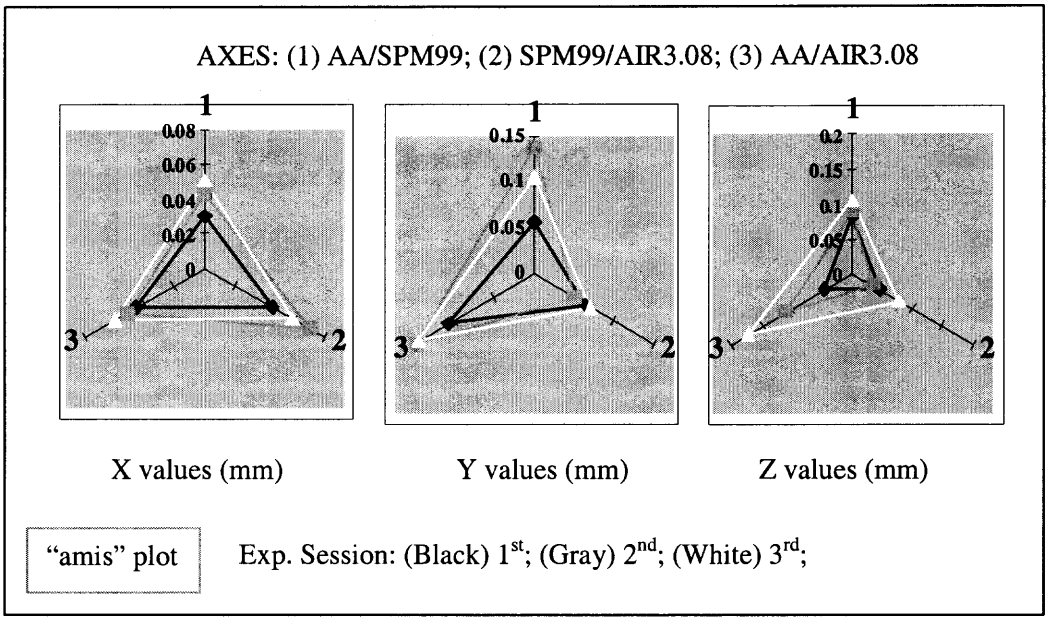

(a)

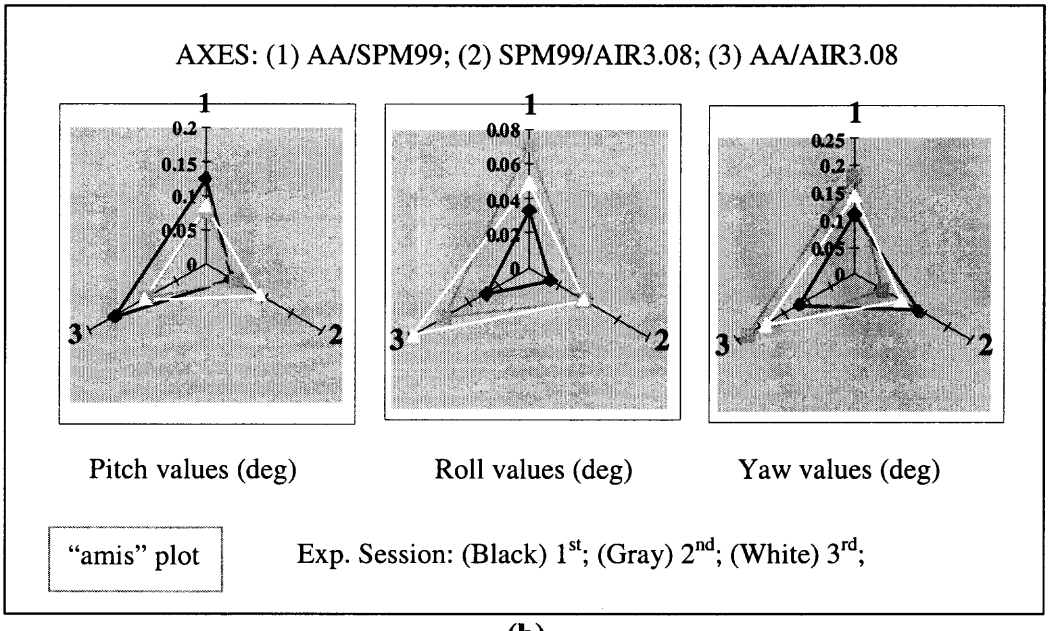

(b)

Figure 7.1 "Amis" Plot across Algorithms for 1st 2nd and 3rd Experimental Sessions

"amis" values were reported in table 5.1 of chapter 5, for each of the six registration parameter's estimate. Their plot show plane triangles within which, the true value should be contained; (a) x, y, z; (b) pitch, roll, yaw.

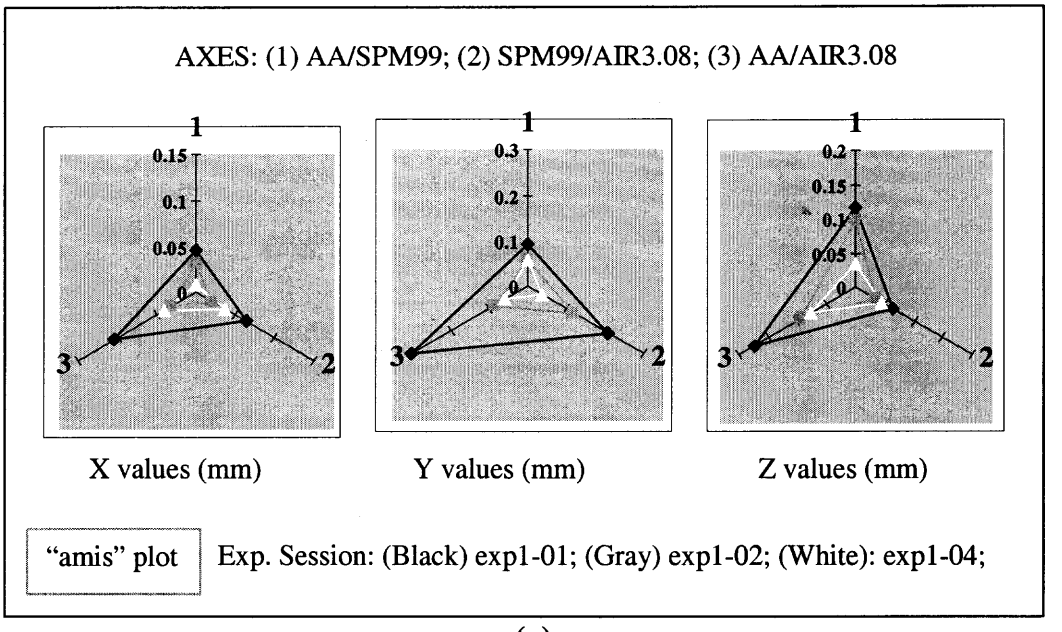

(a)

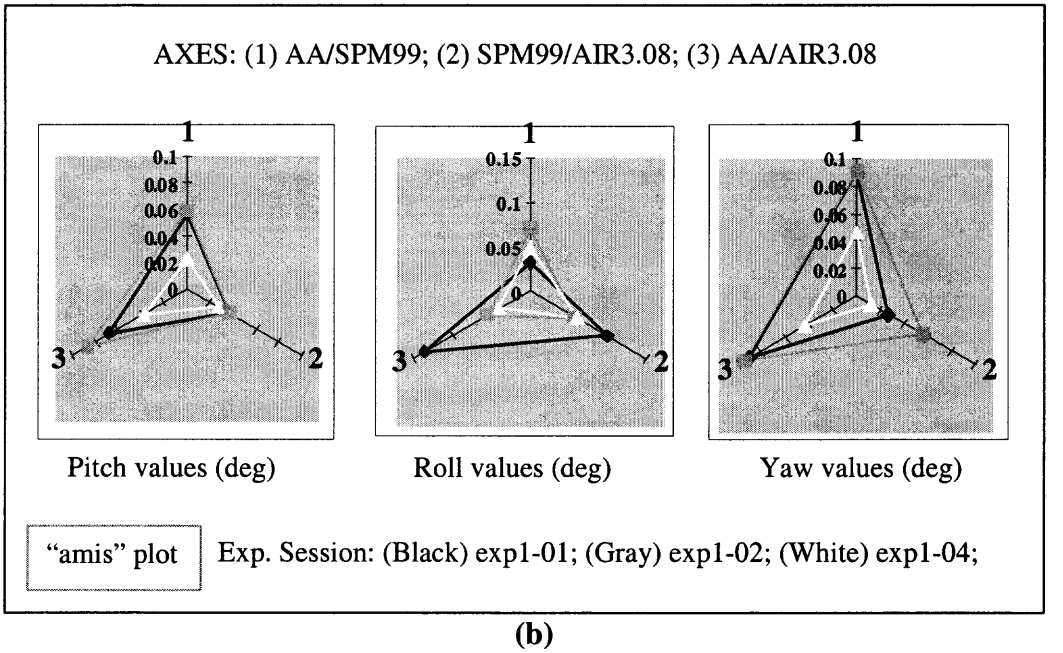

(b)

Figure 7.2 "Amis" Plot across Algorithms for exp1-01, exp1-02 and exp1-04 Experimental Sessions

"amis" values were reported in table 5.1 of chapter 5, for each of the six registration parameter's estimate. Their plot show plane triangles within which, the true value should be contained; (a) x, y, z; (b) pitch, roll, yaw.

7.4 Summary

AUTOALIGN is a retrospective technique that performs inter-image motion correction of fMRI time series. It does not make use of optimization processes of similarity measures and demonstrates the feasibility of fiducial based registration in fMRI. It does overcome the serious limitation of affixing markers to the subject's head, typical of any fiducial based approach. The algorithm allows low computational cost by using a tensor-based approach to localize markers on the subject's head.

AUTOALIGN alignment accuracy strictly depends on how precise is the localization of the three fiducial markers in the brain images of the time series. Estimation of average values obtained with real fMRI data used for validation indicates AUTOALIGN to be more than 0.697 mm accurate. Furthermore, it proves to be accurate for fMRI volumes with low (16-28) sampling resolutions along one axis. This is accomplished by constructing the head coordinate system by the 3-fiducial point technique (Ciulla and Deek 2001a). Such a solution allows extending the applicability of tensor-based registration to problems that could not be solved successfully earlier (Faber and Stokely 1988).

Comparison of AUTOALIGN motion parameter values with those of SPM99 and AIR3.08 suggests similarity of results. AUTOALIGN is respectively 1:2 and 1:5 faster than the latter two registration algorithms, but its alignment accuracy drops of about 1:10 with exponentially (2^N) increasing noise. Thus, the benefit of speed of computation may pay off in cases of low noise fMRI recording.

7. 5 On the Future of fMRI Alignment Research

This paragraph concludes this dissertation by pointing out a general lesson that has been learned by comparing performances of AUTOALIGN, SPM99 and AIR3.08. Results presented in chapter 5, show that AUTOALIGN is faster (1: 2-5), but less robust to noise than the other two algorithms. Erone's triangles (Table 7.2) confirmed that as far as the estimation of the 6 rigid-body motion parameters in fMR volumes with unknown head motion in it, the three algorithms are very much alike. Therefore, the question that can summarize an overall conclusion is: "Which one of the three algorithms is the most efficient?"

It is due of mention recent work done in the field by Freire and Mangin (2001) because of its relevancy in term of diversity of similarity functions (i.e. alignment algorithms typology) used. The authors brought to the attention of the research community that when the motion is small relative to the voxel size, it might not be convenient to resample brain volumes (i.e. apply an interpolation paradigm). This is because of motion artifacts (i.e. failures in correcting voxel intensity) that the interpolation itself might introduce into the brain images. This signifies that even though alignment is performed in order to remove motion, because of the approximate nature of any interpolation paradigms, it might produce a detrimental effect especially in those cases in which the motion to remove is very small.

Therefore, according to Freire and Mangin (2001), the overall question that future research needs to answer is: "How small is the motion that a registration algorithm can remove without producing artifacts?" To add up to Freire and Mangin (2001), this dissertation presents in the next paragraph a mathematical

assertion which claims that for a given interpolation paradigm (e.g. tri-linear) there is a "region of efficacy" outside which, motion correction is not beneficial. Thus, the overall question for future research becomes: "Where into the voxel is the region of efficacy of a motion correction algorithm?"

To answer above question would allow choosing an alignment algorithm for fMRI time series instead of another on the simple basis that the one that performs better would be the one that estimate motion within the "region of efficacy" of the interpolation paradigm and does it so in the shortest computational time.

7.5.1 On the Tri-linear Interpolation Effectiveness

Here is presented a theorem that explains in what circumstances Tri-linear interpolation paradigm is efficient in correcting intensity at sub-voxel accuracy. It is auspicial that this knowledge would contribute to future efforts in fMRI alignment research.

Definition I

Let $V_1 = (0, 0, 0)$, $V_2 = (1, 0, 0)$, $V_3 = (1, 1, 0)$, $V_4 = (0, 1, 0)$ be the quadruple of vertices of the rectangle α. Let α be lying on a plane π_1 of equation $C * z + D = 0$ $\|$ to the XY plane of an absolute right handed reference coordinate system (Ξ) of origin O. Let $V_5 = (0, 0, 1)$, $V_6 = (1, 0, 1)$, $V_7 = (1, 1, 1)$, $V_8 = (0, 1, 1)$ be the quadruple of vertices of the rectangle β. Let β be lying on a plane π_2 of equation $C * (z + \xi_1) + D = 0$ $\|$ to the same XY plane and with ξ_1 being a constant. While V_i ($i = 1 \ldots 4$) follow each other counter-clock wise on α, V_i ($i = 5 \ldots 8$) do it on β. These

eight vertices are located at the boundary surface Σ of a parallelepiped Ψ (voxel) as shown by figure 7.3.

Definition II

Let $V_1 = (0, 0, 0)$, $V_4 = (0, 1, 0)$, $V_5 = (0, 0, 1)$, $V_8 = (0, 1, 1)$ be the quadruple of vertices of the rectangle δ. Let δ be lying on a plane π_3 of equation $A * x + D = 0 \parallel$ to the ZY plane of Ξ (absolute right handed reference coordinate system) of origin O. Let $V_2 = (1, 0, 0)$, $V_3 = (1, 1, 0)$, $V_6 = (1, 0, 1)$, $V_7 = (1, 1, 1)$ be the quadruple of vertices of the rectangle γ. Let γ be lying on a plane π_4 of equation $A * (x + \xi_2) + D = 0 \parallel$ to ZY; with ξ_2 being a constant. While V_i (i =1, 4, 5, 8) follows each other counter-clock wise on δ, V_i (i =2, 3, 6, 7) does it on γ. Also, these eight vertices are located at the boundary surface Σ of a parallelepiped Ψ (voxel) as shown by figure 7.3.

Definition III

Let $V_9 = (X, 0, 0)$, $V_{10} = (1, Y, 0)$, $V_{11} = (X, 1, 0)$, $V_{12} = (0, Y, 0)$ be respectively any points of the segments $[V_1, V_2]$, $[V_2, V_3]$, $[V_3, V_4]$, $[V_4, V_1]$ and $V_{13} = (X, 0, 1)$, $V_{14} = (1, Y, 1)$, $V_{15} = (X, 1, 1)$, $V_{16} = (0, Y, 1)$ be respectively any points of the segments $[V_5, V_6]$, $[V_6, V_7]$, $[V_7, V_8]$, $[V_8, V_5]$. Also, let $V_{17} = (1, 0, Z)$, $V_{18} = (1, 1, Z)$ be respectively any points of the segments $[V_4, V_8]$, $[V_3, V_7]$ and $V_{19} = (0, 0, Z)$, $V_{20} = (0, 1, Z)$ be respectively any points of the segments $[V_1, V_5]$, $[V_2, V_6]$. Where $X \in [0, 1]$, $Y \in [0, 1]$ and $Z \in [0, 1]$ and V_i (i = 9...20) is located at the boundary surface Σ of a parallelepiped Ψ (voxel) as shown by figure 7.3.

Definition IV

Let f be a continuous function that takes the form:

$$f(X,Y,Z) = f(0,0,0) + x\,[f(1,0,0) - f(0,0,0)] + y\,[f(0,1,0) - f(0,0,0)] + z\,[f(0,0,1) - f(0,0,0)] + xy\,[f(0,0,0) - f(1,0,0) - f(0,1,0) + f(1,1,0)] + zy\,[f(0,0,0) - f(0,1,0) - f(0,0,1) + f(0,1,1)] + xz\,[f(0,0,0) - f(1,0,0) - f(0,0,1) + f(1,0,1)] + xyz\,[f(1,1,1) - f(1,1,0) - f(0,1,1) - f(1,0,1) + f(0,0,1) + f(0,1,0) + f(1,0,0) - f(0,0,0)] \quad (7.1)$$

Where: f(0,0,0), f(1,0,0), f(1,1,0), f(0,1,0) and f(0,0,1), f(1,0,1), f(1,1,1), f(0,1,1) are respectively its two quadruple of values at the vertices of the two rectangles α and β of the parallelepiped Ψ.

Definition V

Let $\delta^2 f / \delta x \delta y = \delta^2 f / \delta y \delta x = [f(0,0,0) - f(1,0,0) - f(0,1,0) + f(1,1,0)] + z\,\omega_f$, $\delta^2 f / \delta x \delta z = \delta^2 f / \delta z \delta x = [f(0,0,0) - f(1,0,0) - f(0,0,1) + f(1,0,1)] + y\,\omega_f$ and $\delta^2 f / \delta y \delta z = \delta^2 f / \delta z \delta y = [f(0,0,0) - f(0,1,0) - f(0,0,1) + f(0,1,1)] + x\,\omega_f$ be the second order derivatives of the function f respectively in xy, xz and yz, where: $\omega_f = [f(1,1,1) - f(1,1,0) - f(0,1,1) - f(1,0,1) + f(0,0,1) + f(0,1,0) + f(1,0,0) - f(0,0,0)]$.

Definition VI

Let $\theta_{xy} = \theta_{yx} = -[f(0,0,0) - f(1,0,0) - f(0,1,0) + f(1,1,0)] / \omega_f$, $\theta_{xz} = \theta_{zx} = -[f(0,0,0) - f(1,0,0) - f(0,0,1) + f(1,0,1)] / \omega_f$ and $\theta_{yz} = \theta_{zy} = -[f(0,0,0) - f(0,1,0) - f(0,0,1) + f(0,1,1)] / \omega_f$ be the slopes of respectively $\delta^2 f / \delta x \delta y$, $\delta^2 f / \delta x \delta z$ and $\delta^2 f / \delta y \delta z$ functions.

Definition VII

The function f = f (X, Y, Z) is a hyperbolic paraboloid that exists for each (X, Y, Z) ϵ Ψ and estimates intensity at sub-voxel locations. Let $\Omega = \{(X, Y, Z) : | \delta^2 f / \delta x \delta y |_{z=Z} = | \delta^2 f / \delta y \delta x |_{z=Z} \leq Z\ \theta_{xy}$ and $| \delta^2 f / \delta x \delta z |_{y=Y} = | \delta^2 f / \delta z \delta x |_{y=Y} \leq Y\ \theta_{xz}$ and $| \delta^2 f / \delta y \delta z |_{x=X} = | \delta^2 f / \delta z \delta y |_{x=X} \leq X\ \theta_{yz} \}$ be the region of efficacy in Ψ.

Observation I

Let $b_{xy} = -[f(0,0,0) - f(1,0,0) - f(0,1,0) + f(1,1,0)]$, $b_{xz} = -[f(0,0,0) - f(1,0,0) - f(0,0,1) + f(1,0,1)]$ and $b_{yz} = -[f(0,0,0) - f(0,1,0) - f(0,0,1) + f(0,1,1)]$. From definition VII it follows that if f = f (X, Y, Z) is efficient in P = (X, Y, Z), then $| \delta^2 f / \delta x \delta y |_{z=Z} = | \delta^2 f / \delta y \delta x |_{z=Z} \leq Z\ \theta_{xy}$ and $| \delta^2 f / \delta x \delta z |_{y=Y} = | \delta^2 f / \delta z \delta x |_{y=Y} \leq Y\ \theta_{xz}$ and $| \delta^2 f / \delta y \delta z |_{x=X} = | \delta^2 f / \delta z \delta y |_{x=X} \leq X\ \theta_{yz}$, which can be rewritten as:

$$|-b_{xy} + Z\ \omega_f| \leq Z\ (b_{xy} / \omega_f) \tag{7.2}$$

$$|-b_{xz} + Y\ \omega_f| \leq Y\ (b_{xz} / \omega_f) \tag{7.3}$$

$$|-b_{yz} + X\ \omega_f| \leq X\ (b_{yz} / \omega_f) \tag{7.4}$$

Thus, if f is efficient in P = P (X, Y, Z), then from equations (7.2), (7.3) and (7.4) it follows respectively that:

$$Z \leq \omega_f\ b_{xy} / (\omega_f^2 - b_{xy}) \tag{7.5}$$

$$Z \geq \omega_f\ b_{xy} / (\omega_f^2 + b_{xy}) \tag{7.6}$$

$$Y \leq \omega_f\ b_{xz} / (\omega_f^2 - b_{xz}) \tag{7.7}$$

$$Y \geq \omega_f\ b_{xz} / (\omega_f^2 + b_{xz}) \tag{7.8}$$

$$X \leq \omega_f\ b_{yz} / (\omega_f^2 - b_{yz}) \tag{7.9}$$

$$X \geq \omega_f b_{yz} / (\omega_f^2 + b_{yz}) \qquad (7.10)$$

For convenience, let $\omega_f\ b_{xy} / (\omega_f^2 - b_{xy}) = Z^{(1)}$ and $\omega_f\ b_{xy} / (\omega_f^2 + b_{xy}) = Z^{(2)}$; $\omega_f\ b_{xz} / (\omega_f^2 - b_{xz}) = Y^{(1)}$ and $\omega_f\ b_{xz} / (\omega_f^2 + b_{xz}) = Y^{(2)}$; $\omega_f\ b_{yz} / (\omega_f^2 - b_{yz}) = X^{(1)}$ and $\omega_f b_{yz} / (\omega_f^2 + b_{yz}) = X^{(2)}$.

Theorem

The function f is efficient if and only if $P = (X, Y, Z) \in \Omega$.

Proof:

Claim (i): If $P = (X, Y, Z) \in \Omega$, then f is efficient.

Given $P = (X, Y, Z) \in \Omega$, it follows from definition VII that $| \delta^2 f / \delta x \delta y |_{z=Z} = | \delta^2 f / \delta y \delta x |_{z=Z} \leq Z\ \theta_{xy}$ and $| \delta^2 f / \delta x \delta z |_{y=Y} = | \delta^2 f / \delta z \delta x |_{y=Y} \leq Y\ \theta_{xz}$ and $| \delta^2 f / \delta y \delta z |_{x=X} = | \delta^2 f / \delta z \delta y |_{x=X} \leq X\ \theta_{yz}$, thus f is efficient in P.

Claim (ii): If f is efficient in $P = (X, Y, Z)$, then $P \in \Omega$.

If f is efficient in $P = (X, Y, Z)$ then from observation I it follows that $\delta^2 f / \delta x \delta y |_{z=Z} \leq Z\ \theta_{xy}$ and $\delta^2 f / \delta x \delta y |_{z=Z} \geq -Z\ \theta_{xy}$; $\delta^2 f / \delta x \delta z |_{y=Y} \leq Y\ \theta_{xz}$ and $\delta^2 f / \delta x \delta z |_{y=Y} \geq -Y\ \theta_{xz}$; $\delta^2 f / \delta y \delta z |_{x=X} \leq X\ \theta_{yz}$ and $\delta^2 f / \delta y \delta z |_{x=X} \geq -X\ \theta_{yz}$.

Now assume the absurd that $P = (X, Y, Z) \notin \Omega$. Then from Observation I it follows that $Z > \omega_f\ b_{xy} / (\omega_f^2 - b_{xy})$ and $Z < \omega_f\ b_{xy} / (\omega_f^2 + b_{xy})$; $Y > \omega_f\ b_{xz} / (\omega_f^2 - b_{xz})$ and $Y < \omega_f\ b_{xz} / (\omega_f^2 + b_{xz})$; $X > \omega_f\ b_{yz} / (\omega_f^2 - b_{yz})$ and $X < \omega_f b_{yz} / (\omega_f^2 + b_{yz})$. Therefore, $Z\ \theta_{xy} > Z^{(1)}\ \theta_{xy}$ and $Z\ \theta_{xy} < Z^{(2)}\ \theta_{xy}$ $(-Z\ \theta_{xy} > -Z^{(2)}\ \theta_{xy})$; $Y\ \theta_{xz} > Y^{(1)}\ \theta_{xz}$ and $Y\ \theta_{xz} < Y^{(2)}\ \theta_{xz}$ $(-Y\ \theta_{xz} > -Y^{(2)}\ \theta_{xz})$; $X\ \theta_{yz} > X^{(1)}\ \theta_{yz}$ and $X\ \theta_{yz} < X^{(2)}\ \theta_{yz}$ $(-X\ \theta_{yz} > -X^{(2)}\ \theta_{yz})$. But, then $| \delta^2 f / \delta x \delta y |_{z=Z} \leq Z\ \theta_{xy}$ and $| \delta^2 f / \delta x \delta z |_{y=Y} \leq Y\ \theta_{xz}$ and $| \delta^2 f / \delta y \delta z |_{x=X} \leq X\ \theta_{yz}$ are not necessarily true, thus the assumption of f being efficient in $P = (X, Y, Z)$

is contradicted. Therefore since to assume $P = (X, Y, Z) \notin \Omega$ leads to an absurd, it must be $P = (X, Y, Z) \in \Omega$.

7.5.2 Implications for Future Research

It was presented a mathematical assertion claiming that for the tri-linear interpolation function, there exists a "region of efficacy" outside which, motions correction is not beneficial. Both size and boundary of such a sub-voxel region depends on the intensity of the eight neighboring voxels. It is then straightforward to assume that the "region of efficacy" can be different from voxel to voxel. Thus, within a brain volume, for given motion estimate, it is suggested that the decision to re-sample should be made locally (i.e. voxel by voxel) when the motion is contained within the region of "efficacy" into the voxel.

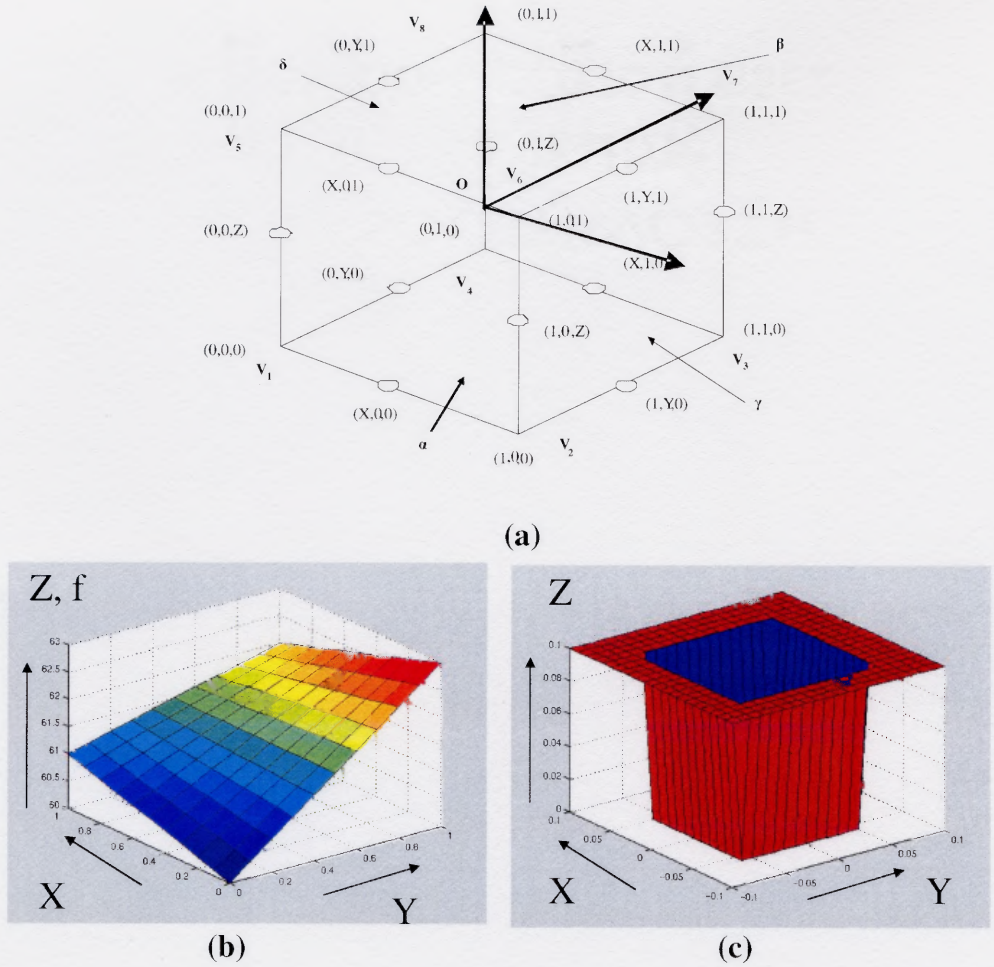

Figure 7.3 Voxel Ψ (a), Trilinear Function (b) and Region of Efficacy (c)

(a) Schematic representation of a Voxel. The origin of the coordinate system is at the center. (b) Plot of the trilinear function f obtained with arbitrary values of intensity at the eight neighbor voxels. (c) Plot of the "Region of Efficacy" (equations 7.5 - 7.10) scaled to represent $0 < Z < 0.1$, (10% of voxel's size) and $X, Y \in [-0.1, 0.1]$ (20% of voxel's size) and obtained with the values of intensity used for the plot shown in (b).

APPENDIX A

AUTOALIGN DATA DESCRIPTION

This Appendix lists and describes data that flows within the modules of the AUTOALIGN computer based system. It also serves as a legend of Chapter 4 pictures.

A.1 AUTOALIGN Level 0 Diagram

Data of Figure 4.6	**Description**
Accuracy Estimation	Registration accuracy measured at the markers location
Alignment Parameters	Three angles (Pitch, Roll and Yaw) and three Coordinates X, Y and Z
Available Memory	Workstation Memory
fMRI Volumes	Brain Images obtained with functional MRI
Hardware (Computation Speed)	Platform Dependent
Image Noise	Signal Detected not attributable to the subject
Sampling Axial Resolution	Resolution of the Brain Image along X, Y and Z
Subject's motion	Head motion
Voxel's Size (X, Y and Z)	3D brain pixel size

A.2 AUTOALIGN Level 1 Diagram (Two fMRI Scans)

Data of Figure 4.7	Description
Accuracy Estimation	Registration accuracy measured at the markers location
Alignment Parameters	Three angles (Pitch, Roll and Yaw) and three Coordinates X, Y and Z
Aligned fMRI Volume	Test fMRI Volume after alignment
Axis of Head Coord System	Numerical values of unit vectors
fMRI Volume ID	Brain Image's file name
Head Physical Constraints	Subject's head-neck constraints
Image Noise	Signal Detected not attributable to the subject
Misalig of Coord Sys O	X, Y and Z Coordinate difference between reference and test Images
Numerical Display	Data of Gradient Computation
Origin of Head Coord System	Numerical values of X, Y and Z Coordinates
Orthogonal of U Vectors	Orthogonal Axes of the Head Coord System
Pitch, Roll and Yaw Angles	Angles of Rigid-body rotation matrix
Reference Scan Parameters	Reference Scan Rigid-body Parameters
Sampling Axial Resolution	Resolution of the Brain Image along X, Y and Z
Subject's motion	Head motion

Test fMRI Volume	Brain image to align to the reference
User's Interactions	Mouse and Keyboard usage
Visual Display	Brain Image Displayed in 3 2D Composite views
Voxel's Size (X,Y and Z)	3D brain pixel size
3-Fiducial Markers	Reference points used to build Coord System
3D plane equations	Equations of the planes of the Head Coord System

A.3 AUTOALIGN Level 1 Diagram (All fMRI Scans)

Data of Figure 4.8	**Description**
Accuracy Estimation	Registration accuracy measured at the markers location
Aligned fMRI Volume	Test fMRI Volume after alignment
Alignment Parameters	Three angles (Pitch, Roll and Yaw) and three Coordinates X, Y and Z
Axis of Head Coord System	Numerical values of unit vectors
Brain Images Format	Files Format
Head Physical Constraints	Subject's head-neck constraints
Image Noise	Signal Detected not attributable to the subject
Interpolation	Intensity Correction due to misalignment
No. of fMRI Volumes	Brain Images file names

Numerical Display	Data of Gradient Computation
Origin of Head Coord System	Numerical values of X, Y and Z Coordinates
Orthogonal U Vectors	Orthogonal Axes of the Head Coord System
Misalig of Coord Sys O	X, Y and Z Coordinate difference between reference and test Images
Pitch, Roll and Yaw Angles	Angles of Rigid-body rotation matrix
Reference Scan Parameters	Reference Scan Rigid-body Parameters
Sampling Axial Resolution	Resolution of the Brain Image along X, Y and Z
Subject's motion	Head motion
Test fMRI Volume	Brain image to align to the reference
User's Interactions	Mouse and Keyboard usage
Visual Display	Brain Image Displayed in 3 2D Composite views
Voxel's Size (X,Y and Z)	3D brain pixel size
3-Fiducial Markers	Reference points used to build Coord System
3D plane equations	Equations of the planes of the Head Coord System

A.4 AUTOALIGN Level 2 Diagram (Display Scan)

Data of Figure 4.9	**Description**
Analog Data	Brain Image data converted into 0-255 scale
Eigenvalues	Radices of Inertia matrix

Eigenvectors	Orthogonal Components extracted from symmetric Inertia matrix
fMRI Volume ID	Brain Image's file name
Gradient Brain Image	Gradient Magnitude Image
Gradient Magnitude	Sum of squared Gx and Gy values, pixel by pixel
Gx Convolution	Convolution with a third order operator
Gy Convolution	Convolution with a third order operator
Image Noise	Signal Detected not attributable to the subject
Inertia matrix	Symmetric matrix with inertial components as entries
Jacobi's Rotation	90 degrees rotation
Matrix Symmetry	Constraint to ensure orthogonal eigenvectors
Orthogonalization	Constraint
Sampling Axial Resolution	Resolution of the Brain Image along X, Y and Z
Scaling of Pixel's Coord	Scaling to control for sampling axial resolution
Scaling of Pixel's Intensity	Scaling to control for pixel intensity
Subject's motion	Head motion
Threshold	Threshold
User's Interactions	Mouse and Keyboard usage
Visual Display	Brain Image Displayed in 3 2D Composite views

Voxel's Size (X, Y and Z)	3D brain pixel size
Zero-Crossing	Points of null derivative

A.5 AUTOALIGN Level 2 Diagram (Unit Vectors)

Data of Figure 4.10	**Description**
Determinant Function	Routine to compute 2x2 Determinant
Physical Head Constraint	Constraint
Plane through 3 Points	Constraint
Plane XY Coefficients	Axy, Bxy, Cxy, Dxy
Plane ZY Coefficients	Azy, Bzy, Czy, Dzy
Plane ZX Coefficients	Azx, Bzx, Czx, Dzx
Unit Vectors	Unit vectors of head coordinate system
2 Points Constraint	Constraint
3-Fiducial Markers	Reference points used to build Coord System

A.6 AUTOALIGN Level 2 Diagram (Align Scan)

Data of Figure 4.11	**Description**
Accuracy Estimation	Accuracy measured at the three markers location
Original grid Coord Val	Original grid X, Y and Z values for each pixel
Orthogonalization	Constraint
Ref Vol. Center of G	Center of gravity of reference brain image

Rigid-body transf	6 parameters transformation
R Matrix	Rotation Matrix (Pitch, Roll and Yaw)
RT Matrix	Rotation-Translation Matrix
Sin, Cos, Atan	Formulas
Test Vol. Center of G	Center of gravity of test brain image
T Vector	Translation Vector
Unit Vectors of Ref Vol.	Unit vectors of Reference volume head coordinate system
Unit Vectors of Test Vol.	Unit vectors of Test volume head coordinate system

A.7 AUTOALIGN Level 2 Diagram (ReDisplay)

Data of Figure 4.12	**Description**
Aligned Volume	Aligned brain image
Analog Conversion	Conversion of brain data into 0-255 range
Analog Data	Pixel's intensities in 0-255 range values
Image Noise	Signal Detected not attributable to the subject
New grid Coord Values	Values of coordinates X, Y and Z for each pixel after alignment
Original grid Coord Val	Original grid X, Y and Z values for each pixel
Parabolic Function	Function used to approximate pixel intensities

Rigid-body assumption	Rigid-body assumption (6 parameters transformation)
RT Matrix	Rotation-Translation matrix
Sampling Axial Resolution	Resolution of the Brain Image along X, Y and Z
Subject's motion	Head motion
Test Volume	Brain Images obtained with functional MRI
Tri-Linear Interpolation	First order interpolation scheme
User's Interactions	Mouse and Keyboard usage
Visual Display	Brain Image Displayed in 3 2D Composite views
Voxel's Size (X, Y and Z)	3D brain pixel size

A.8 AUTOALIGN Level 2 Diagram (Diff. Image)

Data of Figure 4.13	**Description**
fMRI Volumes	Brain Images obtained with functional MRI
Image Noise	Signal Detected not attributable to the subject
Sampling Axial Resolution	Resolution of the Brain Image along X, Y and Z
Subject's motion	Head motion
User's Interactions	Mouse and Keyboard usage
Visual Display	Brain Image Displayed in 3 2D Composite views
Voxel's Size (X,Y and Z)	3D brain pixel size

A.9 AUTOALIGN Level 2 Diagram (Align All to Ref.)

Data of Figure 4.14	Description
Accuracy Estimation	Registration accuracy measured at the markers location
Aligned Volume	Aligned brain image
Alignment Parameters	Three angles (Pitch, Roll and Yaw) and three Coordinates X, Y and Z
Analog Data	Brain Image data converted into 0 - 255 scale
Convolution	X and Y Convolution with a third order operator
Determinant Function	Routine to compute 2 x 2 determinant
Gradient	Gradient Magnitude Image
Inertia	Symmetric matrix with inertial components as entries
Eigenvectors	Eigenvectors of inertia matrix
fMRI Volumes	Brain Images obtained with functional MRI
Image Noise	Signal Detected not attributable to the subject
New grid Coord Values	Values of coordinates X, Y and Z for each pixel after alignment
Numerical Display	Numerical data on the output screen

Original Grid Coord Val	Original grid X, Y and Z values for each pixel
Orthogonalization	Constraint
Parabolic Function	Function used to approximate pixel intensities
Rigid-body assumption	Rigid-body assumption (6-parameters transformation)
Sampling Axial Resolution	Resolution of the Brain Image along X, Y and Z
Subject's motion	Head motion
Tri-Linear Interpolation	First order interpolation scheme
Unit Vectors	Unit vectors of brain volume head coordinate system
User's Interactions	Mouse and Keyboard usage
Voxel's Size (X, Y and Z)	3D brain pixel size
3-Fiducial Markers	Reference points used to build Coord System

APPENDIX B

PRELIMINARY TEST OF THE AUTOALIGN TECHNIQUE

Four experimental sessions are described in this Appendix. They aimed to preliminary test AUTOALIGN technique and compare results to those obtainable by SPM99 with same data (Ciulla and Deek 2001a).

It has been used a T2*-weighted Magnetic Resonance volume (fMRI) having sampling resolution 64 (3.75 mm), 64 (3.75 mm) and 28 (5.00 mm) respectively in the x, y and z directions. The fMRI volume has been subject of controlled motion simulation. Artificial volumes were created in which, pitch, roll and yaw rotations (respectively about x, y and z axes) were introduced at steps of 1° by ROTRA software system (Ciulla 2000) either individually (e.g. pitch = 0; roll = 0 and yaw $\in$ [-10°; 10°]) or simultaneously (pitch, roll and yaw $\in$ [-10°; 10°]).

Tests were conducted to see how the angles were estimated by AUTOALIGN and SPM99. Results are shown in figures B.1 - B.4. In figures B.1 -B.3, two of the three angles were expected to be estimated as zero lines (white), as imposed in the artificial test volumes; while the third angle was expected to be as close as possible to the ideal line (black). In figure B.1 estimation results for pitch $\in$ [-10°; 10°], roll = 0 and yaw = 0 are plotted respectively for AUTOALIGN (a) and SPM99 (b). Figures B.2 and B.3 show estimation results of AUTOALIGN (a) and SPM99 (b) respectively for pitch = 0, roll $\in$ [-10°; 10°] and yaw = 0; and pitch = 0, roll = 0 and yaw $\in$ [-10°; 10°]. In general from a visual inspection of the three figures it can be seen that AUTOALIGN performed similarly to SPM99. "Amis" values (eq. 134,

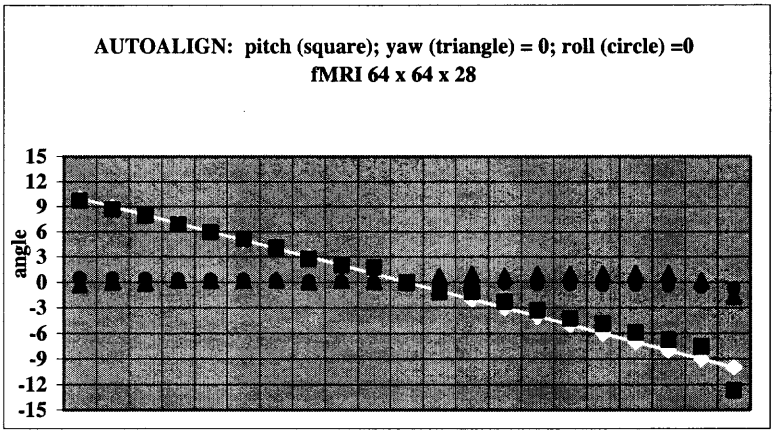

(a)

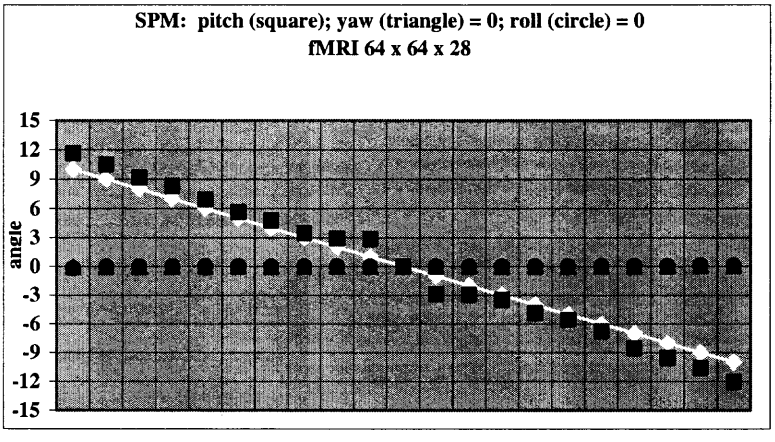

(b)

Figure B.1 AUTOALIGN and SPM99 Estimation of Pitch Angles

The white line connects values of the angles that were used to create the artificial volumes, and represents the ideal performance of the two systems. The rigid body transformation is applied to the volume at steps of 1° as pitch $\in$ [-10°; 10°], roll = 0 and yaw = 0. Pitch (■), yaw (▲) and roll (●) express the actual performance of the two systems: AUTOALIGN (a) and SPM99 (b).

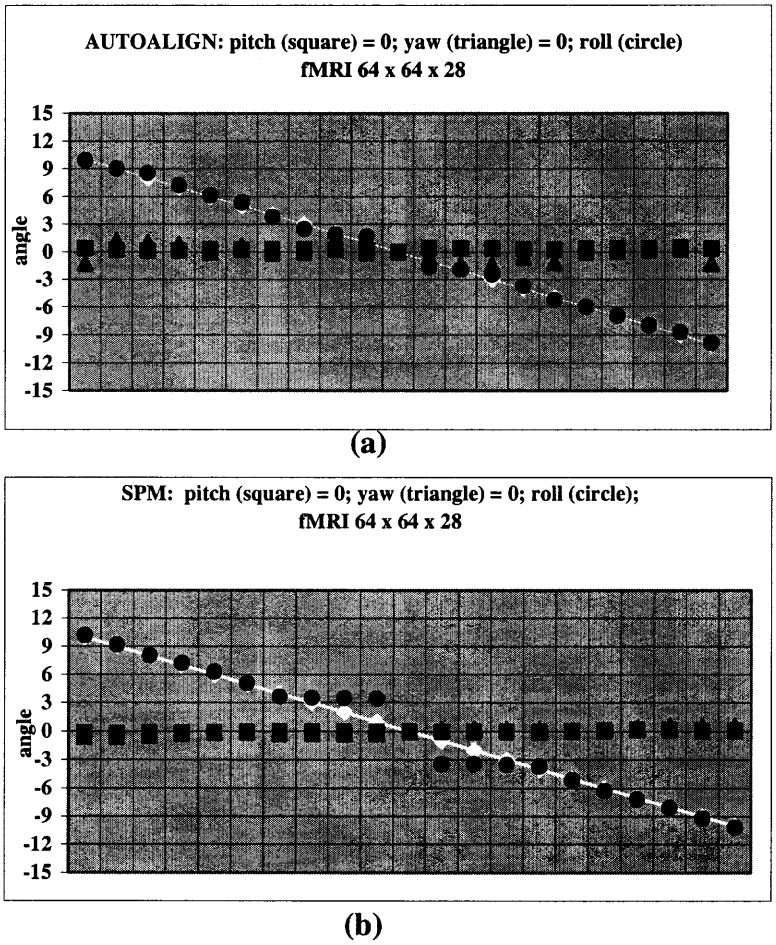

Figure B.2 AUTOALIGN and SPM99 Estimation of Roll Angles

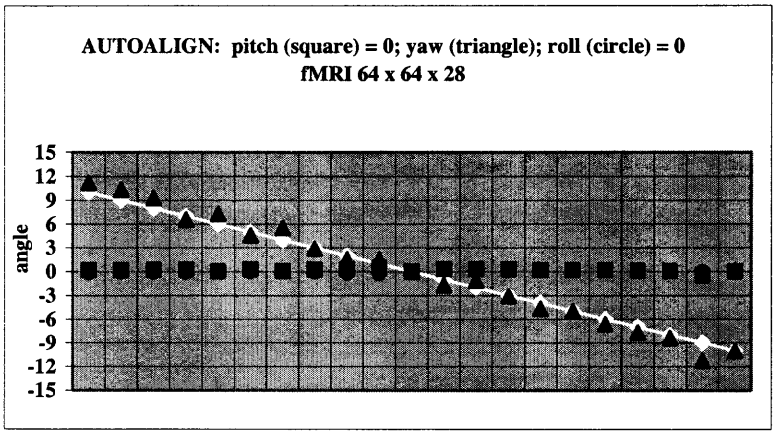

(a)

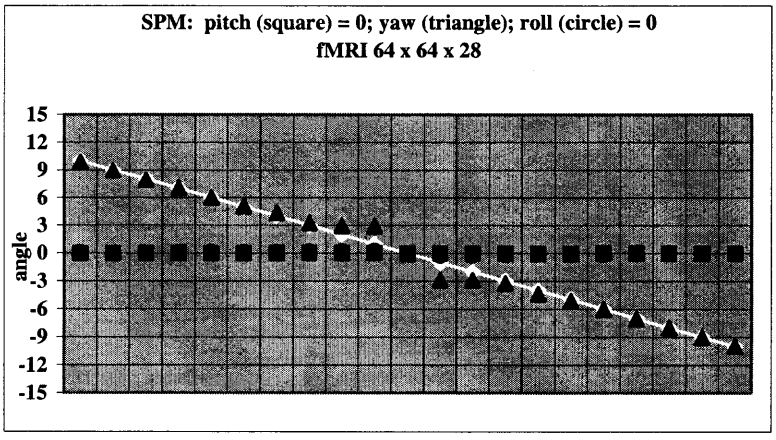

(b)

Figure B.3 AUTOALIGN and SPM99 Estimation of Yaw Angles

Chapter 5) were computed to measure average misalignment in the estimation of angles of rotation within [-10°; 10°]. Results of "amis" values are summarized in table B.1. From table B.1 it can be inferred that within [-10°; 10°] SPM99 performed generally better than AUTOALIGN except for the estimation of pitch and roll angles.

When the experiments were conducted in order to see how AUTOALIGN and SPM99 performed estimation of the three angles imposed concurrently (pitch, roll and yaw ϵ [-10°; 10°]), it was discovered that AUTOALIGN performs better than SPM99 only for large rotations (angles greater than 5° in their absolute value). These last results are presented in figure B.4 respectively for AUTOALIGN (a) and SPM99 (b). Similarly, Friston et al. (1995) reported that the Statistical Parametric Mapping has an accuracy of 100μm, which, decreases when the spatial misalignments approach the resolution of the brain images.

Figure B.5 shows a sample result of the realignment performed by AUTOALIGN. An original fMRI slice is shown in (a). The original fMR image has been realigned (b) after being rotated by 3° about the Z-axis. The mis-estimation of the yaw angle from the expected value (3°) was 0.07° and the mis-registration along the Y-axis direction, at the location indicated by the arrow, was 0.08 mm (18 pixels * 3.75 mm * tan (0.07)), which is less than the sampling axial resolution (3.75 mm). From the figure, it is visible that artifacts are still present after realignment and they can be attributed, in part, to the nearest neighbor interpolation scheme adopted at this stage of AUTOALIGN development.

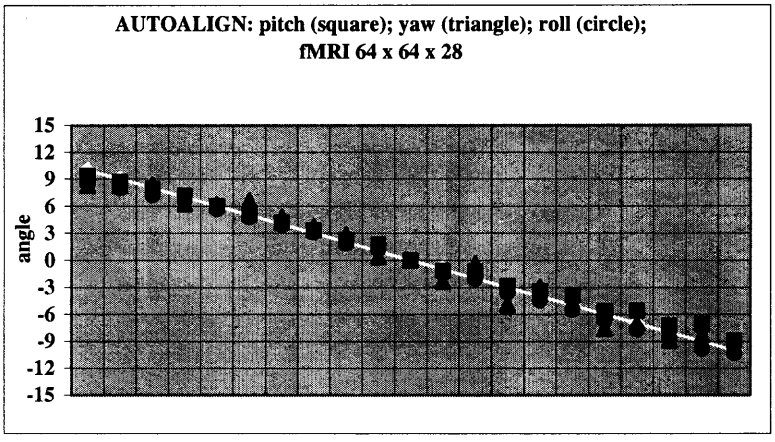

(a)

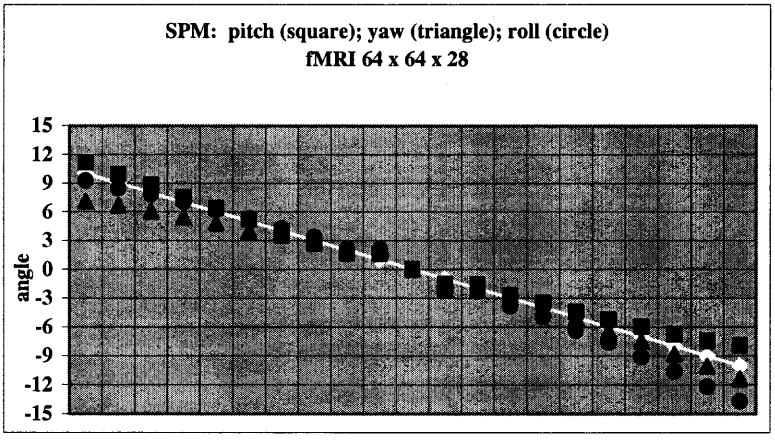

(b)

Figure B.4 AUTOALIGN and SPM99 Estimation of Pitch, Roll and Yaw Angles

Rotations were simulated simultaneously at steps of 1° (pitch, roll and yaw $\in$ [-10°; 10°]) to the 64 x 64 x 28 fMRI volume. Pitch (■), yaw (▲) and roll (●) are the estimations of the two software systems: AUTOALIGN (a), SPM99 (b); and they are plotted together with the ideal line (white).

Table B.1 Preliminary Test Results of the AUTOALIGN Technique

For each experiment and for each of the two software systems (AUTOALIGN and SPM99), the table shows "amis" values. Data can be read together with figures B.1- B4 and they are relevant to the experiment conducted to estimate pitch, roll and yaw both individually (e.g. pitch ϵ [-10°; 10°], roll = 0 and yaw = 0) and concurrently (pitch, roll and yaw ϵ [-10°; 10°]).

Range [-10 deg; 10 deg]			
	fMRI 64 x 64 x 28		
AUTOALIGN	*pitch*	*yaw=0*	*roll=0*
amis	*0.416*	*0.358*	*0.183*
	pitch=0	*yaw=0*	*roll*
amis	*0.195*	*0.413*	*0.161*
	pitch=0	*yaw*	*roll=0*
amis	*0.148*	*0.471*	*0.108*
	pitch	*yaw*	*roll*
amis	*0.35*	*0.594*	*0.314*
	fMRI 64 x 64 x 28		
SPM99	*pitch*	*yaw=0*	*roll=0*
amis	*0.752*	*0.016*	*0.02*
	pitch=0	*yaw=0*	*roll*
amis	*0.05*	*0.208*	*0.375*
	pitch=0	*yaw*	*roll=0*
amis	*0.014*	*0.242*	*0.067*
	pitch	*yaw*	*roll*
amis	*0.453*	*0.592*	*0.703*

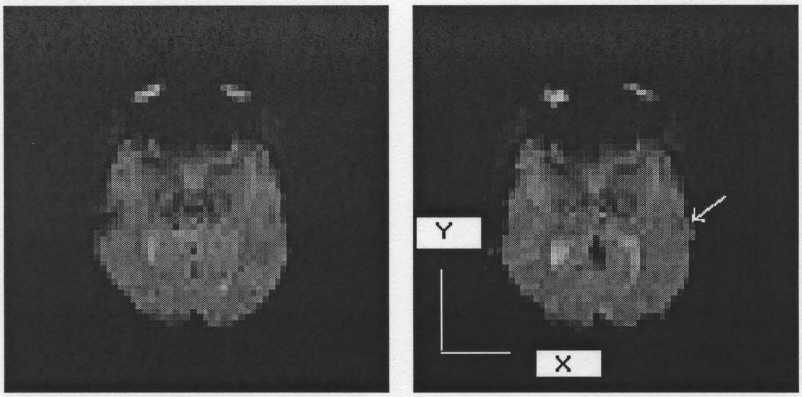

(a) (b)

Figure B.5 Sample Alignment Result of AUTOALIGN

An original 64 x 64 fMRI slice (a) and the same image after manipulation (applying a 3° rotation about the Z-axis which, is perpendicular to the image and passing through the center of gravity) and alignment (b). The fMR Image shown in (b) was processed twice with nearest neighbor interpolation.

REFERENCES

Alpert, N.M., Brandshaw, J.F., Kennedy, D. and Correia, J.A.
The Principal Axes Transformation - A method for Image Registration. The Journal of Nuclear Medicine, 1990, 31: 1717-1722.

Althof, R.J., Wind, M.G.J. and Dobbins, J.T.
A Rapid and automatic image registration algorithm with sub-pixel accuracy. IEEE Transactions on Medical Imaging, 1997, 16: 308-316.

Andersson, J.L.R., Hutton, C., Ashburner, J.,Turner, R. and Friston, K.
Modeling geometric deformations in EPI time series. Neuroimage, 2001, 13: 903-919.

Arendsen, R. and Bentum, M.
Design and realization of computer system for high speed single exposure dual-energy image-processing. Master Thesis, University of Twente. The Netherlands, 1991.

Arun, K.S., Huang, T.S. and Blostein, S.D.
Least-square fitting of two 3-D point sets. IEEE Trans. Pattern Anal. Machine Intell., 1987, PAMI-9: 698-700.

Ashburner, J., Andersson, J.L.R. and Friston, K.J.
High-dimensional image registration using symmetric priors. Neuroimage, 1999, 9: 619-628.

Atkinson, D., Hill, D.L.G., Stoyle, P.N.R., Summers, P.E. and Keevil, S.F.
Automatic Correction of Motion Artifacts in Magnetic Resonance Images Using and Entropy Focus Criterion. IEEE Transactions on Medical Imaging, 1997, 16: 903-910.

Audette, M.A., Ferrie, F.P. and Peters, T.M.
An algorithmic overview of surface registration techniques for medical imaging. Med. Image Anal., 2000, 4: 201-217.

Banerjee, P.K. and Toga, A.W.
Image alignment by integrated rotational and translational transformation matrix. Phys. Med. Biol., 1994, 39: 169-1988.

Bellers, E. B. and De Bruijn, F.J.
On the automation of single exposure dual-energy computed-radiography. Master Thesis. University of Twente, The Netherlands, 1993.

Besl, P.J. and McKay. N.D.
A Method for Registration of 3-D Shapes. IEEE Transactions on Pattern Analysis and Machine Intelligence, 1992, 14: 239-256.

Betting, F. and Feldmar, J.
3D-2D projective registration of anatomical surfaces with their projections. Bizais, Y. and Barillot, C. Eds. Information Processing in Medical Imaging. Kluwer Academic Publishers, Dordecht, 1995, 275-286.

Biswal, B.B. and Hyde, J.S.
Contour-Based Registration Technique to Differentiate Between Task-Activated and Head Motion-Induced Signal Variations in fMRI. MRM, 1997, 38: 470-476.

Boesecke, R., Bruckner, T. and Gabriele, E.
Landmark based correlation of medical images. Phys. Med. Biol., 1990, 35(1): 121-126.

Bookstein, F.L.
Principal Warps: Thin plate splines and the decomposition of deformation. IEEE Trans. Pattern Anal. Mach. Intell., 1989, 11: 567-585.

Borgefors, G.
Hierarchical chamfer matching: a parametric edge-matching algorithm. IEEE Transactions on Pattern Analysis and Machine Intelligence, 1988, 10: 849-865.

Brown, L.G.
A survey of image registration techniques. ACM Comput. Surv., 1992, 24: 325-376.

Buckner, R.L., Snyder, A.Z., Sanders, A.L., Raichle, M.E. and Morris, J.C.
Functional brain imaging of young, nondemented and demented older adults. Journal of Cognitive Neuroscience, 2000, 12 Supplement 2: 24-34.

Castleman, K.R.
Digital Image Processing. Prentice Hall, Englewood Cliffs, New Jersey, 1996, 116-119.

Ciulla, C., Takeda, T. and Endo, H.
MEG Characterization of Spontaneous Alpha Rhythm in the Human Brain. Brain Topography, 1999, 11(3): 211-222.

Ciulla, C., Takeda, T., Endo, H., Kumagai, T., Morabito, M. and Xiao, R.
MEG measurements of 40Hz auditory evoked response in human brain. In: Aine, C., Okada, Y., Stroink, G., Swithenby, S. and Wood, C. (Eds),

Biomag96: Proceedings of the Tenth International Conference on Biomagnetism, Springer-Verlag, 2000.

Ciulla, C.
Development and Characterization of Techniques for Neuroimaging Alignment. Master's Thesis. New Jersey Institute of Technology. Newark, NJ, USA, 2000: 1-59.

Ciulla, C. and Deek, F.P.
Development and Characterization of an Automatic Technique for the Alignment of fMRI time Series. Brain Topography, 2001a, 14(1): 41-56.

Ciulla, C. and Deek, F.P.
Performance Assessment of an Algorithm for the Alignment of fMRI Time Series. Submitted to Brain Topography, 2001c.

Chen, M., Kanade, T., Pomerleau, D. and Schneider, J.
3-D deformable registration of medical images using a statistical atlas. CMU-RI-TR-98-35. Robotics Institute, Carnegie Mellon University, 1998.

Chen, M., Kanade, T., Pomerleau, D. and Schneider, J.
Probabilistic registration of 3-D medical images. CMU-RI-TR-16. Robotics Institute, Carnegie Mellon University, 1999.

Clarkson, M.J., Rueckert, D., King, A.P., Edwards, P.J. et al.
Using texture mapping to register video images to tomographic images by optimizing mutual information. L.G. Hill and D.J. Hawkes. Medical Image Understanding and Analysis, 1999, Oxford, UK. July 19-20.

Coley, M.D., Ansorge, R.E., Hall, L.D. and Carpenter, A.
A locally adaptive registration technique for high precision registration of 3-D MRI data. Neuroimage, 2000, 12: 574-581.

Collignon, A., Maes, F., Dalaere, D., Vandermeulen, D. et al.
Automated multi-modality image registration based on information theory. Information Processing in Medical Imaging. Y. Bizais, C. Barillot and R. Di Paola, Eds. Kluwer Academic, Dordrecht, The Netherlands, 1995a, 263-274.

Collignon, A., Vandermeulen, D., Suetens, P. and Marchal, G.
Automated multimodality image registration based on information theory. Computer Imaging and Vision, 1995b, 3: 263-274.

Collignon, A., Vandermeulen, D., Suetens, P. and Marchal, G.
3D multi-modality medical image registration using feature space clustering. N. Ayache, Eds. CVRMed, Vol. 905 of Lecture notes in

Computer Science, Springer-Verlag, Berlin, 1995c, 195-204.

Collins, D.L., Holmes, C.J., Peters, T.M. and Evans, A.C.
Automatic 3-D model-based neuroanatomical segmentation. Hum. Brain Map., 1995, 3: 190-208.

Cox, R.W.
AFNI: Software for analysis and Visualization of Functional Magnetic Resonance Neuroimages. Computer and Biomedical Research, 1996, 29: 162-173.

Davatzikos, C.
Spatial normalization of 3D brain images using deformable models. J. Comput. Assist. Tomography, 1996, 20: 656-665.

De Castro, E. And Morandi, C.
Registration of Translated and Rotated Images using finite Fourier Transforms. IEEE Trans. PAMI, 1987, 5: 700-703.

Demmel, J.W.
Applied numerical linear algebra. SIAM, Society for Industrial and Applied Mathematics. 1997, 195-264.

Dobbins, J.T., Rice, J.J., Goodman, P.C., Patz, E.F.Jr. and Ravin, C.E.
Variable Compensation chest radiography performed with a computed radiography system: Design, considerations and initial clinical experience. Radiol., 1993, 187: 55-63.

Eddy, W.E., Fitzgerald, M. and Noll, D.C.
Improved Image Registration by Using Fourier Interpolation. MRM, 1996, 36: 923-931.

Erickson, B.J. and Jack, C.R.Jr.
Correlation of single photon emission CT with MR image data using fiduciary markers. A. J. Neuroradiology, 1993, 14: 713-739.

Evans, A.C., Beil, C., Marrett, S., Thompson, C.J. and Hakim, A.
Anatomical-functional correlation using an adjustble MRI-based region of interest. Atlas with positron emission tomography. Journal of Cerebral Blood Flow and Metabolism, 1988, 8: 513-529.

Evans, A.C., Marrett, S., Collins, L. and Peters, T.M.
Anatomical-functional correlative analysis of the huban brain using three dimensional imaging systems. Schneider, R.H., Dwyer III, S.J. and Jost, R.G. (Eds). Medical Imaging: Image Processing, SPIE, Bellingham WA, 1989, 1092: 264-274.

Evans, A.C., Neelin, P., Marrett, S., Meyer, E., Dai, W. and Collins, L.
Combined stereotactic mapping of MRI and PET Studies of Cognitive activation in human brain. Annual International Conference of the IEEE Engineering in Medicine and Biology Society, 1991, 13(1).

Faber, T.L. and Stokely, E.M.
Orientation of 3-D Structures in Medical Images. IEEE Transactions on Pattern Analysis and Machine Intelligence, 1988, 10(5): 626-633.

Fitzpatrick, J.M, West, J.B. and Maurer, C.R. Jr.
Predicting Error in Rigid-body Point-based Registration. Special Issue of IEEE Trans. Med. Imaging on Image Registration, 1998a, 17, 694-702.

Fitzpatrick, J.M., Hill, D.L.G., Shyr, Y., West, J., Studholme, C. and Maurer, C.R.
Visual Assessment of the Accuracy of Retrospective Registration of MR and CT Images of the Brain. IEEE Transactions on Medical Imaging, 1998b, 17(4): 571-585.

Fitzpatrick, J.M., Hill, D.L.G. and Maurer, C.R.
Image Registration. In: Handbook of Medical Imaging, Vol. 2: Medical Imaging Processing and Analysis. Sonka, M. and Fitzpatrick, J.M. (Eds). SPIE Vol. PM80, 2000.

Fitzpatrick, J.M. and West, J.B.
The distribution of terget registration error in rigid-body point-based registration. IEEE Transactions on Medical Imaging, 2001, 20(9): 917-927.

Freire, L. and Mangin, J.F.
Motion correction algorithms may create spurious brain activations in the absence of subject motion. Neuroimage, 2001, 14: 709-722.

Friston, K.J., Frith, C.D., Liddle, P.F. and Frackowiak, R.S.J.
Comparing functional (PET) images: the assessment of significant change. J. Cereb. Blood Flow Metab., 1991a, 11(4): 690-699.

Friston, K.J., Frith, C.D., Liddle, P.F. and Frackowiak, R.S.J.
Plastic Transformation of PET images. J. Computer Assisted Tomography, 1991b, 15(4): 634-639.

Friston, K.J., Ashburner, J., Frith, C.D., Poline, J.B. et al.
Spatial registration and normalization of images. Hum. Brain Mapp., 1995, 2: 165-189.

Friston, K.J., Williams, S., Howard, R., Frackowiak, R.S.J. and Turner, R.
Movement-Related effects in fMRI time series. MRM. 1996, 35: 346-355.

Grachev, I.D., Berdichevsky, D., Raunch, S.L., Heckers, S. et al.
A method for assessing the accuracy of intersubject registration of the human brain using anatomic landmarks. Neuroimage, 1999, 9: 250-268.

Grootoonk, S., Hutton, C., Ashburner, J., Howseman, A.M., Josephs, O. et al.
Characterization and correction of interpolation effects in the realignment of fMRI time series. Neuroimage, 2000, 11: 49-57.

Hajnal, J.V., Saeed, N., Oatridge, A., Soar, E.J., Young, I.R. and Bydder, M.G.A.
A registration and interpolation procedure for subvoxel matching of serially acquired MR images. J. Comput. Assit. Tomogr., 1995, 19: 289-296.

Hastreiter, P., Rezk-Salama, C., Nimsky, C., Lurig, C., Greiner, G. and Ertl., T.
Registration techniques for the analysis of the brain shift in neurosurgery. Computers & Graphics, 2000, 24: 385-389.

Hawkes, D.J., Hill, D.L.G., Lehmann, E.D., Robinson, G.P., Maisey, M.N. et al.
Preliminary work on the interpretation of SPECT images with the aid of registered MRI images and an MR derived neuro-anatomical atlas. In: 3D Imaging in Medicine algorithms, Systems, Applications. K.H.Hoehne, H Fuchs and S.M. Pizer, Eds. Springer-Verlag, Berlin, 1990: 241-252.

Hedley, M., Yan, H. and Rosenfeld, D.
Motion Artifact Correction in MRI Using Generalized Projections. IEEE Transactions on Medical Imaging, 1991a, 10(1): 40-46.

Hedley, M., Yan, H. and Rosenfeld, D.
An Improved Algorithm for 2-D Translational Motion Artifact Correction. IEEE Transactions on Medical Imaging, 1991b, 10(4): 548-553.

Hemler, P.F., van den Elsen, S.P.A., Napel, S. and Adler, J.R.
A versatile system for multimodality image fusion. J. Image Gui. Surg., 1995, 1: 35-45.

Henri, C.J., Collins, D.L. and Peters, T.M.
Multimodality image integration for stereotaxic surgical planning. Med. Phys., 1991, 18: 167-177.

Hill, D.L.G., Hawkes, D., Crossman, J.E., Gleeson, M.J., Cox, T.C.S. et al.
Registration of MR and CT images for skull base surgery using point-like anatomical features. British Journal of Radiology, 1991, 64: 1030-1035.

Hill, D.L.G., Hawkes, D.J., Harrison, N. and Ruff, C.F.
A strategy for automated multimodal registration incorporating anatomical knowledge and imagery characteristics. Information Processing in Medical

Imaging. H. H. Barret and A. F. Gmitro, Eds. Springer-Verlag, Berlin, 1993, 182-196.

Hill, D.L.G. and Hawkes, D.J.
Voxel Similarity measures for automated image registration. Visualization in Biomedical Computing. vol. Proc. SPIE 2359, 1994, 205-216.

Hill, D.A.G., Stoyle, P.N.R., Summers, P.E. and Keevil, S.F.
Automatic correction of motion artifacts in magnetic resonance images using and entropy focus criterion. IEEE Trans. on Medical Imaging, 1997, 16(6): 903-910.

Hill, D.L.G. and Hawkes, D.J.
Across-modality registration using intensity-based cost functions. In: Handbook of Medical Imaging: Processing and Analysis, Bankman, I.N., (Eds), 2000, 537-553.

Hogan, R.E., Cook, M.J., Kilpatrick, C.J., Binns, D.W., Desmond, P.M. et al.
Accuracy of coregistration of single-photon emission CT with MR via a brain surface matching technique. A. J. Neuroradiol., 1995, 17: 793-797.

Hogan, R.E., Lowe, V.J. and Bucholz, R.D.
Triple-Technique (MR Imaging, Single-Photon Emission CT, and CT) Coregistration for Image-Guided Surgical Evaluation of Patients with Intractable Epilepsy. A. J. Neuroradiol., 1999, 20: 1054-1058.

Holden, M., Hill, D.L.G., Denton, E.R.E., Jarosz, J.M. Cox, T.C.S. et al.
Voxel Similarity Measures for 3-D Serial MR Brain Image Registration. IEEE Transactions on Medical Imaging, 2000, 19: 94-102.

Iosifescu, D.V., Shenton, M.E., Warfield, S.K., Kikinis, R., Dengler, J. et al.
An automated registration algorithm for measuring MRI subcortical brain structures. Neuroimage, 1997, 6: 13-25.

Jacq, J.J. and Roux, C.
Registration of 3-D images by genetic optimization. Patt. Recognit. Lett., 1995, 16: 823-841.

Jiang, H., Holton, K.S. and Robb, R.A.
Image Registration of multimodality 3-D medical images by chamfer matching. Biomedical Image Processing and Three-Dimensional Microscopy. vol. Proc. SPIE 1660, 1992a: 356-366.

Jiang, H., Robb, R.A. and Holton, K.S.
A new Approach to 3-D Registration of multimodality medical images by surface matching. Visualization in Biomedical Computing. vol. Proc. SPIE

1808, 1992b: 196-213.

Kybic, J., Thevenaz, P. and Unser, M.
Multiresolution spline warping for EPI registration. Proc. Of the SPIE Conference on Mathematical Imaging: Wavelet Applications in Signal and Image Processing. VII, Denver, CO, USA, 1999, 3813: 571-579.

Kybic, J. and Unser, M.
Multidimentional Elastic Registration of Images Using Splines. Proc. of the IEEE Int. Conf. On Imag. Proc. Vancouver, 2000, II: 455-548.

Kybic, J., Thevenaz, P., Nirkko, A. and Unser, M.
Unwarping of unidiretionally distorted EPI images. IEEE Transactions on Medical Imaging, 2000, 19: 80-93.

Kruggel, F. and Yves von Cramen, D.
Alignment of magnetic resonance brain datasets with the stereotactical coordinate system. Medical Image Analysis, 1999, 3(2): 175-185.

Lavalle, S., Szeliski, R. and Brunie, L.
Matching 3-D smooth surfaces with their 2-D projections using 3-D distance maps. In Geometric Methods in Computer Vision. vol. SPIE, San Diego, CA, July 1991.

Lee, C.C., Jack, C.R.Jr., Grimm, R.C., Rossman, P.J., Felmlee, J.P. et al.
Real-Time Adaptive Motion Correction in Functional MRI. MRM, 1996, 36: 436-444.

Lee, C.C., Grimm, R.C., Manduca, A., Felmlee, J.P. Ehman, R.L. et al.
A Prospective Approach to Correct for Inter-Image Head Rotation in fMRI. MRM, 1998, 39: 234-243.

Lemieux, L., Wieshmann, U.C., Moran, N.F., Fish, D.R. and Shoovon, S.D.
The detection and significance of subtle changes in mixed signal brain lesions by serial MRI scan matching and spatial normalization. Med. Image Anal., 1998, 2(3): 227-242.

Lemoine, D., Barillot, C., Gibaud, B. and Pasqualini, E.
An anatomical based 3D registration of multimodality and atlas data in neurosurgery. A. Colchester and D. Hawkes, Eds. Information Processing in Medical Imaging. Proceedings of the 12th International Conference. Springer-Verlag, Berlin, 1991, 154-164.

Lemoine, D., Liegeard, D., Lussot, E. and Barillot, C.
Multimodal registration system for the fusion of MRI, CT, MEG, and 3D or stereotactic angiography data. Medical Imaging. Image Capture Formatting

and Display. vol. Proc. SPIE, 1994, 46-56.

Li, H., Manjunath, B.S. and Mitra, S.K.
Registration of 3-D multimodality brain images by curve matching. Proc. IEEE Conference on Medical Imaging, San Francisco, 1993, 1744-1748.

Liu, A., Pizer, S.M., Eberly, D., Morse, B., Rosenman, J. and Carrasco, V.
Volume registration using the 3D core. Proc. SPIE Medical Imaging VIII. Newport Beach, CA, 1994.

Maas, L.C., Frederick Blaise, deB. and Renshaw, P.F.
Decoupled Automated Rotational and Translational Registration for Functional MRI Time Series Data: The DART Registration Algorithm. MRM, 1997, 37: 131-139.

Maes, F., Collignon, A., Vandermeulen, D., Marchal, G. and Suetens, P.
Multimodality image registration by maximization of mutual information. IEEE Trans. Medical Imaging, 1997, 16(2): 187-198.

Maes, F., Vandermeulen, D. and Suetens, P.
Comparative evaluation of multiresolution optimization strategies for multimodality image registration by maximization of mutual information. Medical Image Analysis, 1999, 3(4): 373-386.

Maguire, G.Q. Jr., Noz, M.E., Rusinek, H., Jaeger, J., Kramer, E.L. et al.
Graphics applied to medical image registration. IEEE Comput. Graph. Appl., 1991, 11: 20-29.

Maintz, J.B., van den Elsen, P.A. and Viergever, M.A.
Using geometrical features to match CT and MR brain images. Beolchi and Kuhn Eds. Medical Imaging analysis of multimodality 2D/3D images. Studies in Health, Technology and Informatics. IOS Press, Amsterdam, 1994, 19: 43-52.

Maintz, J.B.A., van den Elsen, P.A. and Viergever, M.A.
Comparison of feature-based matching of CT and MR brain images. Computer Vision, Virtual Reality and Robotics in Medicine. N. Ayache, Eds. Springer-Verlag, Berlin, 1995: 219-228.

Maintz, J.B.A., van den Elsen, P.A. and Viergever, M.A.
Comparison of edge-based and ridge-based registration of CT and MR brain images. Medical Image Analysis, 1996a, 1(2): 151-161.

Maintz, J.B.A. van den Elsen, P. A. and Viergever, M.A.
Evaluation of ridge seeking operators for multimodality medical image matching. IEEE Trans. Pattern Anal. Mach. Intell., 1996b, 18: 353-365.

Maintz, J.B., van den Elsen, P.A. and Viergever, M.A.
Registration of 3D medical images using simple morphological tools. J. Duncan and G. Gindi, Eds. IPMI 97, Volume 1230 of Lecture Notes in Computer Science. Springer Verlag, 1997, 204-217.

Maintz, J.B.A., Meijering, E.H.W. and Viergever, M.A.
General Multimodal Elastic Registration Based on Mutual Information. Hanson, K.M., Eds. Medical Imaging. Image Processing. Bellingham, 1998, 3338 SPIE: 144-154.

Maintz, J.B. and Viergever, M.A.
A Survey of Medical Registration. Medical Image Analysis, 1998, 2(1): 1-36.

Malandain, G., Fernandez-Vidal, S. and Rocchisani, J.M.
Rigid Registration of 3-D objects by motion analysis. Proc. 12th Int. Conf. Pattern Recognition, 1994a, 579-581.

Malandain, G., Fernandez-Vidal, S. and Rocchisani, J.M.
Improving Registration of 3-D medical images using a mechnical based method. 3rd European Conference on Computer Vision (ECCV 94), 1994b, 131-136.

Malandain, G., Fernandez-Vidal, S. and Rocchisani, J.M.
Physically based rigid registration of 3-D form objects: Application to medical imaging. Tech. Rep. 2453, INRIA, Sophia Antipolis Cedex France, 1995.

Mandava, V.R., Fitzpatrick, J.M., Maurer, C.R.Jr., Maciunas, R.J. and Allen, G.S.
Registration of multimodal volume head images via attached markers. Medical Imaging VI: Image Processing. vol. Proc. SPIE, 1992, 1652: 271-282.

Mangin, J.F., Frouin, V. and Bendriem, B.
Nonsupervised 3-D registration of PET and MRI data using chamfer matching. Conference on Medical Imaging. Nuclear Science Symposium. Orlando. Florida. October 1992.

Maurer, C.R., Fitzpatrick, J.M., Wang, M.Y. and Maciunas, R.J.
Estimation of localization accuracy for markers in multimodal volume images. Proc. Annu. Int. Conf. IEEE Eng. Med. Biol. Soc., 1993, 15: 124-125.

Maurer, C.R. and Fitzpatrick, J.M.
A Review of medical image registration. Interactive Image-Guided Neurosurgery. R.J. Maciunas, Eds. Park Ridge, IL. American Association

of Neurological Surgeons, 1993, 17-44.

Maurer, C.R., Aboutanos, G.B., Dawant, B.M., Gadamsetty, S. et al.
Effect of geometrical distortion correction in MR on image registration accuracy. Medical Imaging. Image Processing. vol. Proc. SPIE 2167, 1994, 200-213.

Maurer, C.R., Aboutanos, G.B., Dawant, B.M., Margolin, R.A. et al.
Registration of CT and MR brain images using a combination of points and surfaces. Medical Imaging: Image Processing. vol. Proc. SPIE 2434, 1995, 109-123.

Maurer, C.R., Aboutanos, G.B., Dawant, B.M., Gadamsetty, S. et al.
Effect of geometrical distortion correction in MR on image registration accuracy. J. Computer Assist. Tomogr., 1996, 20: 666-679.

Maurer, C.R., Fitzpatrick, J.M., Wang, M.Y., Galloway, R.L. et al.
Registration of head volume images using implantable markers. IEEE Transactions on Biomedical Imaging, 1997, 16(4): 447-462.

Meyer, C.R., Leichtman, G.S., Brunberg, J.A., Wahl, R.L. and Quint, L.E.
Simultaneous Usage of Homologous Points, Lines and Planes for Optimal, 3-D, Linear Registration of Multimodality Imaging Data. IEEE Transactions on Medical Imaging, 1995, 14(1): 1-11.

Meyer, C.R., Boes, J.L., Kim, B., Bland, P.H., Zasadny, K.R., Kison, P.V. et al.
Demonstration of accuracy and clinical versatility of mutual information for automatic multimodality image fusion using affine and thin-plate spline warped geometric deformations. Medical Image Analysis. 1997, 1 (3): 195-206.

Miller, M.I., Christensen, G.E., Amit, Y. and Grenander, U.
Mathematical textbook of deformable neuroanatomies. Proc. Natl. Acad. Sci. USA, 1993, 90: 11944-11948.

Morris, E.D., Muswick, G.J., Ellert, E.S., Steagall, R.N. et al.
Computer aided technique for aligning interleaved sets of non-identical medical images. SPIE vol. 1898. Image Processing, 1993.

Levin, D.N., Pellizzari, C.A., Chen, G.T.Y., Chen, C. and Cooper, M.D.
Retrospective geometric correlation of MR, CT and PET images. Radiology, 1988, 169: 817-823.

Nikou, C., Heitz, F., Armspach, J.P., Namer, I.J. and Grucker, D.
Registration of MR/MR and MR/SPECT Brain Images by Fast Stocastic Optimization of Robust Voxel Similarity Measure. Neuroimage, 1998, 8:

30-43.

Ostuni, J.L., Santha, A.K.S., Ventaka, S.M., Weinberger, D.R. et al.
Analysis of interpolation effects in the reslicing of functional MR images. Journal of Computer Assisted Tomography, 1997, 21(5): 803-810.

Panigrahy, A., Caruthers, S.D., Krejza, J., Barnes, P.D., Faddoul, S.G. et al.
Registration of Three-Dimensional MR and CT Studies of the Cervical Spine. A. J. Neuroradiol., 2000, 21: 282-289.

Pavia, J., Ros, D., Catafau, A.M., Lomena, Huguet, M. and Setoin, I.
Three-dimensional realignment of activation brain single-photon emission tomographic studies. Eur. J. Nucl. Med., 1994, 21: 1298-1302.

Pellizzari C.A., Chen G.T.Y., Spelbring D.R., Weichselbaum R.R. and Chin-Tu C.
Accurate Three-Dimensional Registration of CT, PET, and/or MR Images of the Brain. Journal of Computer Assisted Tomography, 1989, 13: 20-26.

Pennec, X., Ayache, N. And Thirion, J.P.
Landmark-based registration using features identified through differential geometry. In: Handbook of Medical Imaging: Processing and Analysis, Bankman, I.N., (Eds), 2000, 499-513.

Powell, M.J.D.
An efficient method for finding the minimum of a function of several variables without calculating derivatives. Comput. J., 1964, 7: 155-163.

Rouet, J.M., Jacq, J.J. and Roux, C.
Genetic Algorithms for a robust 3-D MR-CT Registration. IEEE Transactions on Information Technology in Biomedicine, 2000, 4: 126-136.

Rousseau, J., Cvlarysse, P., Blond, S., Gibon, D., Vasseur, C. and Marchandise, X.
Validation of a new method for stereotactic localization using MR imaging. J. Comp. Assist. Tomogr., 1991, 15: 291-296.

Schonemann, P.H.
A generalizaed solution of the orthogonal procrustes problem. Psychometrika, 1966, 31: 1-10.

Schormann, T., Henn, S. and Zilles, K.
A new approach to fast elastic alignment with application to human brains. Lecture Notes Comput. Sci., 1996, 1131: 437-442.

Strasters, K.C., Little, J.A., Burman, J., Hill, D.L.G. and Hawkes, D.J.
Anatomic landmark image registration: validation and comparison. CVR Med/MRCAS, 1997.

Studholme, C., Hill, D.L.G. and Hawkes, D.J.
Automated 3D registration of MR and CT images of the head. Medical Image Analysis, 1996, 1: 163-175.

Studholme, C., Hill, D.L.G. and Hawkes, D.J.
Automated three-dimentional registration of magnetic resonance and positron emission tomography brain images by multiresolution optimization of voxel similarity measures. Medical Phys., 1997, 24(1): 25-35.

Talairach, J. and Tournoux, P.
Co-planar Stereotaxic Atlas of the Human Brain. 3-Dimensional Proportional System: An Approach to Cerebral Imaging. Thieme medical, New York, 1988.

Thirion, J.
Extremal points: definition and application to 3D image registration. Proc. CVPR. Los Alamitos, CA. IEEE Computer Society Press., 1994, 587-592.

Thevenaz, P. and Unser, M.
An Efficient Mutual Information Optimizer for Multiresolution Image Registration. Proc. of the 1998 IEEE Int. Conf. on Image Processing, 1998a, 833-837.

Thevenaz, P., Ruttimann, U.E. and Unser, M.
A pyramid Approach to Subpixel Registration Based on Intensity. IEEE Transactions on Image Processing, 1998b, 7(1): 27-41.

Thevenaz, P. and Unser, M.
Optimization of mutual information for multiresolution image registration. IEEE Trans. on Image Processing, 2000, 9(12): 2083-2099.

Thompson, P.M. and Toga, A.W.
A surface based technique for warping three dimensional images of the brain. IEEE Trans. Med. Imaging, 1996, 15(4): 402-417.

Thompson, P. and Toga, A.W.
Elastic Image registration and pathology detection. In: Handbook of Medical Imaging: Processing and Analysis, Bankman, I.N., (Eds), Academic Press, 2000: 569-601.

Thompson, P. and Toga, A.W.
Warping strategies for intersubject registration. In: Handbook of Medical Imaging: Processing and Analysis, Bankman, I.N., (Eds), Academic Press, 2000: 569-601.

Thompson, P.M., MacDonald, D., Mega, M.S., Holmes, C.J. and Evans, A.C.

Detection and mapping of abnormal brain structure with a probabilistic atlas of cortical surfaces. J. Comput. Assist. Tomogr., 1997, 21(4): 567-581.

Toga, A.W.
Visualization and warping of multi-modality brain imagery. Functional Neuroimaging: Technical Foundations. R.W. Thatcher, M. Halle, T. Zeffiro, J.E. Roy and M. Huerta. Eds. Academic Press. San Diego, CA, 1994, 171-180.

Toga, A.W. and Thompson, P.
The role of image registration in Brain Mapping. Image and Vision Computing Journal, 2000.

Turkington, T.G., Jaszczak, R.J., Pellizzari, C.A. et al.
Accuracy of registration of PET, SPECT and MR images of a brain phantom. J. Nucl. Med., 1993, 34: 1587-1594.

Unser, M., Thevenaz, P., Lee, C. and Ruttiman, U.E.
Registration and Statistical Analysis of PET Images Using the Wavelet Transform. IEEE Engineering in Medicine and Biology, 1995, 14(5): 603-611.

Van den Elsen, P.A., Maintz, J.B.A., Pol, E.J.D. and Viergever, M.A.
Image fusion using geometric features. R.A. Robb, Eds. Visualization in Biomedical Computing. vol. 1808 of Proc. SPIE. SPIE Press, Bellingham, WA, 1992, 172-186.

Van den Elsen, P.A., Pol, E-J.D. and Viergever, M.A.
Medical Image Matching. A review with classification. IEEE Eng. in Medicine and Biol., 1993a, 26-38.

Van den Elsen, P.A., Maintz, J.B.A. and Viergever, M.A.
Geometry driven multimodality matching of brain images. Brain Topography, 1993b, 5: 153-158.

Van den Elsen, P.A., Pol, E.J.D., Sumanaweera, T.S., Hemler, P.F. et al.
Grey value correlation techniques used for automatic matching of CT and MR brain and spine images. Visualization in Biomedical Computing. vol. Proc. SPIE 2359, 1994, 227-237.

Van den Elsen, P.A., Maintz, J.B.A., Pol, E.J.D. and Viergever, M.A.
Automatic Registration of CT and MR brain Images using Correlation of Geometrical Features. IEEE Trans. on Medical Imaging, 1995, 14(2): 384-396.

Vemuri, B.C., Huang, S., Sahni, S., Leonard, C.M., Mohr, C. et al.

An efficient motion estimator with application to medical image registration. Medical Image Analysis, 1998, 2: 79-98.

Viola, P. and Wells III, W.M.
Alignment by maximization of mutual information. Proc. IEEE Int. Conf. on Computer Vision, Boston, MA, 1995, 15-23.

Wang, M.Y., Maurer, C.R., Fitzpatrick, J.M. and Maciunas, R.J.
An automatic technique for finding and localizing externally attached markers in CT and MR volume images of the head. IEEE Transactions on Biomedical Engineering, 1996, 43(6): 627-637.

Wang, Y. and Staib, L.H.
Physical model-based non-rigid registration incorporating statistical shape information. Medical Image Analysis, 2000, 4: 7-20.

Warfield, S., Dengler, J., Zaers, J., Guttaman, C.R.G., Wells, W.M. et al.
Automatic identification of gray matter structures from MRI to improve the segmentation of white matter lesions. J. Image Guided Surg., 1996, 1(6): 326-338.

Wells III, W.M., Viola, P. and Kikinis, R.
Multi-modal volume registration by maximization of mutual information. Medical Robotics and Computer Assisted Surgery. Wiley-Liss, New York, 1995, 55-62.

Wells III, W. M., Viola, P., Atsumi, H., Nakajima, S. and Kikinis, R.
Multimodal volume registration by maximization of mutual information. Medical Image Analysis, 1996, 1(1): 35-51.

West, J. et al.
Comparison and Evaluation of retrospective Intermodality Brain Image Registration Techniques. Journal of Computer Assisted Tomography, 1997, 21: 554-566.

West, J., Fitzpatrick, J.M., Wang, M.Y., Dawant, B.M., Maurer, C.R. et al.
Retrospective intermodality registration techniques for images of the head: Surface-based versus Volume-based. IEEE Transactions on Medical Imaging, 1999, 18(2): 144-149.

West, J. et al.
Fiducial point placement and the accuracy of point-based, rigid body registration. Neurosurgery, 2001, 48: 810-817.

Woods, R.P., Cherry, S.R. and Mazziotta, J.C.
Rapid automated algorithm for aligning and reslicing PET images. Journal

of Computer Assisted Tomography, 1992, 16: 620-633.

Woods, R.P., Mazziotta, J.C. and Cherry, S.R.
MRI-PET Registration with Automated Algorithm. Journal of Computer Assisted Tomography, 1993, 17: 536-546.

Woods, R.P. Grafton, S.T., Holmes, C.J., Cherry, S.R. and Mazziotta, J.C.
Automated image registration: I. General methods and intrasubject, intramodality validation. J. Comput. Assist. Tomogr., 1998a, 22(1): 139-152.

Woods, R.P. Grafton, S.T., Watson, J.D., Sicotte, N.L. and Mazziotta, J.C.
Automated image registration: II. Intersubject validation of linear and nonlinear models. J. Comput. Assist. Tomogr., 1998b, 22(1): 153-165.

Woods, R.P.
Within-modality registration using intensity-based cost functions. In: Handbook of Medical Imaging: Processing and Analysis, Bankman, I.N., (Eds), 2000a: 529-536.

Woods, R.P.
Validation of registration accuracy. In: Handbook of Medical Imaging: Processing and Analysis, Bankman, I.N., (Eds), 2000b: 491-497.

Zhang, J., Levesque, M.F., Wilson, C.L.
Multimodality imaging of brain structures for stereotactic surgery. Radiology, 1990, 175: 435-441.